UNIVERSITY OF CALIFORNIA

Santa Barbara

Spectroscopy as a Window into History: Photochemistry as It Pertains to Archeology, Pigments, and Early Earth Nucleobases

A Dissertation submitted in partial satisfaction of the requirements for the degree Doctor of Philosophy in Chemistry

By

Ann Karen Williams

Committee in charge

Professor Mattanjah S. de Vries, Chair

Professor Steven K. Buratto

Professor Joan Emma Shea

Professor Stuart Tyson Smith

December 2021

The dissertation of Ann Williams is approved.

_____

Stuart Tyson Smith

_____

Steven K. Buratto

_____

Joan Emma Shea

_____

Mattanjah S. de Vries, Committee Chair

November 2021

Spectroscopy as a Window into History: Photochemistry as It Pertains to Archeology, Pigments, and Early Earth Nucleobases

By

Ann Karen Williams

ACKNOWLEDGEMENTS

First off, I would like to acknowledge my family. It is only with deep roots that great heights can be achieved. Even though physical distance was far our emotional connection never faltered or wavered. This steady source of love and support was a constant source of strength and optimism. Thank you.. for without you I wouldn't have achieved so much. Lastly to Nana, God rest her soul, thank you for always believing in me. I know if you were here today you would be so proud of me.

Secondly, to my friends As they say " make new friends but keep the old" To my old friends Tom and Logan, we've had quite the adventures. You've always been faithful encouraging companions. With the confidence your friendship gives me, I can journey anywhere. To my new friends – Greta, Vani and Shannon- has a group of strong women ever been more inspirational? You've made me laugh. You've helped me cry. You've kept me strong and determined and helped me keep going no matter what to reach my goals. You've been my cheerleaders as well helping me celebrate the successes, no matter how small. The university as a whole is better off from your presence in it.

Lastly to my love, Joseph.. where to begin. Grad school started this and I am so happy it didn't end it. When home and comfort felt far away you brought it close again. For that, I can never thank you enough.

To my advisor Mattanjah de Vries, thank you for support, your patience and your teaching over the years. To my colleagues- Trevor, Nathan, Greg, Michael, Si Young and Krystal- as we all know this lab does not produce work that is the result of a single person. It is only through our collaboration and teamwork that we have all succeeded and produced such good work. Lastly, I would like to acknowledge the efforts of my committee members- Dr. Buratto, Dr. Smith, Dr. Shea- and my collaborators- Dr. Anabel Ford and Dr. Rafal Szabla.

ANN WILLIAMS

(678) 698-4748 | annwilliams@ucsb.edu | www.linkedin.com/in/a-k-williams

SUMMARY OF QUALIFICATIONS

- 3 years experience of in-depth understanding of highly technical instrumentation, initiative in improving the technique, and creative problem solving for a home built instrument.
- 8 months experience in quality control with a production company, illustrating my ability to work as part of team to meet production deadlines.
- 5 months mass spectrometry facility manager maintaining an ESI-MS, MALDI, and GC-MS instruments, including minor repairs, analyzing organic and non-organic samples.
- Demonstrated success at completion of projects and distillation of complex information into accessible written and oral formats through **2** first author publications, **2** second author publications and **7** presentations.

EDUCATION

Ph.D. Candidate, Physical Chemistry
(Expected) December 2021

University of California, Santa Barbara (UCSB), Goleta, CA

B.S. in Chemistry, Minor in Anthropology, *Summa Cum Laude*
May 2017

Valdosta State University (VSU), Valdosta, GA

Award: ACS Undergraduate Award in Analytical Chemistry, Scholarship for Excellence in Chemistry, 2016 Who's Who Among Students in American Universities and Colleges

Publications

Nucleobases as molecular fossils of prebiotic photochemistry: Excited state dynamics of C2 and C6 substituted purines. G. Gate, **A. Williams**, M. R. Haggmark, N. Svadlenak, and M. S. de Vries. Royal Society of Chemistry. Book Title: Prebiotic Chemistry. (**June 2021**)

The Enolic Form of Curcumin in the Gas Phase. G. Gate[a], **A. Williams[a].** M. Haggmark, M. S. de Vries

The tautomer-specific excited state dynamics of 2,6-diaminopurine illuminated by REMPI and quantum calculations. G. Gate, **A. Williams** M. S. de Vries, R. Szabla.

[a] *these authors contributed equally*

SKILLS

- **Instrumentation:** Mass Spectrometry (GC-MS, MALDI-MS, ESI-LC-MS, UPLC-MS/MS), high vacuum pumps, mechanical pumps, and vacuum detectors.
- **Spectroscopy:** gas phase spectroscopy (REMPI, pump-probe, double resonance, transient absorption); alignment, maintenance, and troubleshooting of multiple laser systems (OPO/OPA, OPG, Nd-YAG, Excimer, Dye); optics- dichroics, mirrors, beam splitters, waveplates, polarizers.
- **Software**: Labview, Mathematica, Gaussian
- **Leadership:** Girl Scout Gold Award (2014), VSU Leadership Award from Honors College (2016)
- **Presentation Awards:** Received best presentation from Southern Regional Honors Conference (2017)

RELEVANT INDUSTY EXPERIENCE

Quality Control Technician, *Oil-Dri Corporation| 2017-2018*

- Worked with a team of 5 colleagues on scientific collection, testing, and quality control of manufacturing products
- Prepared accurate lab reports, sample logs, and certificates of analysis
- Worked under pressure to effectively deliver product by production deadlines.

RELEVANT CHEMISTRY EXPERIENCE

Graduate Student Researcher, Chemistry Dept., *UCSB*
Sept. 2018-Current

- Worked with a team of ~5 researchers to maintain all lab equipment. Equipment is home built so use, maintenance and repairs requires intricate understanding of the technique and creative problem solving skills.
- Independently developed and managed 2-year interdisciplinary research project that quantifies and analyzes biomarkers in archeological fragments
- Taken initiative by improving our instrumentation, redesigning our group website to attract new members, reorganizing our filing system and data organization
- Collaborated with 2 colleagues for the data collection and writing on multiple projects studying nucleobase derivatives utilizing gas phase spectroscopy and TOF-MS to elucidate excited state dynamics.
- Utilized management skills through training of new lab members in all techniques and equipment, development of an undergraduate mentoring worksheets and providing constructive feedback.
- Distilled complex information into accessible visual, written, and oral formats.

Interim Mass Spectrometry Facility Manager/ Facility Assistant, *UCSB* Apr.-Jun.2019, May. 2021-Current

- Analysis of organic and inorganic small molecules and peptides through GC-MS, ESI-LC-MS, and MALDI
- Upkeep, calibration, and maintenance of all three facility instruments
- Communication of results to students and faculty at all levels of understanding
- Preserved all old data as appropriate to ensure safe backup
- Received Facility Manager promotion upon successful accomplishments at Assistant-level
- Sample analysis with ESI-LC-MS and MALDI-MS of organic and inorganic compounds.
- Assisted in preventative maintenance and repairs of the ESI-LC-MS

LEADERSHIP EXPERIENCE

Co-chair, Chemistry Professional Development, *UCSB* *Aug. 2020-Current*

- Collaborated with a committee of 5 grad students by monthly meetings to plan, delegate, and host career development events
- Contacted alumni and company representatives as workshop host or panelist.

Programing Co-Chair, Beyond Academia Conference, *UCSB* Oct. 2020-Apr. 2021

- Collaborated in a committee of 10 graduate students to delegate tasks and oversaw planning of a 2-week virtual conference with 30 company reps and 300 attendees.
- Co-led weekly meetings to discuss details and ensure completion of tasks that required problem solving and initiative.

Executive member, Honors Student Association, *VSU* May.2015-May. 2018

- Worked independently to plan, host, and market monthly events to engage students in research. Attended weekly meetings with a committee of 6 other students to plan club and university wide events.

ABSTRACT

Spectroscopy as a Window into History: Photochemistry as It Pertains to Archeology, Pigments, and Early Earth Nucleobases

Ann Karen Williams

Spectroscopy is a broad tool set that can be applied to further the understanding of many interdisciplinary questions. The technique of jet-cooling, laser-desorption, resonance-enhanced-multi-photon-ionization, mass spectrometry (LD-JC-REMPI-MS) was used to study the photodynamics of pigments and alternative nucleobases as well as quantify residues in archeological pottery. LD-JC-REMPI-MS as a cold gas phase technique offers the benefits of simplifying absorption spectra to individual vibronic transitions unique to individual tautomeric forms of a molecule. As a form of action spectroscopy, mass spectrometry is the detector, while the intermediate REMPI step allows for ps level detection of lifetimes and relaxation mechanisms.

The earliest interdisciplinary question of historical interest our technique has been applied to is the understanding of the early earth conditions that lead to the selection of canonical nucleobases over alternative forms. The same reactions responsible for the canonical nucleobases would've synthesized many other molecules similar in structure. Recent research has shown that many of these alternative molecules could have successfully functioned in DNA or RNA. Thus, it is not biological pressures that selected the canonical nucleobases. What then was the selection method that led to only the 5 nucleobases

inclusion in DNA and RNA over these many alternative forms? Photochemistry, specifically distinct differences in excited state lifetimes, are the answer.

The second question in the historical timeline that our technique has been applied to is the identification of cacao residues in Maya pottery. Cacao is an important ritualistic beverage made from the combination of hot water and the dried, roasted, ground seeds of the *Theobroma cacao* plant. Compounds characteristic for cacao are part of a molecular family known as xanthines. These compounds are variations of some of the same molecules we studied for the first question. We therefore applied the knowledge acquired about their spectroscopy in part one to develop an analytical technique to detect cacao residues. Our study has focused on vessel fragments from the Maya site of El Pilar located in modern day Belize, part of a project led by Dr. Anabel Ford. In this study LD-JC-REMPI-MS is used as the analytical technique to detect theophylline as an indicator of cacao.

Finally, the last window of history our technique was applied to is an understanding of pigments. Conservationists value highly the study of pigments as an understanding of photochemistry can predict fading. Pigments with faster excited state lifetimes are much less likely to undergo fading as the fast decay prevents the molecules from undergoing damaging reactions from absorption of UV light. As pigments similar in structure can have vastly different decay pathways, each pigment must be studied individually to determine the lifetime and thus its lightfastness. Previous studies have shown that excited state proton or hydrogen transfer is often one of the fast decay pathways that prevents fading of pigments. Both curcumin and indigo studied in this dissertation are dominated by an excited state

proton/hydrogen transfer. Both are studied in the deuterated form to further study the role of excited state proton/hydrogen transfer as a decay pathway, as well as contribute a broader understanding of both pigments.

TABLE OF CONTENTS

I- INTRODUCTION

Photochemistry in its most basic definition is the intersection between light and matter. This intersection of the tangible and intangible is responsible for such a portion of the beauty of life. For it is the absorption and emission of light from objects that gives them color. Light and the photochemistry it produces is even likely responsible for choosing the building blocks from which all of life is built. While light can result in so much life, the high energy nature of UV light can also be highly damaging. The absorption of damaging, high energy light is what causes most pigments to fade over time. This same high energy UV light can also damage the very fabric of life by causing our DNA to undergo damaging reactions. Thus a molecule that absorbs UV light must be able to quickly dissipate this energy to prevent undergoing chemical reactions. Consequently, understanding the lifetime of a molecule can predict if a painting's colors will last a century or a year and even decide if a molecule becomes a fundamental building block of life.

Photochemistry can also be utilized as an invaluable tool through the skillset of spectroscopy. Spectroscopy uses photochemistry to determine the pathways and lifetimes of a molecule. Many techniques can be used to collect this data, this dissertation will focus on only one technique with a few other mentioned as relevant. In our experimental set up, action spectroscopy is used which means that molecules absorb light which then causes them to react in ways that are detectable by non-spectroscopic methods. In this case, light reacts with matter to change phase, produce ions, generate an absorption event, characterize excited states, but the outcome measured is actually the production of ions.

The combination of photochemistry and mass spectrometry studied here is called laser-desorption, jet-cooling, resonance-enhanced-multiphoton-ionization, mass spectrometry (LD-JC-REMPI-MS). This type of action spectroscopy allows a wide variety of molecules to be studied as cold neutral isolated gas phase molecules with an ionization step that collects spectroscopic information in a way that distinguishes between isomers and allows for the detection of molecules with relatively low absorption cross sections. Spectra generated show absorption bands corresponding to individual vibronic transitions from a specific tautomer, from which the lifetime of each transition can be determined.

In addition, the isolated cold gas phase also narrows the observed tautomers to only these lowest in energy such that IR techniques assign individual absorption bands to a specific tautomer. IR techniques can also be used to identify the tautomers present in the technique.

In this dissertation, this technique has been applied to study alternative nucleobases, dyes and archeological organic residues. While seemingly vastly difference in nature these compounds are often all substituted purines. Additionally, each different type of study often relies on the fact that molecules can be similar in structure while having vast differences in photochemistry. Because of these similarities, photochemistry can be applied to many interdisciplinary areas often of historical importance. Thus this dissertation will begin in an early earth, move to ancient Maya civilization, and, lastly, end in dye making and medicinal pigments in Asia and Europe. For each window of history, spectroscopy and the application of our technique LD-JC-REMPI-MS will offer up invaluable information.

II DESCRIPTION OF LD-JC-REMPI-MS AS A PHOTOCHEMICAL AND ANALYTICAL TECHNIQUE

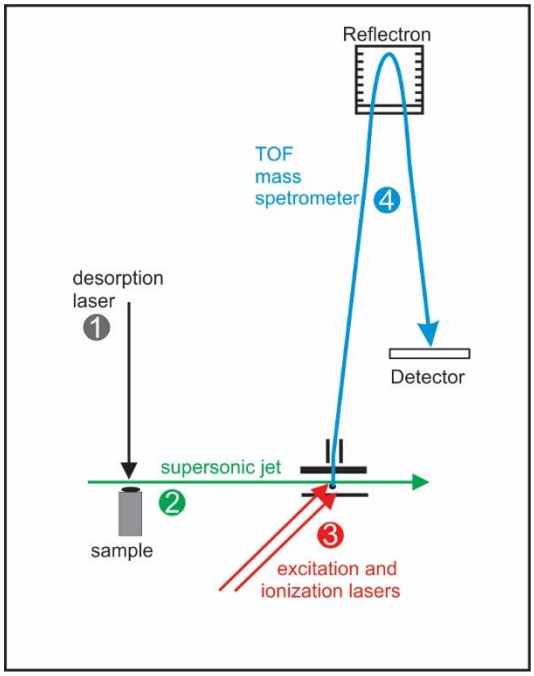

Figure 1- Schematic of the instrumental set up. Desorption is in black, jet cooling green, resonance enhanced multi-photon ionization red, reflectron TOF mass spectrometer blue

All studies in the following work were done on a homebuilt instrument that combines gas phase spectroscopy and mass spectrometry. In brief, this is a four step process that involves laser-desorption (1), jet-cooling (2), resonant enhanced multi-photon ionization (REMPI; 3), and reflectron time-of-flight mass spectrometry (re-TOF-MS: 4). Succinctly, all samples are usually powdered samples combined with graphite and placed on a translating graphite bar under high vacuum. The sample graphite mixture is then desorbed by a Nd:YAG laser pulse, placing the sample in the gas phase while minimizing fragmentation. This desorption event takes place in front of a pulse valve which produces a supersonic molecular beam that collisionally cools the desorbed molecules to ~ 20 K. The desorbed, cooled molecules are then

ionized through a two-photon resonant process that allows for a variety of spectroscopic information to be gathered. The ionized molecules are then detected by a reflectron time-of-flight mass spectrometer (reTOF-MS). This will be explained in detail in the following sections.

This technique offers two key benefits- cold gas phase spectra simplify broad absorption transitions into individual vibronic transitions. The lack of solvent, isolation of individual molecules and cooling are responsible for the simplification of the spectra. With such simplified spectra, different molecules, isomers, and tautomers are easily distinguishable from each other. The presence of solution creates many different microhydration states leading to minute shifts in absorption transitions. When added up in bulk, this contributes to the broad absorption bands characteristic of solvent phase data. In addition, at room temp, a single molecule will have multiple vibrational bands of the ground state populated, allowing for a variety of different excited state transitions. Cooling of isolated molecules depopulates the vibrational bands of the ground state, leading to fewer possible transitions and thus highly simplified spectra. Lastly, due to the low pressure of our instrument, molecules can each be treated as isolated molecules being too separated to have any effect on each other's photochemistry.

The second benefit of this technique is the combination of very high sensitivity with unprecedented specificity by combining mass spectrometry with optical spectroscopy[1-3]. By using both wavelength and mass selectivity, this technique can easily distinguish between compounds with similar structures and is even capable of distinguishing between different isomers or tautomers[4-8]. This combination of laser spectroscopy and mass spectrometry

provides simultaneous wavelength and mass specificity for the identification of compounds, resulting in unprecedented accuracy and unambiguous identification. The addition of optical spectroscopy also increases the overall resolution as the optical resolution provided by the typical laser bandwidth as a fraction of a wavenumber is several orders of magnitude better than a conventional mass resolution. By separating the desorption and ionization steps, this technique can selectively ionize and detect a specific molecule from a complex sample. Absorption spectra in solution phase are usually characterized by broad absorption bands that are very similar if not identical for molecules close in structure. These differences in absorption allow for selective ionization of the desired molecule, provided that the absorption spectrum of the analyte is known

II.1 LASER DESORPTION

Laser desorption is a commonly used technique, usually coupled with molecular beams to generate gas phase molecules without ionization, fragmentation, or high sample volatility.

Laser desorption first appeared in 1963 when Honig and Woolston used a focused ruby laser to vaporize and ionize samples detected by a mass spectrograph[9]. They detected electrons, most likely emitted through thermionic emission, and singly charged positive ions for metals, semiconductors, and an insulator. In 1969, Vastola and Pirone expanded upon the abilities of laser desorption with a ruby laser and 1-hexyl sulfonate salts to show that it could be used for the vaporization of organic salts. Their mass spectra show no fragmentation, but only alkali metal ions and ions due to the attachment of an alkali cation to the desorbed molecules

[10]. Later in 1978, Posthumus showed that laser desorption could be further expanded to also work with large nonvolatile, bio-organic molecules like sucrose, and adenosine [11]. Their method used a pulsed TEA-CO_2 laser with a magnetic sector mass spectrometer. For all compounds, they were able to observe either the protonated or alkali cation attached form of the molecule. All spectra also showed a high degree of fragmentation. Later studies in the 1980's, like the one by Karas and Hillenkamp used laser desorption in the UV to desorb molecules up to 250,000 Da[12-15]. This relies on using a matrix to absorb the light which then transfers the energy to the compound causing desorption [13].

By 1986, lasers had been used for roughly 20 years for the vaporization and ionization of a variety of molecules[16, 17]. By this point enough studies had been done to show that laser desorption was a fairly soft technique resulting in little fragmentation. Lasers had been used from 193 nm to 1060 nm, but almost always pulsed and always focused. At this point, scientific interest shifted from the application of laser desorption to determining the mechanism of laser desorption[18-20]. Later work would transition to either discovering the mechanism of laser desorption or combining laser desorption with other laser ionization techniques that would greatly increase the signal intensity and available spectral information [12]

With later advances in jet cooling and the combination of laser desorption with laser spectroscopy and mass spectrometry, laser desorption became essential for the study of nonvolatile or thermally labile compounds[21].

Initial studies had primarily used laser desorption as both the desorption and ionization technique, but later papers quickly realized that the majority of desorbed molecules were neutrals not ions [22]. This ratio depends to a first approximation on the laser power due to the surface temperature induced by the laser power[21]. Thus, signal would be greatly increased by separating the desorption and ionization steps. In addition by separating the desorption and ionization events, surface and adsorbate interactions can be prevented[23]. In the late 1980's laser desorption began to be combined with supersonic jet cooling as a highly effective way to study thermally labile or nonvolatile compounds with jet cooling[24, 25] [21, 24, 26]. Initial studies by Li and Lubman and by Cable, Tubergen and Levy demonstrate the capabilities of laser desorption to be combined with jet cooling to study molecules such as tyramine, tyrosine, Trp-Gly, and Trp-Gly-Gly.

Further studies were done to determine the cooling of desorbed molecules, desorption placement vs jet entrainment, and the limit of detection. In 1988, Arrowsmith, de Vries, Hunziker, and Wendt used perylene to experimentally answer "the fraction of adsorbate entrained in the jet which will appear in the detection volume"[1]. They varied instrument parameters such as horizontal and vertical sample height in relation to the center of the molecular beam and then measured the concentration profiles of entrained perylene vapors. By measuring the fluorescence of perylene at different distances along the molecular beam path, they were able to find the optimal instrumental conditions[1]. A later study in 1990 by Meijer, de Vries, Hunziker, and Wendt uses anthracene to determine the vibrational cooling of the desorbed molecules after entrainment in the molecular beam[2].

The exact mechanism by which laser desorption happens is still highly debated. There are two key proposed mechanisms. 1) Laser desorption is the result of a nonequilibrium process where the surface-adsorbate bond is broken without the energy being well distributed enough to break internal adsorbate bonds[27-30]. 2) Laser desorption is the result of thermal equilibrium kinetics at high temperatures. In this regime, preexponential factors dominate the kinetics causing desorption to happen rapidly before decomposition occurs[31]. Many studies have been done to support both mechanisms.[30]

The first mechanism is initially suggested by Zare and Levine in 1987[27]. They state that the lowest energy bonds in the molecule are not broken during laser desorption because of the existence of a bottleneck for intramolecular vibrational energy transfers. In this method, a solid substrate absorbs the energy of the desorption laser. The adsorbate molecule can then either desorb or dissociate. The bond between the surface and adsorbate is a weak van der Waals bond which will transfer the vibrational energy in the surface well[32]. The bonds within the adsorbate are much higher in frequency and thus will not transfer the desorption energy well. In this case, the surface adsorbate bond acts as a bottleneck which restricts the flow of energy into the adsorbate molecule, causing the molecule to desorb rather than dissociate[27].

Later studies done in 1994 and 1995 by Voumard, Zenobi, and Zhan support this desorption mechanism.[29, 30] In their 1994 study, they began developing a method of measuring the internal vibrational temperature of aniline desorbed from a crystal surface. In this first attempt, they aren't able to observe enough of the spectrum to find a suitable transition[29]. Then in 1995, they successfully use REMPI to measure the vibrational/ rotational contour of

aniline to determine if thermal equilibrium was reached during the rapid laser-induced desorption process. If the internal degrees of freedom of aniline match the expected surface temperature than this would support the second mechanism but instead if the internal degrees of freedom indicate a lower temperature than the surface than the first mechanism would be supported. For the origin transition of aniline, the rotational band contour of aniline was calculated from 1 to 1000 K. From these calculations a rotational temperature around 300-400 K best match the experimental data, which is significantly lower than the calculated surface temperature of 575 K[30].

The second mechanism was originally suggested by Hall in 1987. In this mechanism, the dominance of desorption over decomposition is due to Arrhenius-type equations for thermal equilibrium kinetics at high temperatures. At the typical laser desorption heating rate of 10^{11} K s^{-1} , surface reactions do not have time to occur because they are restricted kinetically[31].

In our experimental conditions, laser desorption is preformed on a graphite bar with a thin layer of analyte on top. The desorption event happens in front of the pulse valve that will be discussed in the next section. The graphite bar is prepared by wiping the bar clean with acetone and a kim whipe, rubbing the outer surface off on an acetone soaked paper towel, using sandpaper to abrade the surface, and then rubbing a graphite sample mixture onto the abraded surface. The prepared graphite bar is then placed on a translating stage that ensures that fresh sample is available to each new laser shot. This stage also allows for adjustments to be made to the bar height in order to allow for signal optimization. The desorption laser

used is a Nd:YAG laser that is a Continuum Minilite 1 which outputs 1064 nm laser light at 10 Hz with 1 mJ per pulse.

II.2 JET COOLING

Supersonic molecular beams and their use for jet cooling in gas phase spectroscopy have allowed for high precision spectroscopy. Jet cooling couldn't be done without first the development of supersonic molecular beams. Supersonic molecular beams allow for the cooling of a molecule that allows it to stay in a highly isolated manner while still being cooled to a few Kelvin which allows for highly specific spectroscopic information to be gathered. Supersonic molecular beams are very unique in their ability to satisfy these demands. Most other techniques cannot achieve this high degree of cooling without also freezing the sample or complicating the spectrum such that vibrational and rotational detail is no longer available.

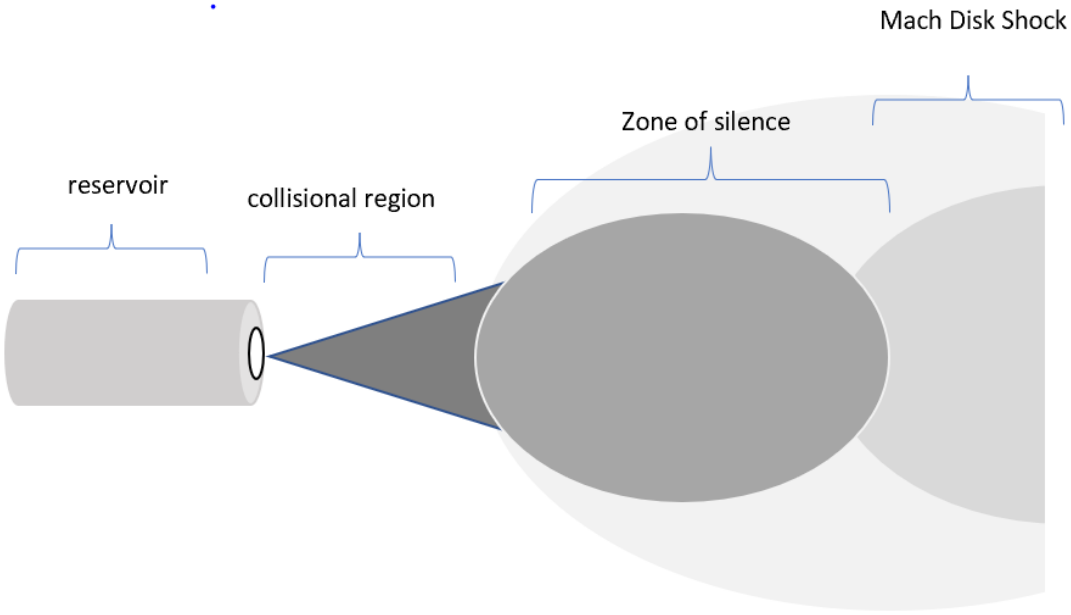

Figure 2- Illustration of the supersonic expansion of a gas

It is important to understand the nature of supersonic molecular beams so that their advantages can be best understood. A high-pressure gas leaving a reservoir into vacuum can create an effusive beam or a supersonic beam. In order for a supersonic beam to be produced, $\lambda_0 >> D$ where λ_0 is the mean free path of gas molecules in the reservoir and D is the diameter of the expansion orifice[33]. In the case of supersonic beams, the gas after entering the low pressure region undergoes an adiabatic, isentropic expansion. During which collision convert the random molecular motion into directed mass flow, also resulting in a reduction in temperature[34]. In an idealized continuum model, these collisions would continue happening with no limit to the high velocities or low temperatures possible. In reality, the frequency of

collisions decreases till eventually degrees of freedom no longer change and become the permanent state of the molecule. A real supersonic beam will reach a terminal Mach number described by Eq 1[33].

$$M_T = G\,(\sqrt{2\sigma p_0 D_\varepsilon}\ ^{(\gamma-1)/\gamma} \qquad \text{Eq. 1}$$

If a greater degree of cooling is required then the product p_0 D must be increased where p_o is the reservoir pressure.

A supersonic molecular beam can be described by different regions. Directly outside of the expansion orifice is the collisional region which is roughly ten lengths of the pulse valve orifice long. Past the collisional region is the barrel shock region where in the expansion and cooling is mostly complete. Inside the barrel shock region is the zone of silence where collisions are rare[35]. These processes are illustrated in Figure 2. It is called the zone of silence because the speed of sound is nearing zero. Also as the gas expands its pressure gets closer to that of background gas. If the background gas is high in density then a shock zone is created where the thickness is dependent on the background gas density. The first shock zone is a barrel shock zone which ends at the Mach disk which is the beginning of the second shock zone[33]. Somewhere after the Mach disk has begun is where the skimmer should be placed. The distance of the Mach disk from the orifice is calculated by Eq. 2[33].

$$\frac{x_m}{D^*} = 0.67\ \frac{P_0{}^{\frac{1}{2}}}{P_1} \qquad \text{Eq. 2}$$

A skimmer is essential to select the core portion of the supersonic beam and transfer it into the high vacuum region. Additionally, skimming allows for a pressure differential to be obtained between the chamber and the TOF tube. Good skimming requires that the normal shock is attached to the skimmer lip[36]. Many studies have focused on determining the correct size, position and shape of a skimmer. Otherwise a skimmer can disturb the generated molecular beam enough to damage the achieved cooling[37].

In our case, supersonic beams are used for the process of jet cooling. In jet cooling a small portion of sample is seeded into a molecular beam that then proceeds to cool the sample through collisions. The cooling of the sample is determined by the total number of collisions between the sample and the carrier gas[38]. Eventually as the collisional region is surpassed, collisional cooling is terminated freezing the sample in a particular rotational, translational, and vibrational state. This collisional cooling is somewhat complicated by the fact that two-body collisions will cool while three body collisions will instead lead to condensation[39]. Early research showed that temperatures of 0.5 K where possible before condensation was achieved [38]. Not only does jet cooling through collisions reduce the velocity distribution of the sample thus reducing the translational temperature but it also relaxes the molecule to the lowest energy conformers[40]. It was shown by Ruoff that higher energy conformers are relaxed only by heavier carrier gasses. While gasses like He were sufficient to produce very low translational temperature, it was unable to relax to lower energy conformers[40]. By using heavier gasses like Ar, spectra can be even further simplified by limiting the conformers of a sample to only the lowest energy forms.

Supersonic molecular beams were first proposed theoretically by Kantrowitz and Grey in 1951.[41] Previously the intensity of a molecular beam was limited by the rate of effusion through the first slit. It had been established that the slit width should be equal to the mean free path of the gas. If instead this first slit was shaped like a nozzle with a second slit then the beam intensity could be increased greatly. This nozzle converts the random translational and internal energy of the gas into mass motion. The ratio between the mass velocity and the molecular velocity is equal to the ratio of the radius of the molecular beam compared to the distance between the two slits.

This situation has the added benefit of monochromatizing the molecular velocities in the beam such that all molecules in the beam should have a uniform translational velocity. In the same year, Kistiakowsky and Slichter designed the first functional supersonic molecular beam[42]. Using the nozzle design proposed by Kantowitz and Grey, they were able to produce Mach 4 at the slit using ammonia as the gas in the molecular beam.

From 1965-1984, studies by researchers like Campargue and Fenn improved and optimized the experimental conditions of molecular beams[35, 37, 43-45]. There was a lot of difficulty in experimentally producing beams as intense as those predicted by theory[37]. In 1965, Anderson and Fenn reduced the skimmer interference to produce intense molecular beams with a velocity distribution of a molecular beam of argon with a Mach number of 23[37]. A study by Roger Campargue looked in detail at this problem of skimmer interference with the molecular beam[35, 43].

Besides for optimizing the skimmer, understanding and optimizing the influence of background gas on the molecular beam was essential. One major step in reducing the negative influence of the background gas was transitioning from a continuous supersonic beam to a pulsed beam. The pulse length could be tuned in such a way to achieve the same cooling as a continuous beam while reducing the background gas considerably. In 1983, Saenger and Fenn published a study determining the optimal pulse length for a supersonic beam[45]. One way to minimize the influence of background gas is counterintuitive by increasing the pressure to 10^{-1} to 1 torr.

In the late 70's, many studies began to show how jet cooling could be used to benefit spectroscopy. In 1977, Smalley et al. compared spectra of a room-temperature sample and jet cooled NO_2 to display the benefits of simplifying spectra so that individual vibronic bands are well separated[46]. Initially these studies were done on many smaller well studied molecules like naphthalene[47]. Comprehensive reviews by Levy in 1980 and 1981 describe in detail the benefits of jet cooling and how it can offer unprecedented levels of spectroscopic resolution[48, 49]. Normally in all but the smallest of molecules, a very large number of quantum states are populated creating very complex spectra. Extreme cooling of the molecule as in the conditions of jet cooling simplifies the number of populated quantum states thus simplifying a spectrum greatly. If cooling was done with a refrigerant, a molecule would still be subjected to many intermolecular interactions that would highly complicate a spectra. Because jet cooling relies more on kinetics than thermodynamics a gas phase sample can be produced at very low temperatures while still remaining highly isolated[48, 49].

In our experimental set up, the molecular beam is introduced by a pulsed nozzle (General Valve) with a nozzle orifice diameter of 0.5 mm and pulses 100 to 120 us in length. The molecular beam is argon with a backing pressure of 6 bar. Diffusion pumps are used to keep the background pressure at 2×10^{-6} in both the chamber and the TOF-tube. The molecular beam passes through a conical skimmer before entering the source of the TOF tube.

II.3 RESONANCE ENHANCED MULTI-PHOTON IONIZATION

There are many different ways of ionizing a molecule when the ionization and desorption step are separated. Each method has limitations and benefits with the major ionization methods being single photon, non-resonant two photon, and resonant two photon ionization. By splitting the desorption and ionization step, the ionization step can be used to gather wavelength specific information[2]. Splitting the ionization process into a two-photon process is especially beneficial.

II.3.a SINGLE PHOTON IONIZATION

The first method of ionization discussed here will be single photon ionization. Single photon ionization requires a photon of enough energy to ionize a molecule directly from its ground state. For most molecules this means that the photon must be in the VUV range (vacuum ultra-violet). Thus, if the ionization potential of a molecule is 10 ev the photon will need to be 125 nm at least. VUV light is very difficult experimentally to produce and is rarely tunable. The benefit of this technique is that it is a very soft ionization method that is capable of ionizing a molecule without fragmentation. Additionally, this technique doesn't require a

chromophore to be present. The difficulty in producing VUV light is an extremely limiting factor.

II.3.b NON-REOSNANT TWO PHOTON IONIZATION

Rather than using a single photon to go from the ground state to the ionization potential (IP), two photons can be used. This prevents the need to produce VUV photons and instead can use UV or sometimes even VIS light for the two photons. In this case one photon will usually be absorbed by a virtual state and the next photon will ionize from that virtual state. Because the intermediate state is a virtual state the laser pulse must have a very intense power. Virtual states are probabilistically unlikely but no impossible, if enough photons strike the sample probabilistically eventually some will populate the virtual state. From there the second photon will ionize from this virtual state. Raman spectroscopy is a common type of non-resonant photon ionization.

II.3.c RESONANT ENHANCED TWO-PHOTON IONIZATION

In resonant enhanced multi-photon ionization (REMPI) the first photon is tuned to be resonant with a particular vibronic transition between the ground state and an excited state. Because this first photon is resonant with a transition it requires much less laser power to excite the molecule. Using less laser power prevents fragmentation from happening during the ionization process. This resonance condition also allows for this first photon to gather information about the excited states and decay pathways of a molecule. Then the second photon ionizes out of the excited state while not high enough in energy to ionize directly from

the ground state. Thus, only the molecule of interest will be detected as signal, allowing single analytes to be selected from more complex samples. One limitation of REMPI is that only molecules with chromophores can be studied.

REMPI can be further broken down into a 1C and 2C method. In one color REMPI, the excitation and ionization photons are the same wavelength. Few molecules have a low enough IP to be able to ionized by the one color method. Two color REMPI, also referred to as R2PI, is more commonly used. In this case the energy difference between the ground state and excited state is lower than the difference between the excited state and the IP, which precludes one color from being useful. In our experimental setup, R2PI most often uses 193, 213, or 266 nm light as the ionization photon.

R2PI is also an umbrella term for a variety of scans that are all forms of R2PI but gather different spectral information. R2PI, pump-probe, double resonance, IR-UV double resonance, UV-UV double resonance scans are all subsets of R2PI. The most simple scan type is the R2PI scan where the excitation wavelength is varied to determine the available vibronic transitions. When the excitation wavelength is resonant for one of these transitions, the wavepacket is excited from the ground state to a particular vibrational band of the excited state. Once the excited state is populated, the second photon is able to ionize. Thus the presence and absence of ions can describe the possible vibronic transitions for a molecule.

The next type of scan is the pump-probe scan. In pump probe, the wavelength of the excitation photon is held constant for a particular vibronic transition. Instead of the

wavelength varying, the time between the two photons is delayed. At time zero, where the two photons are overlapped in time, the highest portion of the wavepacket will be ionized. As the time delay increases between the two photons, portions of the wavepacket have time to decay to other energy state so that the full wavepacket is no longer in the original state thus generating fewer ions. This translates to a decrease in the original signal as the intermediate excited state has time to decay. This decay of signal can be fit mathematically with a lifetime.

Double resonance is the next technique that can be used. This technique allows for the ratio of two compounds to be gathered with a high degree of accuracy. For this, a third photon is involved. One photon will excite the first sample of interest, while the second will excite the second sample of interest, then a third photon will ionize both samples. By collecting the signal for the two compounds simultaneously, the noise of shot-to-shot variations is removed from affecting the ratio of the two compounds. Most of the shot-to-shot variation comes from variations in the intensity of the desorption laser so this allows the signal of both samples to be measured from the same desorption event each time.

In IR-UV double resonance, there are three photons with an IR photon added in addition to the excitation and ionization photon. The IR photon can be used in two different modes to provide information about the tautomers present in the spectra. One mode will collect the gas phase IR spectra for the tautomer correlating to the excited state transition the excitation photon is resonant with. Because this IR is taken of a cold gas phase molecule, it is highly

specific to a particular tautomer. The other mode will quantify how many tautomers are present under the experimental conditions.

In mode 1, the gas phase IR spectrum of a specific tautomer is collected. The IR laser is scanned over a range of wavelengths to characterize the ground state vibrational levels. The other excitation and ionization photon are held constant at a resonant vibronic transition. When the IR laser is resonant with a particular ground state transition, the wavepacket is mostly excited into this higher energy vibrational level. This excited portion of the wavepacket is no longer resonant with the excitation photon and thus will no longer produce ions. A small portion of the wavepacket will still be in the lowest level of the ground state and a portion of the wavepacket will still be resonant and produce ions. Consequently, a spectra is generated where a dip in signal corresponds to an IR transition.

In mode 2, the number of tautomers in an R2PI scan is found. The IR laser is held constant at a particular IR stretch specific to a single tautomer. The IR laser will partly deplete the ground state. The excitation laser is scanned and any vibronic transition that is from the tautomer that the IR stretch is resonant for will show a decrease in signal. If another tautomer is present the signal will not be lower because the IR will not be depleting the ground state of that tautomer.

In the studies published in this dissertation, the lasers used in R2PI methods are an OPG, an OPO/OPA, an Excimer and an Nd:YAG.

An Optical Parametric Generator (OPG) produces wavelength tunable pulses in the range of 200-1200 nm. The OPG used in these experiments has a pump laser that produces 355 nm ps pulses. These pulses are then fed into the OPG, where they become tunable in wavelength (20 ps, 500-1000 uJ). The pump laser also generates residual 1064 nm and 532 nm leftover from the harmonic generation of 355 nm (20 ps, 200 uJ). This 1064 nm and 532nm light are combined to harmonically generate 266 nm and 213 nm ps light. This 266 nm and 213 light is used as the ionization light in multiple experiments. The tunable pulse is used as the excitation pulse.

For ns resolution experiments, the excitation pulse can come from an Nd:YAG laser (DCR 11 Quanta Ray) which produces 213 nm or 266 nm light (10 mJ, 10 ns). Additionally, an Excimer can also be used as the excitation pulse. In this case our Excimer is an argon fluoride laser that produces 193 nm light (2 mJ, 10 ns).

For double resonance experiments where IR is needed, an Optical Parametric Oscillator/ Optical Parametric Amplifier (LaserVision) is used to generate the IR pulses from the pump beam of 1064 nm light from an Nd:YAG (DCR 2A, 500 mJ, 10ns).

II.4 REFLECTRON TIME-OF-FLIGHT MASS SPECTROMETERY

It is hard to believe that there was such a recent time in science when the atom was not a widely accepted belief. The same discoveries that identified the proton and the electron led to the development of the earliest mass spectrometers. Before the mass spectrometer could be developed early experiments needed to be done to characterize the velocity, charge, and

mass of cathode and canal rays[50]. At this point in history the nature of cathode rays was a hot topic as people debated whether they were formed of particles or waves[51]. If it was particles, then the mass of the particle needed to be measured as proof. In 1987, Thomson discovered the charged particle that made up cathode rays- the electron[52]. This early work required measuring the e/m ratio of electrons lead to similar techniques being used in the first mass spectrometers.

The mass spectrometer was first developed in 1907 by J. J. Thomson[53, 54]. This instrument generated ions in gas discharge tubes that were passed through parallel electric and magnetic fields which deflected the ions into parabolic trajectories that were detected on a photographic plate. Mass spectrometry was so revolutionary because previously physicist believed in ether and continuum with no widely accepted theory of atoms[53]. The development of mass spectrometry also revolutionized the field of isotopes and our concept of nuclear binding. Later in 1909, J. J. Thomson with the help of his assistant Francis W. Aston characterized two neon isotopes- ^{20}Ne and ^{22}Ne. The discovery of an isotope of neon was the first isotope to be found for a stable element[50].

With the retirement of J. J. Thomson shortly after this, Francis Aston and A. J. Dempster became the two leading scientists in the field of mass spectrometry. Aston's first great contribution was the development of a new instrument, named the mass spectrograph[50]. In this improved instrument, Aston observed four lines in the mass spectrum of neon[55]. Aston went on to characterize 212 of the 287 naturally occurring isotopes[53]. In parallel, Dempster

created the first focusing magnetic mass spectrometer to separate isotopes in 1918. He went on to focus primarily on measuring isotopic abundances[56, 57].

While these early scientists developed the foundational uses and design of the mass spectrometer, this technique was not widely used. Only in the 1940's when Alfred Nier arrived on the scene did the usefulness of mass spectrometry become apparent. He made improvements to the magnetic sector mass spectrometers first made by Dempster. Nier made the first 60 sector field instrument[58, 59]. Even more important than his design of new instruments was his communication with chemists and biologists to show other disciplines besides physicists how useful mass spectrometry could be[51]. One of his projects with biologists used MS to measure isotopes of carbon and lead that could be used to help date things like the earth's crust[60]. Additionally, another great contribution of his was the discovery of 235-U, the radioactive isotope that contributed greatly to the nuclear age[61].

Our mass spectrometer consists of four key parts- the source, the flight tube, the reflectron, and the detector. The source is the region where REMPI is used to form ions and then charged plates propel the ions into the rest of the TOF tube. The source is composed of three main components- the repeller plate, the extraction grid, and the acceleration grid. Our instrument is designed to only work with positive ions, thus the repeller plate and extraction grid are negatively charged, while the acceleration grid is positively charged. After exciting the source, ions will enter the field free region of the TOF tube. During this region the ion packet will begin to separate out based on the mass to charge ratio of the ions with the lighter elements flying faster. In our experimental set up, these flight times are on the order of μs.

The following equations (Eq. 3-6) show how the flight time can be related to the mass-to-charge ratio.

$$E_k = \frac{mv^2}{2} = qV_s = zeV_s = E_{el} \quad \text{Eq. 3}$$

$$v = \sqrt{\frac{2zeV_s}{m}} \quad \text{Eq. 4}$$

$$t = \frac{L}{v} \quad \text{Eq. 5}$$

$$t = \sqrt{\frac{m}{z}}\left(\frac{L^2}{2eV_s}\right) \quad \text{Eq. 6}$$

Equation 3 shows how kinetic energy can be related to mass and velocity which can also be related to the charge and the potential that is applied to accelerate it. Equation 4 is equation 3 reorganized to solve for velocity. Equation 5 calculates the time for an ion to travel a length when moving at a particular velocity. When equation 4 is plugged in to equation 5, the travel time is related to the mass-to-charge ratio[62].

These equations assume that all of the ions have the same initial kinetic energy, but in actually that assumption is not true. These slight variations in kinetic energy result in a broadening of the distribution of the ion packet causing ions with the same mass-to-charge ratio to arrive at slightly different times. This broadening can greatly reduce the resolution of a mass spectrometer. A reflectron was developed to correct for this difference in initial kinetic energy. The reflectron was developed in 1972 by V. Karataev and in 1973 by B. Mamyrin[63, 64]. At the end of the tube, multiple electric potentials are produced that will deflect the ions back

in the direction they came from at a slight angle to then strike the micro-channel plates. Ions moving slightly faster will travel slightly further into the electric field before they are repelled away while slower ions with the same mass-to-charge ratio will penetrate the electric field less and exit the field sooner. This difference in path length will correct for that difference in initial kinetic energy.

II.5 BIBLIOGRAPHY

1. Arrowsmith, P.; de Vries, M. S.; Hunziker, H. E.; Wendt, H. R., Pulsed laser desorption near a jet orifice: Concentration profiles of entrained perylene vapor. *Applied Physics B* **1988,** *46*, 165-173.
2. Meijer, G.; de Vries, M. S.; Hunziker, H. E.; Wendt, H. R., Laser desorption jet-cooling of organic molecules. *Applied Physics B* **1990,** *51*, 395-403.
3. Nir, E.; Kleinermanns, K.; de Vries, M. S., Pairing of isolated nucleic-acid bases in the absence of the DNA backbone. *Nature* **2000,** *408* (6815), 949-951.
4. Callahan, M. P.; Crews, B.; Abo-Riziq, A.; Grace, L.; de Vries, M. S.; Gengeliczki, Z.; Holmes, T. M.; Hill, G. A., IR-UV double resonance spectroscopy of xanthine. *Physical Chemistry Chemical Physics* **2007,** *9* (32), 4587-4591.
5. Callahan, M. P.; Gengeliczki, Z.; de Vries, M. S., Resonant Two-Photon Ionization Mass Spectrometry of Jet-Cooled Phenolic Acids and Polyphenols. *Analytical Chemistry* **2008,** *80*, 2199-2203.
6. Nir, E.; Hünig, I.; Kleinermanns, K.; de Vries, M. S., Conformers of guanosines and their vibrations in the electronic ground and excited states, as revealed by double-resonance spectroscopy and ab initio calculations. *Chemphyschem* **2004,** *5* (1), 131-137.
7. Siouri, F. M.; Boldissar, S.; Berenbeim, J. A.; de Vries, M. S., Excited State Dynamics of 6-Thioguanine. *J Phys Chem A* **2017,** *121* (28), 5257-5266.
8. Nir, E.; Janzen, C.; Imhof, P.; Kleinermanns, K.; de Vries, M. S., Guanine tautomerism revealed by UV-UV and IR-UV hole burning spectroscopy. *Journal of Chemical Physics* **2001,** *115*, 4604-4611.
9. Honig, R. E.; Woolston, J. R., Laser-Induced Emission of Electrons, Ions, and Neutral Atoms from Solid Surfaces. *Applied Physics Letters* **1963,** *2* (7), 138-139.
10. Vastola, F. J.; Mumma, R. O.; Pirone, A. J., Analysis of Organic Salts by Laser Ionization. *Organic Mass Spectrometry* **1970,** *3*, 101-104.
11. Posthumus, M. A.; Kistemaker, P. G.; Meuzelaar, H. L. C.; de Brauw, M. C. T. N., Laser desorption-mass spectrometry of polar nonvolatile bio-organic molecules. *Analytical Chemistry* **1978,** *50* (7), 985-991.
12. Karas, M.; Bahr, U., Laser desorption mass spectrometry. *TrAC Trends in Analytical Chemistry* **1986,** *5* (4), 90-93.

13. Karas, M.; Bahr, U.; Ingendoh, A.; Hillenkamp, F., Laser Desorption/Ionization Mass Spectrometry of Protiens of Mass 100 000 to 250 000 Dalton. *Angewandte Chemie International Edition in English* **1989,** *28* (6), 760-761.
14. Karas, M.; Bahr, F.; Hillenkamp, F., UV laser matrix desorption/ionization mass spectrometry of proteins in the 100000 dalton range. *International Journal of Mass Spectrometry and Ion Processes* **1989,** *92*, 231-242.
15. Tabet, J.-C.; Cotter, R. J., Laser Desorption Time-of-Flight Mass Spectrometry of High Mass Molecules. *Analytical Chemistry* **1984,** *56*, 1662-1667.
16. Brand, J. L.; George, S. M., Effects of laser pulse characteristics and thermal desorption parameters on laser induced thermal desorption. *Surface Science* **1986,** *167* (2-3), 341-362.
17. Mumma, R. O.; Vastola, F. J., Analysis of Organic Salts by Laser Ionization Mass Spectrometry. Sulfonates, sulfates and thiosulfates. *Organic Mass Spectrometry* **1972,** *6*, 1373-1376.
18. Burgess, D. J.; Stair, P. C.; Weitz, E., Calculations of the surface temperature rise and desorption temperature in laser-induced thermal desorption. *Journal of Vacuum Science and Technology A* **1986,** *4*, 1362-1366.
19. van der Peyl, G. J. Q.; van der Zande, W. J.; Kistemaker, P. G., Kinetic energy distributions of ions produced in organic laser desorption. *International Journal of Mass Spectrometry and Ion Processes* **1984,** *62* (1), 51-71.
20. Zhan, Q.; Wright, S. J.; Zenobi, R., Laser Desorption Substrate Effects. *Journal of the American Society for Mass Spectrometry* **1997,** *8*, 525-531.
21. Li, L.; Lubman, D. M., Analytical Jet Spectroscopy of Tyrosine and Its Analogs Using a Pusled Laser Desorption Volatilization Method. *Applied Spectroscopy* **1988,** *42*, 418-424.
22. Sherman, M. G.; Kingsley, J. R.; Hemminger, J. C.; McIver, R. T. J., Surface analysis by laser desorption of neutral molecules with detection by fourier-transform mass spectrometry. *Analytica Chimica Acta* **1985,** *178*, 79-89.
23. Conzemius, R. J.; Capellen, J. M., A review of the application to solids of the laser ion source in mass spectrometry. *International Journal of Mass Spectrometry and Ion Physics* **1980,** *34* (3-4), 197-271.
24. Li, L.; Lubman, D. M., Pulsed laser desorption method for volatilizing thermally labile molecules for supersonic jet spectroscopy. *Review of Scientific Instruments* **1988,** *59*, 557-561.
25. Nir, E.; Grace, L.; Brauer, B.; de Vries, M. S., REMPI spectroscopy of jet-cooled guanine. *Journal of the American Chemical Society* **1999,** *121* (20), 4896-4897.
26. Cable, J. R.; Tubergen, M. J.; Levy, D. H., Laser desorption molecular beam spectroscopy: the electronic spectra of trytophan peptides in the gas phase. *Journal of the American Chemical Society* **1987,** *109* (20), 6198-6199.
27. Zare, R. N.; Levine, R. D., Mechanism for bond-selective processes in laser desorption. *Chemical Physics Letters* **1987,** *136* (6), 593-599.
28. Zenobi, R.; Hahn, J. H.; Zare, R. N., Surface Temperature measurements of dielectric materials heated by pulsed laser radiation. *Chemical Physics Letters* **1988,** *150* (6), 361-365.
29. Voumard, P.; Zenobi, R.; Zhan, Q., Laser-induced thermal desorption of aniline from a quartz surface. *Surface Science* **1994,** *307-309*, 360-366.
30. Voumard, P.; Zenobi, R.; Zhan, Q., Spectroscopic Probe for Energy Transfer during Laser Desorption from Surfaces. *Journal of Physical Chemistry* **1995,** *99*, 11722-11727.
31. Hall, R. B., Pulsed-Laser-Induced Desorption Studies of the Kinetics of Surface Reactions. *Journal of Physical Chemistry* **1987,** *91*, 1007-1015.

32. Lucchese, R. R.; Tully, J. C., Trajectory studies of vibrational energy transfer in gas-surface collisions. *Journal of Physical Chemistry* **1984,** *80*, 6313-6319.
33. Morse, M. D., Supersonic Beam Sources. In *Experimental Methods in the Physical Sciences*, Academic Press, Inc.: 1996; Vol. 29B.
34. Haventith, M., The Molecular Beam. In *Infrared Spectroscopy of Molecular Clusters*, Springer: Berlin, 2002; Vol. 176, pp 35-46.
35. Campargue, R., Progress in Overexpanded Supersonic Jets and Skimmed Molecular Beams in Free-Jet Zones of Silence. *The Journal of Physical Chemistry* **1984,** *88* (20), 4466-4474.
36. Valleau, J. P.; Deckers, J. M., Supersonic Molecular Beams II Theroy of the Formation of Supersonic Molecular Beams. *Canadian Journal of Chemistry* **1965,** *43*, 6-17.
37. Anderson, J. B.; Fenn, J., Velocity Distributions in Molecular Beams from Nozzle Sources. *Physics of Fluids* **1965,** *8* (780).
38. Even, U.; Jortner, J.; Noy, D.; Lavie, N.; Cossart-Magos, C., Cooling of large molecules below 1 K and He clusters formation. *The journal of Chemical Physics* **2000,** *112*, 8068.
39. Hillenkamp, M.; Keinan, S.; Even, U., Condensation limited cooling in supersonic expansions. *Journal of Chemical Physics* **2003,** *118* (19).
40. Ruoff, R. S.; Klots, T. D.; Emilsson, T.; Gutowsky, H. S., Relaxation of conformers and isomers in seeded supersonic jets of inert gasses. *Journal of Physical Chemistry* **1990,** *93* (5).
41. Kantrowitz, A.; Grey, J., A High Intensity Source for the Molecular Beam. Part 1. Theoretical. *Review of Scientific Instruments* **1951,** *22*, 328-332.
42. Kistiakowsky, G. B.; Slichter, W. P., A High Intensity Source for the Molecular Beam. Part 2. Experimental. *Review of Scientific Instruments* **1951,** *22*, 333-337.
43. Campargue, R., Aerodynamic Separation Effect on Gas and Isotope Mixtures Induced by Invasion of the Free Jet Shock Wave Structure. *The journal of Chemical Physics* **1970,** *52* (4).
44. Fenn, J.; Mann, M.; Meng, C.; Wong, S.; Whitehouse, C., Electrospray ionization for mass spectrometry of large biomolecules. *Science* **1989,** *246*, 64-71.
45. Saenger, K. L.; Fenn, J., On the time required to reach fully developed flow in pulsed supersonic free jets. *J. Chem. Phys.* **1983,** *79* (6043).
46. Smalley, R. E.; Wharton, L.; Levy, D. H., Molecular Optical Spectroscopy with Supersonic Beams and Jets. *Accounts of Chemical Research* **1977,** *10*.
47. Beck, S. M.; Monts, D. L.; Liverman, M. G.; Smalley, R. E., Intramolecular vibrational redistribution in electronically excited naphthalene. *The Journal of Chemical Physics* **1979,** *70*, 1062.
48. Levy, D. H., Laser Spectroscopy of Cold Gas-Phase Molecules. *Annual Review of Physical Chemistry* **1980,** *31*, 197-225.
49. Levy, D. H., The Spectroscopy of Very cold Gases. *Science* **1981,** *214* (4518), 263-269.
50. Beynon, J. H.; Morgan, R. P., The development of mass spectroscopy: an historical account. *International Journal of Mass Spectrometry and Ion Physics* **1978,** *27*, 1-30.
51. Griffiths, J., A Brief History of Mass Spectrometry. *Analytical Chemistry* **2008,** *80*, 5678-5683.
52. J., T. J., XL. Cathode Rays. *Philosophical Magazine* **1897,** *5*.
53. Munzenberg, G., Development of mass spectrometers from Thomson and Aston to present. *International Journal of Mass Spectrometry* **2013,** *349-350*

9-18.
54. Thomson, J. J., XLVII. On rays of positive electricity. *Philosophical Magazine* **1907,** *6*.
55. Aston, F. W., XLIV. The constitution of atmospheric neon. *Philosophical Magazine* **1920,** *6*.
56. Dempster, A. J., A New Method of Positive Ray Analysis. *Physics Reivew* **1918,** *11*, 316.

57. Dempster, A. J., New Methods in Mass Spectroscopy. *Proceedings of the American Philosophical Society* **1935,** *75* (8), 755-767.
58. Nier, A. O., A Mass Spectrometer for Isotope and Gas Analysis. *Review of Scientific Instruments* **1947,** *18* (6), 398.
59. Nier, A. O., A Mass Spectrometer for Routine Isotope Abundance Measurements. *Review of Scientific Instruments* **1940,** *11*, 212.
60. Nier, A. O., The Isotopic Constitution of Radiogenic Leads and the Measurement of Geological Time. II. *Physical Review* **1939,** *55*, 153.
61. Nier, A. O., The Isotopic Constitution of Uranium and the Half-Lives of the Uranium Isotopes. *Physical Review* **1939,** *55*, 150.
62. de Hoffman, E.; Stroobant, V., *Mass Spectrometry: Principles and Applications* John Wiley and Sons, LTD. : West Sussex, 2007.
63. B., M., Mass reflectron: a new nonmagnetic time-of-flight high resolution mass spectrometer. **1973,** *64* (1), 82-89.
64. V, K., New Method for Focusing Ion Bunches in Time-of-Flight Mass Spectrometery. *American Institute of Physics* **1972,** *16* (7), 1177-1179.

III THE FIRST WINDOW OF HISTORY: SELECTION OF NUCLEOBASES IN AN EARLY EARTH

III.1 AN EARLY EARTH: THE SOUP FROM WHICH LIFE EMERGED

Spectroscopy can offer up satisfying answers to a variety of questions. One questions that this dissertation applies spectroscopy to is an understanding of early earth and what conditions on an early earth led to the selection of the nucleobases in DNA and RNA. Life on an early earth would've consisted of a soup of molecules similar in structure from which the canonical nucleobases were chosen. As canonical and alternative nucleobases have also been found on meteorites, it is likely that an early earth would've also had many of these same molecules present. Many scientists have studied possible reactions that could've led to the construction of alternative and canonical nucleobases.

In 2001, Miyakawa et al. froze HCN and NH_3 at -75 C for 25 years and then analyzed the resulting mixture. They found that over that time period the HCN and NH_3 had reacted to form adenine, guanine, hypoxanthine, xanthine, 2,6-diaminopurine, uracil, 5-aminouracil, 5-dyroxyuracil, orotic acid, 5-aminoorotic acid, and 4,5-diydroxy-pyrimidine. Another very promising experiment was conducted in 1953 by Harold Urey and Stanley Miller. In this experiment, a flask filled with reduced gasses and heated circulating water was subjected to an electrical discharge. The resulting molecules were identified and found to include many canonical and alternative nucleobases. Another theory is that the soup of molecules on an

early earth were deposited there when meteorites hit the surface[65]. Studies have shown that meteorites contain adenine, guanine, hypoxanthine, xanthine, purine, and 2,6-diaminopurine[65].

With ample proof of a molecular soup present on an early earth containing many pyrimidine and purine based structures, the question becomes what selection factors chose the canonical bases from such a diverse mixture. Scientist have spent much time and effort considering the way in which life developed. What if we had fossils from the earliest time where life began to answer these questions? What if these fossils could tell us something about what factors and mechanisms lead to the development of life? To some degree these fossils exist and are capable of study. Long before what is thought of as life developed, the building blocks of life were chosen. This selection of the molecular building blocks of life was the earliest step in life being chosen. These molecules, their structure, reactivity properties, and their photochemistry is unchanged from prebiotic times. Thus, they can serve as fossils for the earliest selection processes of life.

As shown previously, these building blocks of life would've existed in a primordial soup that contained many different variations of the canonical nucleobases, such as different derivates and analogues. Today only five of these nucleobases are found in DNA and RNA. In contrast, modern research has designed functional genetic lexicons with these alternative forms that biologically function [3, 66, 67]. Thus, some other factor besides biology must have provided the selection process for the canonical nucleobases. Generally, the molecular architecture for

replication seems to require rigid structures, which tend to be aromatic and therefore inevitably prone to UV absorption. An early earth would've had no protective ozone layer and thus would've been bombarded by harmful UV radiation. Since UV excitation is unavoidable for such compounds, it is crucial to understand the possible competing pathways available to process the electronic excitation. The nucleobases that are found in DNA and RNA exhibit short excited state lifetimes, orders of magnitude shorter than their analogues. Without ultrafast excited state lifetimes, purine and pyrimidine molecules will absorb this radiation and undergo damaging reactions. The stability of DNA and life itself relies on the preservation of structure in the nucleobase building blocks. Even slight changes or deviations can have dire consequences. The safe elimination of excess electronic energy in the canonical bases is exquisitely sensitive to molecular structure and much slower relaxation is observed in many closely related structures. The stark difference in response to UV irradiation between these structures suggests the possibility of a photochemical selection of the molecular building blocks of life long before the advent of biological selection. It is thus conceivable that the molecular photo-properties of nucleobases, which we study now, are relics from part of the prebiotic chemistry that occurred 4 billion years ago.

III.2 BRIEF DESCRIPTION OF PHOTOCHEMISTRY RELEVANT TO NUCLEOBASES

DNA and RNA are formed of 5 nucleobases- guanine, adenine, cytosine, thymine, uracil. Out of these five, two are purines (guanine and adenine) and three are pyrimidines (cytosine, thymine, uracil). These five canonical bases have been studied thoroughly photochemically,

but their many derivatives have much less known about them. It is crucial that these analogues be studied in detail to see if clear patterns emerge. There are so many derivatives to study, that it is important to be smart in initially designing a subset of bases to study. If the focus is on the purine bases, then two canonical bases are available. Out of the many alternatives if substitutions at only the C_2 and C_6 position are studied this greatly narrows the available variations. To narrow it even further we choose to look only at oxo- and amino-derivatives. This leaves us with only 6 alternative forms to consider- 2-aminopurine, 2,6-diaminopurine, 2-oxopurine, 6-oxopurine, 2,6-dioxopurine, isoguanine. Each of these purine derivatives could conceivably form alternative base pairs with suitable complementary nucleobases, such as isoguanine with isocytosine, xanthine with 2,4-diaminopyrimidine, or 2,6-diaminopurine with uracil[3, 68, 69]. In addition, these alternative bases have also been found in meteorites or shown to be possible by-products of the same reactions that would've formed the canonical nucleobases[65, 70, 71].

Since UV excitation is unavoidable for such compounds as the alternative and canonical nucleobases, it is crucial to understand the possible competing pathways available to process the electronic excitation. At this point, the relaxation dynamics of the canonical nucleobases are well studied and focus has shifted to their derivatives and analogues. The goal is to determine if there is a mechanistic reason for the unique photostability of the canonical bases.

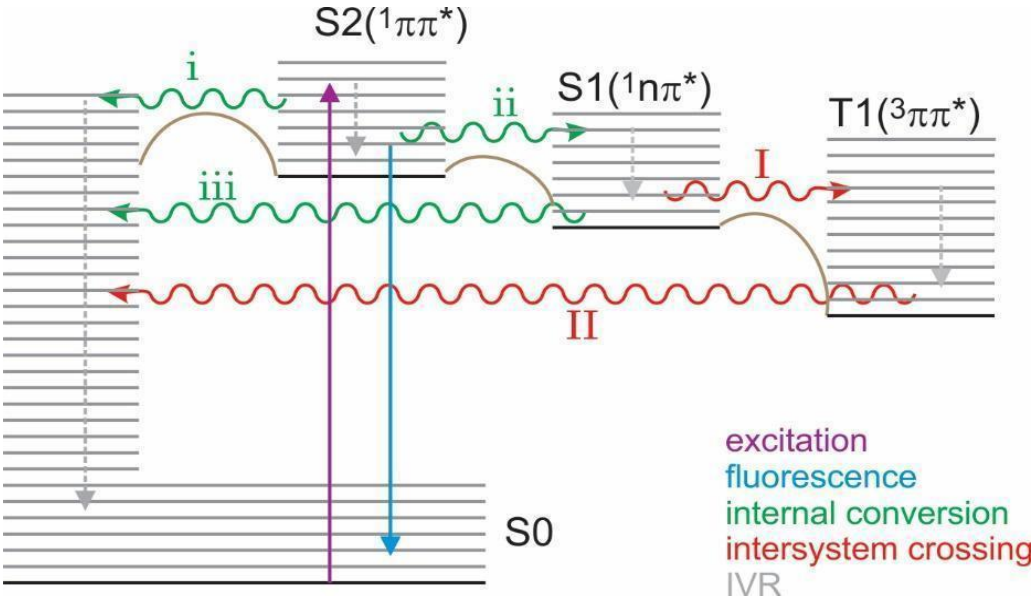

Figure 3: Schematic Jablonski diagram, indicating major competing excited state decay processes. All internal conversion processes (green) can be fast if trajectories are available to conical intersections. Lifetimes can become significantly longer if the system is trapped in a minimum below a potential barrier (barriers are indicated in brown). Intersystem crossing (red) can be fast when El Sayed allowed (I) or very slow when not El-Sayed allowed (II). If the nπ* is higher in energy then the ππ* state. (reproduced from Gate 2021)[72]

Figure 3 shows a schematic Jablonski diagram to illustrate some major competing excited state decay processes following UV absorption (purple). There are four key decay pathways available to an excited molecule- fluorescence, internal conversion, intersystem crossing, and intra-molecular vibrational redistribution. (1) Fluorescence is a radiative decay from an excited singlet state to a lower energy singlet state. This decay is usually on a ns lifetime. (2) Internal conversion (IC) is a nonradiative decay between two singlet states and can have a very fast lifetime in the ps or fs range. Many factors determine the decay lifetime of IC but

Frank Condon factors are a major consideration to determining the lifetime of the decay. Lifetimes can become significantly longer if the system is trapped in a minimum below a barrier in the potential energy surface (PES). Internal conversion most often happens through a conical intersection (CI). In a conical intersection, the potential energy surface of the two states are extremely close together allowing for a very fast relaxation. Physically for this energy transfer to happen, the molecule must undergo some sort of molecular deformation. Literature has discussed several motifs in purines with out-of-plane distortion at C_2 and sometimes at C_6 being very important to the CIs in substituted purines[73-75]. Alternatively, substitution at C_6 has also been discussed as possibly affecting barriers on trajectories toward CIs.[76, 77] (3) Intersystem crossing (ISC) is a transition between a singlet and triplet state. Depending on whether it is El Sayed allowed and the degree of spin orbit coupling. ISC can be fast, on the order of ps or very slow on the order of ns to μs. (4) Finally, the last relaxation method is intramolecular vibration redistribution (IVR). Extremely fast, IVR relaxes from higher vibrational energy levels to lower ones within the same electronic state through dissipation of heat.

For a molecule to be photostable the faster processes have to be more probable than the slow rates. Allowing for extremely fast relaxation of the excess energy prevents damaging reactions. The interplay of these processes are highly dependent on the shape of the energy levels which are more complex than Jablonsky diagrams would lead you to believe. Energy states are better represented by complex multidimensional potential energy surfaces (PES).

Not only is the relative energies of S_1, S_2, T_1, T_2 important to determining the dominant relaxation pathways, but even more so is the complex shapes found in PES including minima, barriers and conical intersections. Furthermore, the potential energy landscape is also affected by tautomeric form[78, 79] and solvent environment, further complicating relaxation pathways and photostability.[80, 81]

III.3 RELATING STRUCTURE AND STABILITY: A CATALOGUE OF RELEVANT SUBSTITUTED

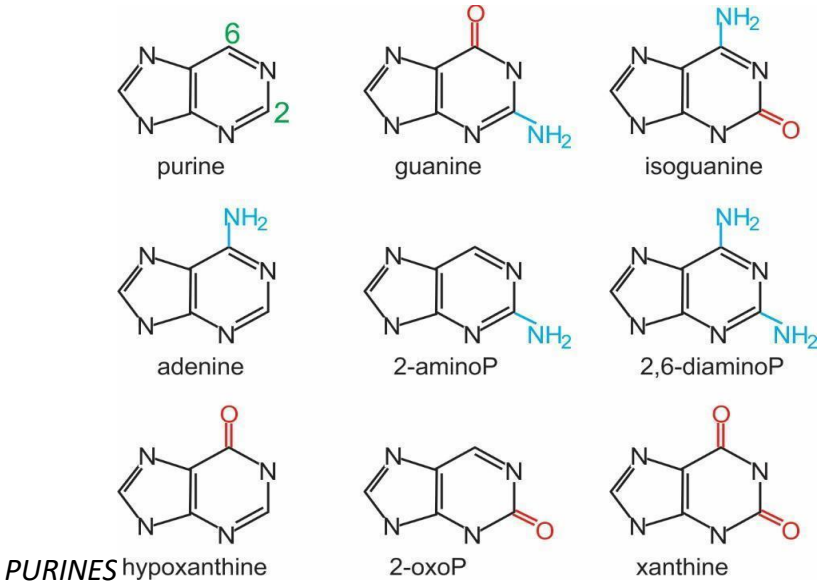

Figure 4- the 9 purine structures formed by all combinations of oxo- and amino- substitutions in the C_2 and C_6 positions. Only one tautomer is shown for each structure. (reproduced from Gate 2021)[72]

The same reactions that formed the canonical nucleobases would have produced a variety of alternative forms. Alternative genetic lexicons have used a variety of these alternative forms in biologically functioning DNA alternatives. With so many options to consider, studying thoroughly the photochemistry of alternative forms is years' worth of work. Thus, alternative

forms must be chosen carefully with extreme consideration for what structural changes are most likely to have a significant effect on lifetime and relaxation dynamics. For this reason, purines substituted at the C_2 and C_6 position were chosen as these are close in form to 2 canonical nucleobases as well as involve points that are important for CI.

The following is a report on the 9 substituted purines structures that involve an oxo- or amino-group at the C_2 or C_6 position. These are all compared in an effort to derive a relationship between structure and lifetime if possible. For most molecules, solvent, gas phase and theoretical data has been collected and will be compared in this review. Solvent phase is the best indicator of how a molecule will behave in nature, but solvation can dramatically change the excited state dynamics found intrinsically in the molecule. Gas phase is a great indicator of the decay pathways intrinsic to the molecule by studying the molecule in an isolated manner. Gas phase data can also be matched to high level computations that further elucidate the decay pathways and PES of the molecule. As some of these systems have multiple tautomers present, both in solution and in the gas phase, we will primarily focus on the biologically relevant tautomer and briefly discuss other tautomers where the data are available to highlight how tautomerization can affect the excited state dynamic

III.3.2 PURINE

The base structure of all 9 of these compounds is purine. Early papers thought that purine as the base structure was what caused some substituents to have an ultrafast lifetime[73, 76]. As

purine has a long lived excited state, it is clear that the story is more complicated. Purine has been studied in the gas phase, in solution and by theory.

In the gas phase, only two studies have been published on purine. Purine appears exclusively as the 9H tautomer.[82] Schneider et al. have reported an R2PI spectrum and determined the lowest electronic state to be of $^1n\pi^*$ character.[83] The narrow linewidths over a long range in the R2PI spectrum suggest a long-lived excited state. To the best of our knowledge, this is the only study that has been done on purine in the gas phase. Based on personal experience, purine is difficult experimentally to study in the gas phase which may contribute to the lack of gas phase studies done on it.

The first thorough solution phase study of purine wasn't until 2015 by Crespo-Hernandez. Solution phase studies, as well, are difficult due to purines low solubility and the near equal populations of the 7H and 9H tautomers. Crespo-Hernandez et al. studied purine and 9-methylpurine with transient absorption spectroscopy, coupled with quantum calculations.[76] The dynamics of 9-methylpurine are compared as that can help determine differences in the dynamics of purine's two tautomers[84, 85]. Calculations were also done to help better understand the complex PES. It was found experimentally and computationally that, absorption goes to the bright $S_2(^1\pi\pi^*)$ with internal conversion to $S_1(^1n\pi^*)$ in 100 fs [73, 86]. In 6-15 ps, vibrational cooling leads to a relaxed $^1n\pi^*$ state. From there, two pathways are possible. Either internal conversion to the ground state or $S_1(^1n\pi^*)/T_2(^3\pi\pi^*)$ intersystem crossing. The triplet yield is expected to be near unity leading to the very long observed

lifetime in purine. This predominance of the triplet state is supported by other solution phase experiments.[87]The authors argue that amino- or oxo- substitution at C_6 prevents $^1n\pi^*$ access, promoting $^1\pi\pi^*/S_0$ internal conversion via a C_2 distortion conical intersection instead.[76]

III.3.b 2-AMINOPURINE

The first alternative nucleobases to be discussed here is 2-aminopurine(2-AP), an isomer of adenine with the amino group at the C_2 instead of the C_6 position. 2-aminopurine has been used as a fluorescent tag in DNA, substituted in position of adenine[88]. 2-aminopurine has also been of great interest because its dynamics are drastically different in the gas phase and solution though the structurally similar adenine does not see such drastic changes between states. In gas phase, 2AP is fairly fast but in solution the lifetime is much longer and is highly fluorescent.

This effect is mainly observed in the 9H tautomer which is the lowest energy and biologically relevant form.[89] Significant contributions to the understanding of the excited state dynamics of 2AP come from studies by Leutwyler and coworkers.[78, 90, 91] The dynamics of 2-AP is complicated by the fact that the S_1 and S_2 states with $^1n\pi^*$ and $^1\pi\pi^*$ character lie so close in energy theorist and experimentalist cannot agree on the order of the states[78, 80, 81, 88, 89, 91-98]. They do agree that the addition of solvent changes the energy difference between the states thus changing the dynamics[78, 80, 81, 88, 89, 91-98]. They were the first to observe 7H-2AP in the molecular beam, ~1600 cm^{-1} to the red and 1000x weaker than 9H-2AP.[78] Additionally, they measured lifetimes of 156 ps and < 5 μs at the origin of isolated 2AP.[80, 90] The fast decay is attributed to internal conversion most likely from S_2 ($^1\pi\pi^*$)/S_1($^1n\pi^*$) allowed via vibrational

coupling then passing through a conical intersection S1($^1n\pi^*$)/GS with ~5 kcal/mol. The ultraslow decay was attributed to $S_1(^1n\pi^*)/T_1(^3\pi\pi^*)$ intersystem crossing. By studying clusters with water they found that microhydration by up to two water molecules increased the faster lifetime 4-100 fold, up to 14.5 ns, depending on the site of hydration. They correlated this lifetime increase with a greater $^1n\pi^* - {}^1\pi\pi^*$ energy gap which led to less vibronic coupling.

In summary, the dynamics of 2-aminopurine are complicated by the extremely close energy of the $^1n\pi^*$ state and the $^1\pi\pi^*$ state. In the gas phase, after absorption into the $^1\pi\pi^*$ state there are 3 pathways. 1) From S_2 an IC to the $S_1(n\pi^*)$ then CI to the GS with a 5 kcal/mol giving a lifetime of 150 ps. 2) Also S_1 ($n\pi^*$) ISC to $T_2(\pi\pi^*)$ with decay in 2 μs. 3) the final pathway is a slight fluorescence with a low QY of 0.006. In solution, the ordering of the $n\pi^*$ state and the $\pi\pi^*$ state flip so that lifetime greatly increases to 11.6 ns or >5 μs with a great increase in the fluorescence QY.

III.3.c 6-AMINOPURINE (ADENINE)

Only two of the substituted purines in this report are canonical nucleobases. The first one to mention is adenine, a mono- substituted purine with an amino- group in the C_6 position. Many studies have been published looking at the solution phase, gas phase and theoretical data of adenine.

The earliest study of adenine in the gas phase was done by Kim et al. in 2000. The first early papers struggled to determine which state is lowest in energy, though this paper accurately

proposed the character of the states as $S_1(n\pi^*)$ and $S_2(\pi\pi^*)$ with the S_2 state being bright and the S_1 state contributing very weak bands. Later papers struggled to confirm this but eventually agreed that this was the most reasonable explanation[89, 99-104]. This first study to consider tautomeric states of adenine was a study by Luhrs et al. that compared the R2PI spectra of adenine and 9-methyladenine. Since 9-methyladenine can only exists in the 9H tautomer instead of the close lying N_7, N_1 and N_3 tautomers possible in adenine, this can help determine if only the 9H biologically relevant tautomer of adenine is found in the gas phase. The R2PI spectra of 9-methyladenine and adenine are identical, clarifying that the gas phase spectra of adenine is in fact dominated by the 9H form. The gas phase data can be summarized as absorption is into the $S_2(\pi\pi^*)$ state, which decays via IC to the $S_1(n\pi^*)$ state and then via another IC to the GS. Decay to the ground state happens in 1ps, though there is also evidence for a decay to a triplet state[100, 101].

While the gas phase data only includes the 9H tautomer, in aqueous solution, adenine exhists in both the 9H and 7H tautomer. The 9H tautomer is the biologically relevant one and decays in 0.2 ps[79, 105-107] , while the 7H tautomer has a longer lifetime of 8 ps.[107] Experimentally, it is unclear whether in solution adenine decays using the $^1n\pi^*$ state. Some studies point to its contribution,[79, 107] while others do not.[108, 109]

III.3.d 2,6-DIAMINOPURINE

2,6-diaminopurine (2,6-dAP) is the structural combination of 2-aminopurine and adenine, but exhibits drastically different photochemistry than both.

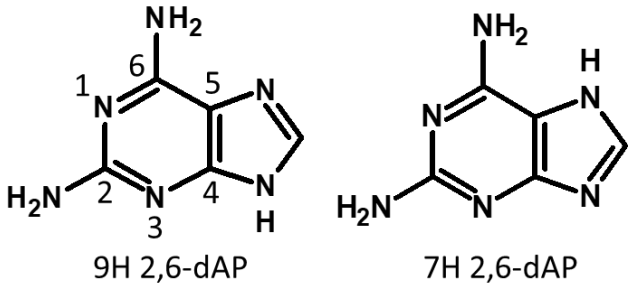

Figure 5- Shows the molecular structure of 2,6-dAP in its 9H and 7H tautomeric form.

Previously, our group studied the 9H and 7H tautomer of 2,6-dAP with ns resolution in the first gas phase study. In the previous work[110], we found 6.3 and 8.7 ns lifetimes for the isolated 9H and 7H tautomers at their respective origins. The following data that is in preparation for publication builds off of these findings by contributing higher order computations and ps resolution spectroscopy. We investigated the dynamics of isolated 2,6-dAP in the picosecond regime and found an additional fast decay pathway with barriers for each tautomer. We discuss the potential mechanisms that could explain observed lifetimes based on accurate quantum chemical calculations. By comparing our experimental and theoretical results with data acquired for adenine and 2AP previously, we attempt to reconcile the excited state dynamics with properties of the molecular structure.

Our results begin with an initial R2PI scan of 2,6-dAP done in ps resolution to identify resonant vibronic transitions. Previously, the R2PI spectrum observed two distinct regions of signal, offset by ~2500 cm^{-1} , with one region having only three transitions. With ps resolution instead of ns, it was revealed that there were other higher energy transitions above those three. Though, the previous work by Gengelickzi et al. already characterized the tautomers

present in the molecular beam, we used mode 1 IR-UV double resonance to identify the 7H and 9H tautomer with the help of theory, and also used mode 2 to show that the tautomers had no overlapping spectral ranges[74]. Confirming the previous findings, the R2PI spectrum of the 7H tautomer of 2,6-dAP ranges from 32216 cm^{-1} to 33616 cm^{-1} (Fig. 6). The origin transition (0-0 transition) is at 32216 cm^{-1}, which matches well with the origin found by Gengeliczki et al (32215 cm^{-1}).[110] This R2PI spectra is the same whether the ionization laser is ns 193 nm or ps 213nm, indicating that the 7H tautomer has no transitions without a ns or greater process. Five major transitions characterize the R2PI spectra with 3 lifetime regimes.

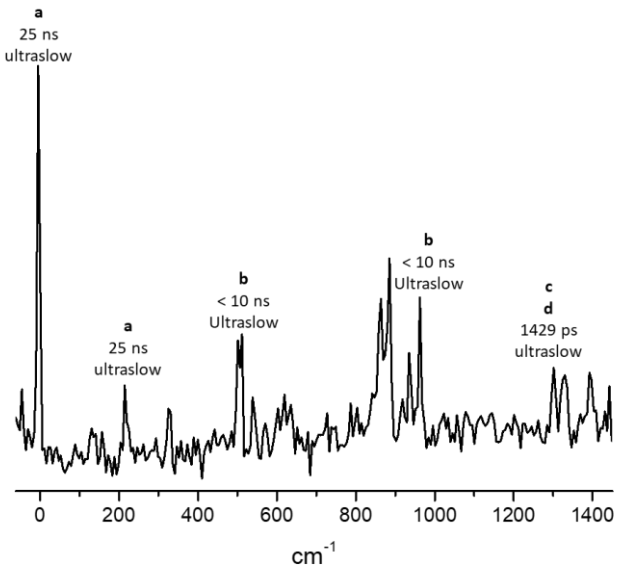

Figure 7. 2C-R2PI spectrum using the nanosecond laser pulse at 193 nm as the probe. Lifetimes are displayed above each peak. All lifetimes were taken from pump probes using the ns 193 nm probe. The only exception is the 1429 ps lifetime, which used the ps 213 nm probe. Lifetimes were measured at the origin, 32216 cm-1, and then +214, +511, +984, and +1307 cm^{-1}, relative to the origin.

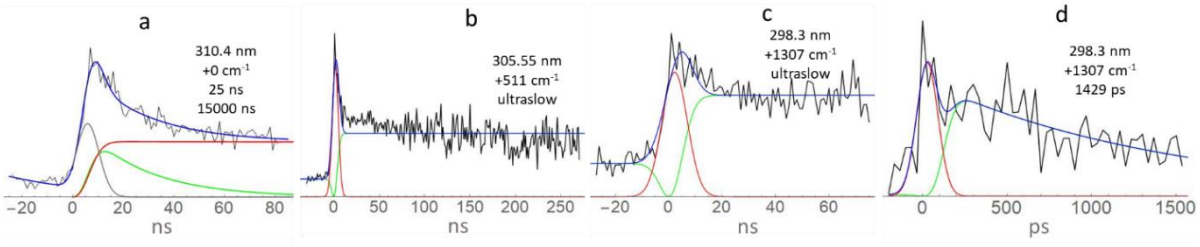

Figure 8. Sample pump probe spectra of 2,6-dAP (7H). (a-c) were pumped with ps pulses and probed with ns 193 nm pulses. (d) was pumped with a ps pulse and probed with ps 213 nm. The origin and +214 cm^{-1} (a) were fit with two exponentials while +511 and +984 cm^{-1} (b) were fit with a monoexponential. +1307 cm^{-1} (c,d) was fit with monoexponentials in the ns and ps regime. Note the change in x-axis units.

Pump probe measurements were done to determine the lifetimes of the transitions. Transitions with the same letter label will look almost identical in lifetime. The pump-probe of a, b, c and d transitions are shown in Figure 8. Pump probe for the *a* transitions (origin and the +214 cm^{-1}) were fit with a biexponential with 25 ns and slow time constants. Note that the origin decay, measured here differs from the one measured by Gengeliczki et al.[110], where the authors derived a single 8.7 ns lifetime. We attribute this difference to differences in the ionization wavelength with 193 nm being used contrary to the 266 nm used in the original work. In fact, the 266 nm probe used previously likely recorded only higher energy vibrational components of the electronic excitation responsible for this shorter photorelaxation channel. This suggests that the probe pulses at 193 nm allowed us to observe a more detailed and accurate picture of the nanosecond photorelaxation channel of 7H 2,6-dAP. Furthermore, it allowed us to observe a slow excited-state decay component that was not observed before likely corresponding to a lower in energy and much longer-lived triplet excited state. Past these two transitions there is no longer a long lived decay component.

The transition b corresponds to the +511 and +984 cm^{-1} higher energy peaks, using the ns 193 nm pump-probe (Fig. 8b). Two different decay components were observed but fit with a monoexponential decay function because the short component matched well with the IRF. We estimate our IRF with the 193 nm probe pulse to be ~10 ns. We could not perform pump probe measurements of the faster decays using the ps probe pulses at 213 nm, due to low signal to noise ratio. Therefore, we estimate the shorter decay to fall within the range between 1 and 10 ns. Fitting of the monoexponential decay function allowed us to identify the same slow photorelaxation channel as in the case of the *a* transitions.

We also performed pump-probe measurements for the peak at +1307 cm^{-1} (denoted with letter c in Fig. 7) from the origin transition using both ns 193 nm (Fig. 8c) and ps 213 nm (Fig. 8d) probe pulses. The nanosecond component was fit with a monoexponential function just as in the case of the *b* peaks and returned a slow lifetime. The ps probe pulse at 213 nm also allowed us to estimate the shorter-lived component with a lifetime of 1429 ps (Fig. 8d).

In summary, we observed two decay components for all 2C-R2PI peaks for the 7H tautomer of 2,6-dAP with a slow component for all peaks. In addition, we recorded a faster component with the time constants equal to 25 ns for the *a* transitions, increased to 1-10 ns for the *b* transitions, and increased to 1.5 ns at the *c* transitions. This change in lifetime is indicative of barrier present in the PES.

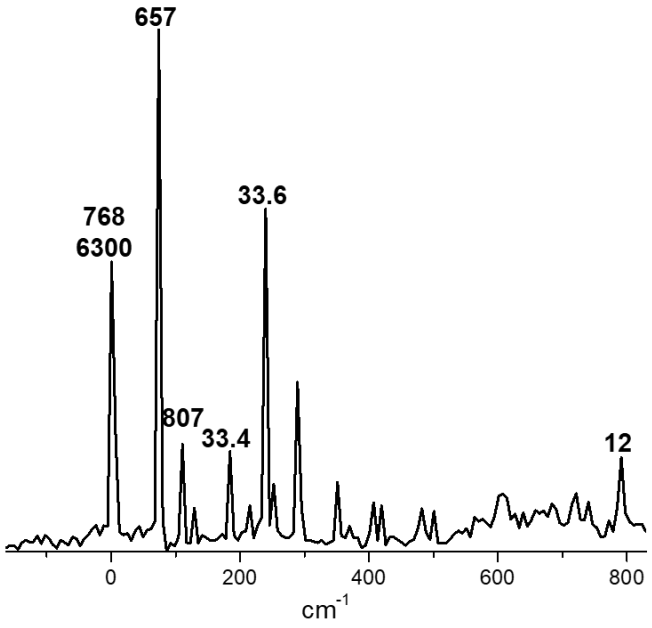

Figure 9. 2C-R2PI spectrum of 9H 2,6-diaminopurine in the gas phase using the ps 213 nm as probe. The origin transition is assigned to 34885 cm^{-1}. Lifetimes for each peak displayed above the corresponding peak, in ps.

The 9H tautomer of 2,6-dAP is the biologically relevant tautomer and corresponds to the absorptions peaks from 34800 to 35650 cm^{-1} . We assign the band at 34885 cm^{-1} to the origin transition of the 9H tautomer in agreement with previous work by Gengliczki et al.[110] Therefore, this origin transition is higher in energy by ~ 2500 cm^{-1} when compared to the origin transition of the 7H tautomer. The lowest-energy vibronic modes for this tautomer are the most intense and the narrowest, indicating a long lifetime. The increase of broadness as well as the lose of intensity at around ~500 cm^{-1} excess energy suggests a corresponding decrease of the excited state lifetime. The lifetime in the picosecond regime quickly decreases by an order of magnitude with an excess of 180 cm^{-1}, and then by another order of magnitude

with an excess 700 cm^{-1}, relative to the origin transition. The pump probe traces for the origin and the observed higher energy peak are shown as example traces in Fig 10.

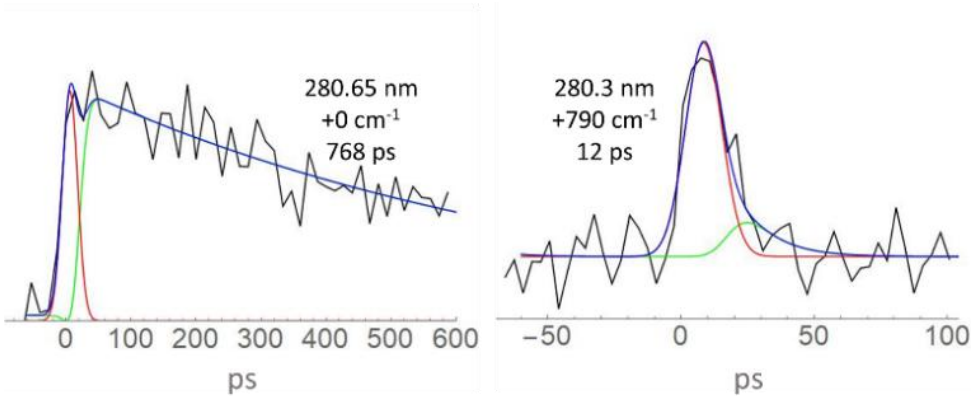

Figure 10. Pump probe traces using ps 213 nm as probe for 2,6-dAP (9H). The left trace was taken at the origin (34885 cm-1) while the right trace was taken at 35675 cm-1.

As we move progressively to higher energies above the origin transition in the R2PI spectrum for 9H 2,6-dAP, the lifetime becomes progressively shorter. Starting at the origin, the first few peaks have lifetimes on the order of 750 ps, in addition to the ns component found in the past study. As excess energy is added (180 cm^{-1}), the 750 ps decreases to 30 ps and the long component is no longer present. With additional excess energy (+790 cm^{-1}), the lifetime further decreases to the same order as the IRF(1-10 ps).

Theoretical calculations were done by Rafal Szabla and colleagues to better understand the PES for both tautomers of 2,6-dAP.

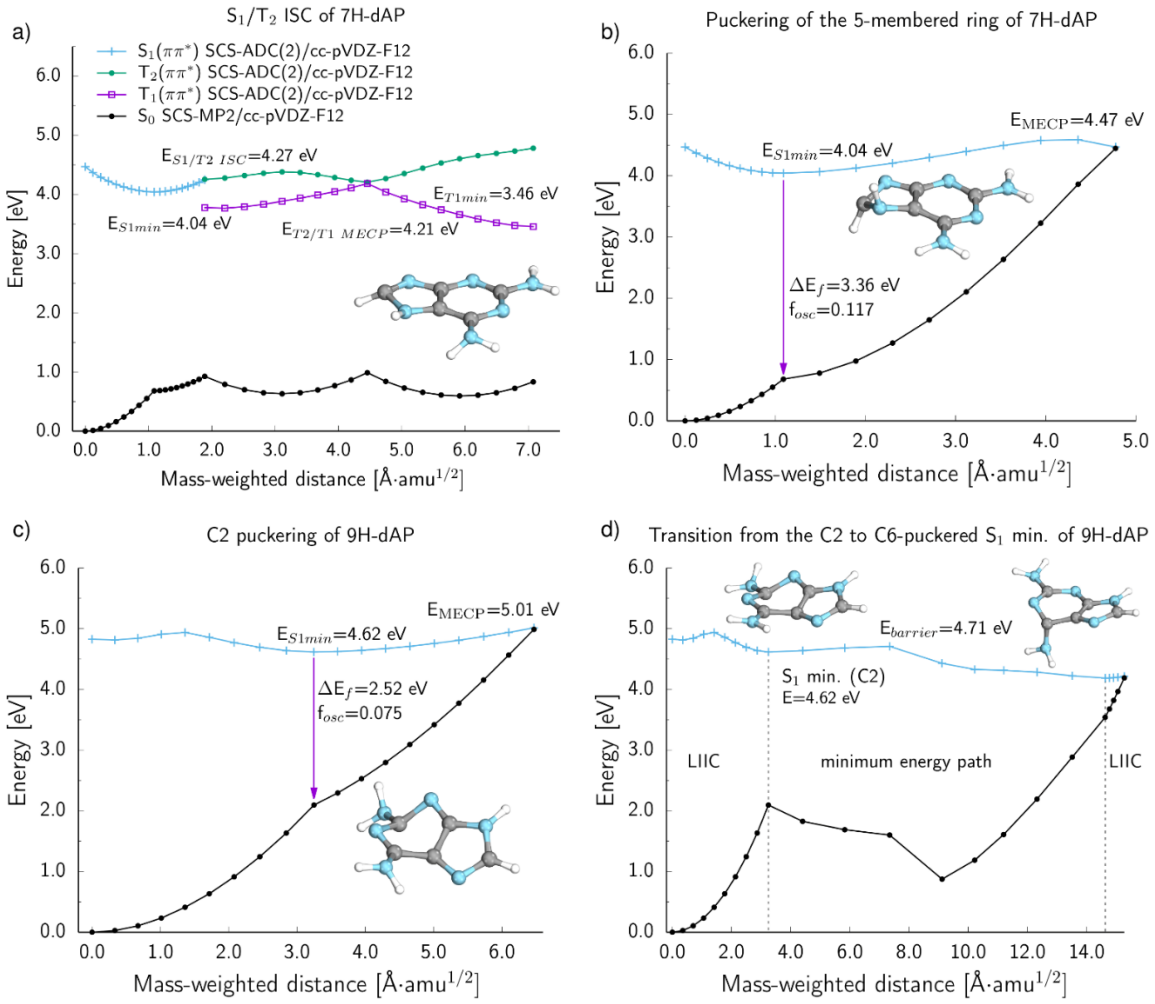

Figure 11. Potential energy profiles for the photorelaxation pathways of the 7H (a and b) and 9H (c and d) tautomers of 2,6-dAP calculated with the excited-state energies calculated at the SCS-ADC(2)/cc-pVDZ-F12 level of theory.

As presented in Fig. 11, both tautomers of 2,6-dAP undergo visible structural changes after the population of the S_1 state, with aromatic ring-puckering mechanisms being the most apparent structural changes than can be observed for both S_1 minima. The S_1 minimum-energy geometry of the 7H tautomer has a strongly puckered 5-membered subunit of the aromatic purine ring, which is the result of C_8=N_7 bond twisting. Population of this minimum

may be followed either by intersystem crossing to the triplet manifold or by direct internal conversion to the electronic ground state via the $S_1(\pi\pi^*)/S_0$ conical intersection (see Fig. 11 a and b). Direct photorelaxation via the $S_1(\pi\pi^*)/S_0$ conical intersection involves stronger puckering of the 5-membered heteroaromatic subunit and is associated with an energy barrier of over 0.4 eV. The presence of this energy barrier is consistent with the experimentally determined lifetime of 25 ns at the origin and with the decrease in lifetime at excess energy above 1300 cm^{-1}. Thus, it is likely that the 25 ns component is descriptive of a nonradiative internal conversion.

Owing to the relatively long timescale of direct internal conversion through the $S_1(\pi\pi^*)/S_0$ conical intersection, UV-excited 7H 2,6-dAP may also undergo intersystem crossing to the triplet manifold of electronic states. Notably, the energy difference between the S_1/T_2 state crossing that the $S_1(\pi\pi^*)$ minimum amounts to merely 0.23 eV and is only slowed down by very low value of spin-orbit coupling (SOC) between these two electronic states, that is 2.34 cm^{-1}. Therefore, in spite of very low degree SOC between the S_1 and T_2 states, the intersystem crossing still enables non-negligible population of triplet states. This allows us to clearly assign the ultralong microsecond time constant to the population of the T_1 state.

In contrast to the 7H tautomer, the photodeactivation of 9H 2,6-dAP from its lowest energy singlet excited state is governed by puckering of the 6-membered subunit of the aromatic purine ring. In particular, the $S_1(\pi\pi^*)$ minimum of 9H 2,6-dAP is characterized by pyramidalization of the C_2 atom. The extent of this pyramidalization and aromatic ring

puckering is increased when the molecule approaches the $S_1(\pi\pi^*)/S_0$ conical intersection (see Fig. 11 c). This state crossing lies nearly 0.4 eV higher in energy than the corresponding $S_1(\pi\pi^*)$ minimum and explains the long photodeactivation time constant, which amounts to 6.3 ns. We emphasize that owing to relatively high oscillator strength of the S_1-S_0 transition from the $S_1(\pi\pi^*)$ minimum, this time constant could indeed be associated with fluorescence when the 9H tautomer is excited at the absorption origin. Alternatively, UV-excited 9H 2,6-dAP could undergo a change in the puckering mode associated with substantial rotation C6-NH_2 amino group out of the plane of the aromatic purine ring and reach another ring-puckered $S_1(\pi\pi^*)/S_0$ conical intersection (see Fig. 11 d). While this latter process is associated with an energy barrier of merely 0.1 eV, it also requires significant structural reorganization of 2,6-dAP, which likely occurs on a picosecond timescale (or longer) and is consistent with the fitting of a picosecond excited-state decay component for the 9H tautomer.

In summary, the experimental and calculations agree on the decay dynamics of 7H and 9H 2,6-dAP. we propose two distinct relaxation mechanisms for the 2,6-dAP (7H) tautomer. The initially bright $^1\pi\pi^*$ of the 7H tautomer can decay directly to the ground state via puckering of the 5-membered subunit or fluorescence, on the order of 25 ns at the origin. Alternatively, 7H 2,6-dAP can undergo intersystem crossing (ISC) to $T_2(^3\pi\pi^*)$. Due to the apparent wavelength-independence in populating the triplet state, both in terms of lifetime and amplitude relative to the faster decay, we assume it must be able to compete with the faster decay. Therefore, it is decaying into this long-lived state just as competitively as the fast decay

is occurring. The relative yields do not appear to be qualitatively changing, based on the relative amplitudes of the short peak and the long tail (Fig. 8).

In comparison, the relaxation model for 2,6-dAP (9H) begins with excitation at the origin leading to population of a bright $^1\pi\pi^*$. A barrier on the order of 400 cm^{-1} prevents the system from undergoing ultrafast nonradiative decay through a $^1\pi\pi^*/S_0$ CI. Therefore, some amount of the wavepacket will relax via fluorescence at the S_1 minimum while the remainder eventually finds its way to a nonradiative decay channel by puckering at the C_6-NH_2 group (Fig. 11d). With increased excitation energy, no amount of fluorescence is observed, outcompeted by the more efficient nonradiative decay.

III.3.e 2-OXOPURINE

Having discussed all amino- substituted purines, now the oxo- substituted purines will be discussed beginning with the alternative nucleobase- 2-oxopurine. 2-oxopurine has been very rarely studied and only observed once experimentally. The first and only experimental observation was in solution in 1954 with a spectra characterized by two transitions at 321 nm and 239 nm[111]. To our knowledge the only two other studies done on 2-oxopurine are two theoretical studies. The first of which in 2008 by Mburu and Mitsika explained that both of these transitions are of ππ* character with two dark nπ* states in between[73]. A 2019 theoretical study by Martinez-Fernandez built off of these findings to characterize the PES as well as the expected photodynamics[77]. They confirmed that the excitation would most likely be into the S1(ππ*) state, as this is the brightest state, whose min lies 3.4 eV above the GS

min. To reach the CI between the S_1/S_0 there is a 0.6 eV barrier from the S_1 min. This CI is characterized by further stretching of the C_2–O and N_3–C_4 bonds, puckering of the C_6 atom and tilting of the H atom at C_6. Calculation of spin orbit coupling shows that the S_1 min also intersects with two triplet states of ππ* character[77].

In conclusion, 2-oxopurine is expected to be very similar to purine with a high triplet yield from ISC out of the bright S_1(ππ*). If studied in the gas phase, we would expect to find a long lifetime due to the ISC and probably a shorter lifetime from the S_1/S_0 CI, but likely not ultrafast due to the slight barrier to reach the CI. Overall, all papers agree that the dynamics of 2-oxopurine is characterized by absorption into the S_1(ππ*) state, with the higher ππ* and nπ* states playing no role. Two triplet states are close in energy to the S_1(ππ*) min with T_2 only a 0.03-0.7 eV energy gap and a high SOC that should allow for considerable intersystem crossing.

III.3.f 6-OXOPURINE

6-oxopurine is better known as hypoxanthine. Hypoxanthine has captivated science due to its function as a rare RNA base in transfer RNA and its extremely short excited state lifetime[112]. The only time hypoxanthine has been studied in the gas phase was done in 1980 by Lin using photoelectron spectroscopy to identify the electron states of hypoxanthine as S_1 (ππ*) and S_2(nπ*)[113].

There were three solution phase experiments all done in 2012, highlighting the decay mechanisms undergone by hypoxanthine and its similar forms of inosine and inosine

monophosphate[112, 114, 115]. In solution, hypoxanthine exists in two keto tautomers- the 7H (0.25 kcal/mol lower in energy) and the 9H. Hypoxanthine and inosine are characterized by absorption into the $S_1(\pi\pi^*)$ state yielding an absorbance at 250 nm that is a superposition of both tautomers in the case of hypoxanthine[112, 114, 115]. Additionally, there is a higher energy band at 200 nm due to three higher energy $n\pi^*$ states[116, 117]. The overlap of the two tautomers made it difficult to determine how similar the ES dynamics of the two tautomers are though the similarity of hypoxanthine dynamics to inosine lead them to believe that the two tautomers are very similar in dynamics. From the experimental data they were able to craft a rough potential energy scheme that yields lifetimes for three processes- a 130 fs decay for the time the wavepacket spends in the FC region, 0.21 ps for the S_1/S_0 CI, and 1.8ps to fully relax the GS[112, 114, 115].

Later theory calculations by Guo supported the lifetime assignment of 130 fs, as well as elucidated on the decay mechanisms responsible for this fast ES lifetime. They found that each tautomer had two different CIs both due to an out-of-plane distortion of the C_2 atom. Both CIs reported were lower in energy than the FC region with no barriers in between. Dynamic simulations show that decay from S_1 to S_0 takes 85.5 in the 7H tautomer and 137.7 fs in the 9H tautomer. The 9H lifetime of 137.7 fs closely matches the 130 fs observed by Chen et al[115]. A study in 2014 by Guo analyzed computationally the photodynamics of hypoxanthine in solution. They found that both tautomers have slight differences in hydrogen bonding that change their photochemistry slightly[116-119]. Stronger hydrogen bonding interactions with 9H place the structure in a less accessible CI geometry which slows the 85.5

fs observed in gas phase to 200-350 fs. Whereas for the 7H tautomer, the hydrogen bonding is much weaker and the lifetime is made slightly faster to 112.6 fs from 137.7 fs previously in gas phase.

Overall, hypoxanthine is incredibly photostable. Hypoxanthine undergoes absorption into the bright $S_1(\pi\pi^*)$ which the quickly passes through an ultrafast barrierless S_1/S_0 CI. Experimental results show that the two tautomers of hypoxanthine present in solution have almost identical dynamics though theory shows that the 7H tautomer should be slightly faster due to the 9H tautomer having stronger hydrogen bonding that leads to a slightly slower conical intersection.

III.3.g 2,6 - DIOXOPURINE

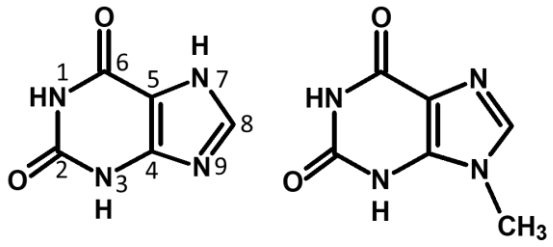

Figure 12. The 7H tautomer of xanthine (left) and 9-methylxanthine (right) with number scheme.

2,6-dioxopurine, better known as xanthine, is the combination of 2-oxopurine and hypoxanthine. Xanthine is found in the human body, as a degradation product of both guanine and adenine[120, 121]. With its flexible hydrogen bonding and base pairing possibilities, it has also been proposed in an early all-purine system of genetic information.[122] The results discussed

below are form a publication in preparation. The intention of the study was to determine the ES dynamics of both the 7H and 9H tautomer of xanthine, but unfortunately, we could not observe xanthine (9H) in our molecular beam, so we used 9-methylxanthine instead. Methylation instead of a hydrogen at N_9 has been shown to have small influence on the excited state dynamics of purines.[119, 123-125]

Xanthine has yet to be studied in the gas phase or the solution phase as it is difficult to dissolve. Theoretically, Domcke et al. wrote an extensive paper on the excited state dynamics of xanthine (7H) and (9H) in the gas phase.[126] They found CIs for both tautomers for both $\pi\pi^*/S_0$ and $n\pi^*/S_0$. The 7H tautomer had an $\pi\pi^*/S_0$ relaxation channel with a small barrier, while the 9H tautomer had a barrier of ~1 eV. Thus, they concluded the 7H tautomer to be photostable while the 9H should not be. Interestingly, the CI coordinates were reached via distortion of the 5-membered ring, similar to what was discussed with 2,6-dAP. The authors excluded crossing of the $n\pi^*/S_0$ CI as it was too high in energy. But the $n\pi^*$ state was isoenergetic or slightly below the $\pi\pi^*$, depending on the method used. Therefore, vibronic coupling between the bright $\pi\pi^*$ and dark $n\pi^*$ states is possible.

In the first gas phase study of xanthine, IR-UV mode I and II is used to determine number of tautomers present as well as collect the gas phase spectra of each tautomer. The gas phase spectra can be matched to theory to identify each tautomer. In addition, R2PI was used to identify and assign lifetimes to each absorption stretch for both xanthine (7H) and 9-methylxanthine (9H).

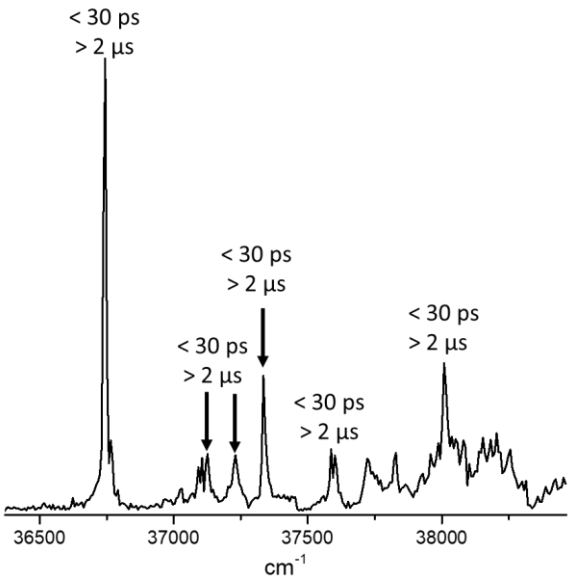

Figure 13. R2PI spectrum of xanthine (7H). The origin is at 36751 cm^{-1}. Lifetimes derived from pump probe traces using ps 213 nm as probe are on top. Lifetimes derived from pump probe traces using ns 193 nm as probe are on bottom. Pump energies were set to the origin 37133, 37230, 37334, 37586 cm^{-1}.

The R2PI spectrum of xanthine (7H) is presented in Fig. 13. It was taken using ns 193 nm as the probe. The R2PI spectrum using ps 213 nm has similar peaks and amplitudes. The origin was found at 36751 cm^{-1}, in good agreement with Callahan et al.[127] The origin peak is by the far largest amplitude peak. The spectrum is sharp for about 700 cm^{-1}, and then broadens out for the next 800 cm^{-1}, at which point it breaks off and no signal is observed. The lifetimes derived from pump probes are displayed above each peak. Lifetimes in the ps regime were derived from pump probes using ps 213 nm as the probe and displayed as the top value. We successfully probed every peak using ps 213 nm and found that all transitions showed similar decays. We attempted to pump probe using ps 266 nm as well, but unfortunately, due to

signal-to-noise issues, we could only successfully pump probe the peaks at 36751 and 37334 cm^{-1} using ps 266 nm.

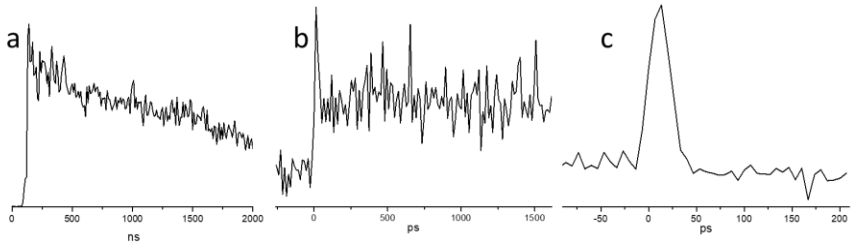

Figure 14. Pump probe of the xanthine (7H). All traces pumped at the origin (36751 cm^{-1}) and probed with ns 193 nm (a), ps 213 nm (b), and ps 266 nm (c). Note the changes in the x-axes. Pump probe traces with ps 213 nm as probe (b) and taken with the pump at the origin, 37133, 37230, 37334, 37586, and 38008 cm^{-1} all looked similar

The ns decays were unable to be fit with an exact lifetime as they were too long lived. Additionally, the traces do not decay exponentially, but linearly, which indicates that the packet of initially excited molecules leave the area of the probe beam. Conversely, the shorter lifetime decays were under the IRF of our system and cannot be characterized accurately either.

Pump probe was attempted using both ps 213 nm and ps 266 nm as probes, a difference of 1.21 eV. Using the lower energy ps 266 nm, the decay traced the instrument response function (IRF), as seen in figure 2(c), which we estimate to be ~30 ps. The trace then returned to baseline. Therefore, the dynamics the ps 266 nm probes is no more than 30 ps, most likely shorter. From our experience, we cannot probe dynamics faster than ~1 ps. 1 ps is therefore the lower bound of what the lifetime could be. Alternatively, probing with the higher energy ps 213 nm shows an IRF trace followed by an elevated baseline for the remainder of the

measurement. In these ps 213 nm decay traces, we attribute the IRF trace to the same dynamics observed with ps 266 nm and the elevated baseline to the decay channel we observe with ns 193 nm. Because the 213 nm has an IRF trace at each peak, we assume the < 30 ps decay mechanism to be present at every peak.

With this in mind, ps 266 nm is ionizing only the highest excited states. The nature of this state(s) will be discussed later. Quickly, xanthine undergoes intramolecular vibrational redistribution (IVR) and possibly internal conversion (IC), lowering its electronic energy, disallowing ps 266 nm to probe from these lower-energy states. This relaxation occurs < 30 ps. Ps 213 nm is high enough in energy to probe both these higher- and lower-energy states. The higher-energy, faster states are shown by the IRF trace. The lower-energy, slower relaxation is shown by the elevated baseline. Alternatively, while ns 193 nm is used as the ionization laser, we cannot observe these faster states due to its much slower time resolution, but can only probe the lower-energy, slower decay. And this slower decay is slow, shown by its lifetime being > 2 μs. Note these dynamics do not noticeably change over the 1300 cm^{-1} we observed, though the signal amplitude did change.

The R2PI spectrum of 9-methylxanthine is presented in Fig. 15. We had to focus the pump and probe beams to get signal on 9-methylxanthine. The spectrum shown was taken using ps 213 nm as probe. Unlike the R2PI spectrum of xanthine (7H), this spectrum has no clear origin or vibronic modes. It is defined by a broad onset of signal. The signal levels off going further to the blue, but no definitive peaks are ever observed. This spectrum is similar to the spectra

of both thymine and uracil.[128, 129] Though not entirely clear, this slow rise in signal may be due to poor Frank-Condon factors at the origin with better overlap to the blue. The spectrum is real, as opposed to an artifact, because we were able to pump probe at all energies. The red arrows indicate where pump probes were taken. We chose those energies to pump probe because they provided sufficient signal without imparting too much excess energy.

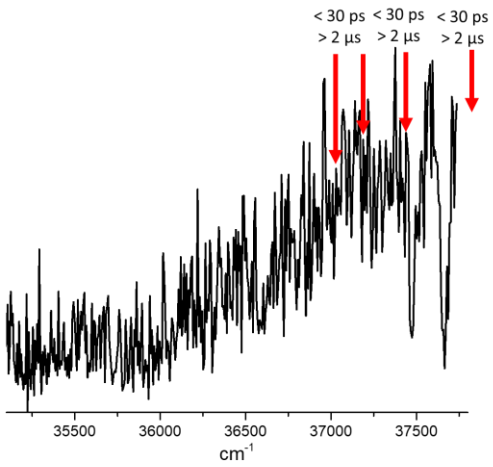

Figure 15. R2PI spectrum of 9-methylxanthine using ps 213 nm as probe. Red arrows indicate where pump probe traces were taken. Pump energies were set to 37037 cm^{-1}, 37174 cm^{-1}, 37453 cm^{-1}, and 37878 cm^{-1}. The dips around 37500 cm^{-1} are laser power artifacts.

Pump probes for 9-methylxanthine were taken using ps 213 nm with a step size of ~30 ps (Fig. 15). Decay traces taken at all pump energies looked similar, showing an IRF followed by elevated background. When taken with a step size of 6.6 ps, the traces again match to IRF with an elevated baseline following. Unfortunately, we could not pump probe using ns 193 nm because we had to focus to get signal. We could not overlap the pump laser with the probe laser well enough to get consistent signal when trying to probe with ns 193 nm.

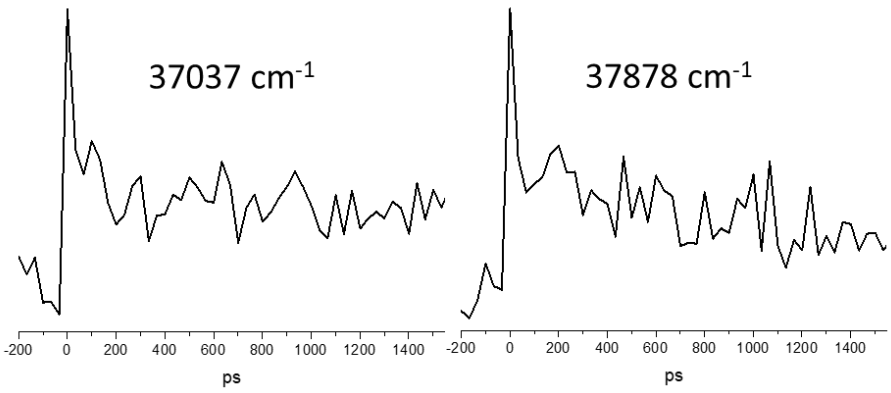

Figure 16. Pump probes of 9-methylxanthine taken in the ps regime using ps 213 nm as probe.

The relaxation dynamics of 9-methylxanthine are similar to xanthine (7H). A < 30 ps decay component is observed followed by a long-lived component. These dynamics do not noticeably change over the 800 cm^{-1} that we observed.

Domcke et al.[126] confirmed using theoretical calculations that only the 7H tautomer of xanthine should be observed in the gas phase. This was based on the fact that the 7H tautomer is the lowest energy tautomer. Further, the Frank-Condon factors for the origin transition of the 7H tautomer are much greater compared to the 9H tautomer. In fact, they say xanthine (9H) should not be observed in the gas phase due to its poor Frank-Condon factors. The poor Frank-Condon factors of xanthine (9H) can potentially explain the R2PI spectrum of 9-methylxanthine, as such a slow rise in signal has been attributed to poor Frank-Condon factors.[128, 129] Potentially, the methylation at the N9 position increases the oscillator strength just enough for it to be observed in the gas phase.

The previous studies on xanthine do not support what we observe in the gas-phase. First, gaseous xanthine (7H) and 9-methylxanthine both have two decay components, one < 30

ps and another slow component. They may have faster components that are beyond the detection limits of our technique. Specifically, the xanthines have been noted for < 1 ps decays in solution, which is supported by theory. This is probably faster than we can observe using R2PI, as stated above. Only Rottger and coworkers noted a small relatively long-lived component of 36 ps when studying XMP in solution.[130] They explained this longer decay to either trapping in the ππ* or transfer of part of the population to a dark nπ*. The IRF traces we do see are most likely attributed to 1-30 ps lifetimes. Therefore, either the ultrafast solution phase dynamics have slowed down in the gas phase or we are observing slower components that could not be seen in solution.

Solvation typically stabilizes ππ* and destablizes nπ* states. So the nearby nπ* state that Domcke describes for isolated xanthine (7H) may not matter in the solution phase because it is too high compared to the ππ*. Therefore, in solution-phase, xanthine may just undergo ultrafast nonradiative decay from ππ* to S_0 as Domcke described for isolated xanthine (7H). But in the gas-phase, the ππ* and nπ* may be close enough for significant vibronic coupling. After excitation, 7H and 9-methylxanthine may internally convert to nπ* and get trapped for a while until it can undergo internal conversion to the ground state. This agrees with Domcke who observed a barrier to nπ*/S_0 CI. This would explain the faster decay we observe which is still on the order of tens of ps and not ultrafast. But once in the nπ*, the system can also do ISC to a very long-lived triplet state. This ISC assignment is based on the long-lived state we observe. No other researchers have talked about a triplet state for xanthines.

In summary, we have found the lowest vibronic transitions of xanthine (7H) and 9-methylxantine. The R2PI spectrum of 9-methylxanthine is noted for its slow, broad onset of signal, most likely due to poor Frank-Condon overlap. Both systems have two decay channels that appear unchanged over the range of at least 800 cm^{-1}. The faster channel has a lifetime < 30 ps and is attributed to prompt $\pi\pi^*$ population transfer to $n\pi^*$, and then internal conversion to the ground state. The slower channel was measured to be > 2 μs for xanthine (7H) and at least tens of ns for 9-methylxanthine, as we were unable to conduct ns pump probe on it. ISC to a long-lived triplet state is assigned to this slower channel.

III.3.h ISOGUANINE

The last alternative nucleobases to discuss is isoguanine with an oxo- group at the C_2 and an amino- at the C_6. Isoguanine gained interest after Rich in 1962 suggested isoguanine and isocytosine could form a highly stable WC base pair as a noncanonical base pair that could biologically be incorporated into DNA[131]. Scientist now believe that the canonical nucleobases are partially chosen because of their stability as in so far that they bond to only one other substituent and exists in only one tautomeric form, later studies show that isoguanine defies both of these standards. Studies have shown that isoguanine exists in multiple different tautomers in DNA[132, 133] and can bond to G,[134] C[132, 135, 136], T[132], and isoC[131] and with C is known to form either parallel strand orientation[135] or tetraplexes[136]. Because of the many important tautomers of isoguanine, two of the most influential early studies by Seela et al. in 1995[137] and Sepiol et al. in 1973[138] focused on assigning the predominant tautomeric forms and agreed upon N_1-H being the dominant form. A study by Eschenmoser

in 1993 also found support for a N_3H tautomer of isoguanine through evidence of an isoG-G base pair where the N_3H tautomer works best.[134] A later study by Blas et al. in 2004 confirms the findings of the previous studies through calculations that identify nine tautomers out of 23 that are the most relevant[132]. These nine forms are a mix of amino-enol, imino-oxo and imino-enol forms.

The first gas phase study of isoguanine was done by Gate et al. in 2019. In this study the gas phase tautomers of isoguanine are assigned and the relaxation dynamics are studied[69]. Their calculations agreed with earlier studies that the enol-N_9H form would be the most stable in the gas phase with the keto-$N_{3,9}$, keto-$N_{1,9}$ keto-$N_{3,7}$, enol-N_7, and keto-$N_{1,7}$ higher in energy as ordered by roughly 8 kcal/mol. They used IR-UV double resonance to identify the tautomers they observed in the gas phase and attributed the signal to the keto- $N_{3,7}$ and enol-N_7 form, meaning that the lowest energy tautomers were not seen in this experimental set up. The keto form was found to have a lifetime at all transitions around 950 ps while the enol form had a much shorter lifetime. Calculations were also done on biologically relevant keto-N_9 and the lowest energy tautomer enol-N_9. Both forms absorb into an $S_1(\pi\pi^*)$ state. The keto state has an S_1 min with $n\pi^*$ character and S_1/S_0 CI 0.98 eV above the min. This barrier explains the longer lifetime observed in the pump-probe experiment. For the enol N_7H form, computations show that there are two S_1/S_0 conical intersections. One is 0.33 eV above the min while the other is 0.4 eV and requires a change in MO character. Consequently, the enol form is expected to have a fast excited state lifetime which explains why only a small amount

of signal was observed and why the pump-probes were unsuccessful. Calculations were also done on the enol-N_9H form, the biologically relevant form that wasn't seen in this experiment and showed that there was no barrier between the S_1 min and the S_1/S_0 CI through puckering of the pyrimidine ring which explains the ultrafast lifetime estimated as 312 fs. [69]

Isoguanine is unique in its many observed tautomeric forms. While many studies have been done to determine the relevant tautomers in gas and solvent phase measurements, few studies have determined the lifetimes and excited state decay mechanisms. For the three tautomers measured in the gas phase, all three are characterized by an absorbance into the S1($\pi\pi^*$) state. The energy barrier between the $S_1(\pi\pi^*)$ min and the S_1/S_0 CI determines the lifetime of the tautomer. The keto-$N_{3,7}$ has the longest measured lifetime of 950 ps roughy at the origin, the enol-N_7H has a faster lifetime, and the enol-N9H, biologically relevant form, is computed to have a lifetime of 312 fs. To determine the lifetime of isoguanine further studies will have to be done in other environments to determine the photostability of different tautomers.

III.3.i GUANINE

Lastly, guanine with an oxo- group at the C_6 position and an amino- at the C_2 position will be discussed. A high resolution gas phase spectrum of guanine was first reported by Nir et al. in 1999,[25] followed by the vibronic spectrum of guanosine.[139] IR-UV double resonance experiments, coupled with calculated structure stabilities were used to assign tautomers in the gas phase. The assignment of the four tautomers was initially wrongly assigned to the

lowest energy tautomers: keto-9H, keto-7H, enol-9H, and enol-7H[8, 140, 141] but it was later confirmed that tautomers 3-7 kcal/mol higher in energy are the ones actually observed in R2PI experiments, namely the enol-9H, enol-7H, and two imino-keto 7H forms.[142-144] The keto-9H, keto-7H, enol-9H (trans), and enol-9H(cis) were observed in helium nanodroplets and IR laser spectroscopy, thus also present in the gas phase.[145, 146] Since R2PI is a form of action spectroscopy, these results suggest that the failure to observe the lowest energy tautomers in R2PI experiments is not indicative of their absence in the molecular beam but of failure to ionize them due to excited state lifetimes that are significantly shorter than the 6 ns laser pulse widths employed in the R2PI experiments. Femtosecond gas phase experiments found < 1 ps lifetimes, but these did not have tautomer selection.[100, 147] The other tautomers have lifetimes on the order of tens of nanoseconds.[7, 141]

Theoretical calculations explain that biological guanine (keto-9H) is not observed in molecular beam experiments due to poor Frank-Condon factors.[144] It is also predicted to have ultrafast decay due to a barrierless $S_1(^1\pi\pi^*)$/ S_0 CI from puckering at C_2. Another barrierless conical intersection opens up via hydrogen-abstraction from a $^1\pi\sigma^*$ state due to stabilization of guanine's large static dipole moment.[144, 148-150] The $^1n\pi^*$ state is negligibly involved in the excited state dynamics due to its high energy. Thiel and co-workers conducted a nonadiabatic dynamics study in simulated aqueous solution and found these dynamics to be faster than *in vacuo.*[151] This difference is due to a smaller energy gap between $^1L_a(\pi\pi^*)$ and $^1L_b(\pi\pi^*)$ and a new conical intersection by out-of-plane motion of the carbonyl group.

Guanine has been scantly studied in solution due to its poor solubility. Instead, solution phase studies have focused on guanosine, GMP, and dGMP. The biologically relevant amino-keto tautomer is found in aqueous solution for guanosine and GMP.[152] Like adenine, these systems have been noted for two low-energy bright states, the $^1L_a(\pi\pi^*)$ and $^1L_b(\pi\pi^*)$. For guanine, the state ordering is reversed though, with $^1L_a(\pi\pi^*)$ lower in energy than $^1L_b(\pi\pi^*)$. The fluorescence spectrum of GMP is much broader and red-shifted relative to other nucleotides with a tail out to 700 nm.[153, 154] This red tail is due to the relatively flat $^1L_a(\pi\pi^*)$ PES leading to the S_1/S_0 conical intersection. Excitation of the higher energy $^1L_b(\pi\pi^*)$ leads to < 100 fs internal conversion to $^1L_a(\pi\pi^*)$.[153-158] The $^1L_a(\pi\pi^*)$ then decays along a barrierless, though flat, PES to the S_1/S_0 conical intersection, leading to a < 1 ps lifetime,

III.4 THE EFFECT ON LIFETIME OF C2 AND C6 SUBSTITUTION IN PURINES

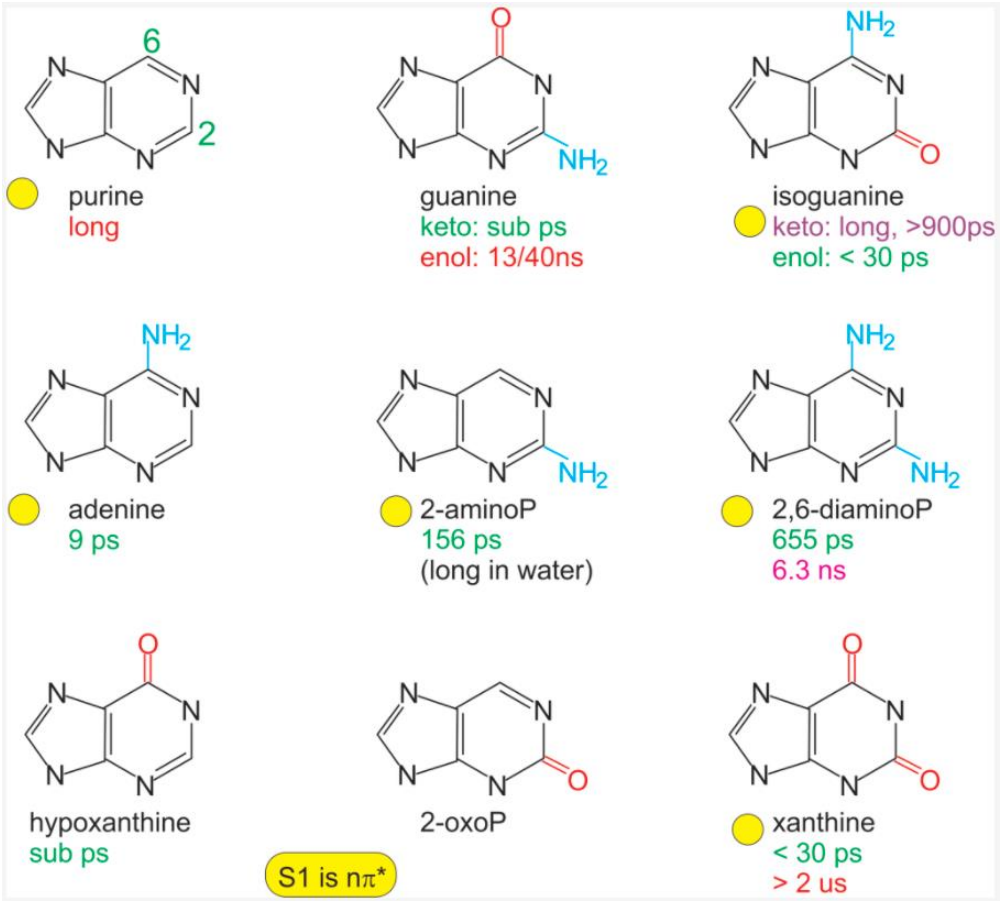

***Figure* 16: Excited state lifetimes as measured at the origin of lowest ππ* transition.**

Photostability follows from the ability to return to the electronic ground state at time scales short enough to outcompete all other possible processes. This scenario requires a potential energy landscape that allows barrierless trajectories to efficient conical intersections. The dependence on structure comes about because even minor changes in the PES can affect the positions and levels of minima, CIs, barriers, or ordering of states which can have large effects on the excited state dynamics. The structure dependence is subtle and even tautomers of the same compound can have excited state lifetimes that differ by orders of magnitude. As a

result, it is hard to formulate general trends. A number of models have been proposed to generalize the structural effects and each of those describe important elements. However, the complete description still appears to require the inclusion of additional details.

While comparing the effects of different C_2 and C_6 substitutions, it should be noted that the excited state lifetimes are not a single number but are, rather, a function of absorption wavelength. The focus is on absorption close to the origin, because the excited state dynamics at threshold energies are the most sensitive measure of the topography of the PE landscapes. Moreover, at high excitation energy, above all barriers, deactivation rates tend to increase and thus may not be an accurate reflection of photostability. For the molecule to rapidly and safely diffuse electronic excitation, no significant part of the spectrum should be trapped in the excited state, including the part absorbed near threshold. In some of the non-canonical bases, such as xanthine and 2AP, ultrafast dynamics occur, but at the same time there is a significant quantum yield for ISC as well, thus threatening the long-term stability upon radiation.

(i) The first motif is the order of ππ* and nπ* states which the substituents modify from purine through stabilization/destabilization effects of the added groups.[73] Generally, the ππ* state is the bright state. If the nπ* is lower in energy in the FC region or its minimum is below that of the ππ* state, then there may be conical intersections between the two that allow the nπ* to be populated and to serve as a doorway state or a dark state.[159, 160] This is the reported arrangement in all cases, except guanine, hypoxanthine, 2-oxopurine and enol isoguanine.

However, while an accessible nπ* state creates a more complex PE landscape, it does not suffice to characterize excited state dynamics. Even when the nπ* state is not accessible, there may or may not be a barrierless path to the ground state, as in keto *vs.* enol guanine. Conversely, when the ^{1}nπ* state can be reached, it may subsequently lead to the ground state, as in adenine, or lead to for example intersystem crossing to a ^{3}ππ* state as in purine and 2-oxopurine, and possibly xanthine, 2,6-diaminopurine, 2-aminopurine.

(ii) A major motif, in many cases, is C_2 puckering in the CI geometry.[77, 161] It has been argued that this geometry is responsible for the short lifetime of two structures without a C_2 substituent, adenine and hypoxanthine. The most often cited example is the lifetime difference between adenine and 2-aminopurine. For 2-aminopurine, it has been argued that the out of-plane rotation of the C_2-amino group takes longer than the C_2-H bond rotation in adenine, resulting in the longer observed lifetime. However, this trend does not hold for purine which has no C_2 substituent but still has a long lifetime. It is also contradicted by the fact that keto-G and enol-isoG with an amino- and oxo- substituent in C_2, respectively, have fast excited state lifetimes.

(iii) Puckering at C_6 can also define conical intersection geometries to a lesser extent.[94] For example, it provides an additional deactivation channel, which becomes significant only at higher excitation energies.[162] C_6 substitution has also been proposed to play a role in modifying the barrier in the ππ* state. The effect is illustrated with the observation that

adenine and hypoxanthine decay fast relative to purine. However, the observations that 2,6-dAP is slower than 2AP and enol-G and keto-isoG are slow complicate this explanation.

(iv)When considering the fate of photoexcited nucleobases the possibility of intersystem crossing is of particular concern. Only rapid return to the ground state, either directly or through a doorway state, effectively transforms electronic excitation to heat but some nonradiative transitions lead to a longer-lived dark state. Purine, 2,6-dAP, and xanthine all have significant ISC with the major pathway involving a $^1n\pi^*/^3\pi\pi^*$ CI, which is El-Sayed allowed. Large spin-orbit coupling, as in the case of 2-oxopurine and 2-aminopurine can also contribute to this strength of this ISC pathway.

It should also be noted that a longer stay in an excited state may not always need to lead to photochemical damage. An example is the formation of excitons in stacked bases, which return to the ground state by charge recombination at a time scale of 100 ps.[163]

One might speculate that the oxo- and amino- substitutions did not only provide the purine and pyrimidine skeletons with the necessary hydrogen bonding structures – for which many combinations were possible – but at the same time also with UV hardiness – for which only a subset was preferred. To understand which structures could provide the fastest deactivation dynamics back to the ground state requires careful computations to map out all potential energy surfaces in comparison with detailed experimental data. In putting these observations and trends together, we observe that the dynamics is governed by distortions of the 6 ring

and the resulting potentials do depend on the structure around the ring. But structural trends combine in very nuanced ways; the effects of individual substitutions don't simply add up and the end result cannot be intuitively predicted.

While from all the data, described here, an extensive picture emerges of the entire landscape of 2, 6 oxo-/amino- substituted purines, a few pieces of the puzzle are still missing. Notably, no gas phase data are yet available for 2-oxopurine, hypoxanthine, and keto guanine. For the latter two, presumably the sub-picosecond excited state lifetime is too short for REMPI detection. Alternative approaches, such as population of the hot ground state following internal conversion may provide additional data.

This field has been progressing, and continues to do so, thanks to parallel developments in experiments and in theory, allowing the study of molecules of increasing size in the gas phase and with ever higher levels of computational theory. Finally, in addition to the prebiotic importance of photostability of the molecular building blocks of life, complete understanding of the structure dependence of photostability might one day help in the design of compounds with desired photochemical properties.

III.5 BIBLIOGRAPHY

3. Nir, E.; Kleinermanns, K.; de Vries, M. S., Pairing of isolated nucleic-acid bases in the absence of the DNA backbone. *Nature* **2000,** *408* (6815), 949-951.

7. Siouri, F. M.; Boldissar, S.; Berenbeim, J. A.; de Vries, M. S., Excited State Dynamics of 6-Thioguanine. *J Phys Chem A* **2017,** *121* (28), 5257-5266.

8. Nir, E.; Janzen, C.; Imhof, P.; Kleinermanns, K.; de Vries, M. S., Guanine tautomerism revealed by UV-UV and IR-UV hole burning spectroscopy. *Journal of Chemical Physics* **2001,** *115*, 4604-4611.

25. Nir, E.; Grace, L.; Brauer, B.; de Vries, M. S., REMPI spectroscopy of jet-cooled guanine. *Journal of the American Chemical Society* **1999,** *121* (20), 4896-4897.
65. Callahan, M. P.; Smith, K. E.; Cleaves, H. J.; Ruzicka, J.; Stern, J. C.; Glavin, D. P.; House, C. H.; Dworkin, J. P., Carbonaceous meteorites contain a wide range of extraterrestrial nucleobases. *Proceedings of the National Academy of Sciences of the United States of America* **2011,** *108* (34), 13995-13998.
66. Abo-Riziq, A.; Grace, L.; Nir, E.; Kabelac, M.; Hobza, P.; de Vries, M. S., Photochemical selectivity in guanine-cytosine base-pair structures. *Proceedings of the National Academy of Sciences of the United States of America* **2005,** *102* (1), 20-23.
67. Weinkauf, R.; Schermann, J. P.; de Vries, M. S.; Kleinermanns, K., Molecular physics of building blocks of life under isolated or defined conditions. *Eur Phys J D* **2002,** *20* (3), 309-316.
68. Boldissar, S.; de Vries, M. S., How nature covers its bases. *Phys Chem Chem Phys* **2018,** *20*, 9701-9716.
69. Gate, G.; Szabla, R.; Haggmark, M. R.; Sponer, J.; Sobolewski, A. L.; de Vries, M. S., Photodynamics of alternative DNA base isoguanine. *Physical Chemistry Chemical Physics* **2019,** *21* (25), 13474-13485.
70. Miyakawa, S.; Cleaves, H. J.; Miller, S. L., The cold origin of life: B. Implications based on pyrimidines and purines produced from frozen ammonium cyanide solutions. *Origins of Life and Evolution of the Biosphere* **2002,** *32* (3), 209-218.
71. Miyakawa, S.; Yamanashi, H.; Kobayashi, K.; Cleaves, H. J.; Miller, S. L., Prebiotic synthesis from CO atmospheres: Implications for the origins of life. *Proceedings of the National Academy of Sciences of the United States of America* **2002,** *99* (23), 14628-14631.
72. Gate, G.; Williams, A.; Haggmark, M. R.; Svadlenak, N.; Hill, G. A.; de Vries, M. S., Nucleobases as Molecular Fossils of Prebiotic Photochemistry: Excited-state Dynamics of C2 and C6 Substituted Purines. In *Prebiotic Photochemistry: From Urey-Miller-like Experiments to Recent Findings*, Saija, F.; Cassone, G., Eds. RSC: 2021.
73. Mburu, E.; Matsika, S., An Ab Initio Study of Substituent Effects on the Excited States of Purine Derivatives. *Journal of Physical Chemistry A* **2008,** *112* (48), 12485-12491.
74. Gengeliczki, Z.; Callahan, M. P.; Svadlenak, N.; Pongor, C. I.; Sztaray, B.; Meerts, L.; Nachtigallova, D.; Hobza, P.; Barbatti, M.; Lischka, H.; de Vries, M. S., Effect of substituents on the excited-state dynamics of the modified DNA bases 2,4-diaminopyrimidine and 2,6-diaminopurine. *Physical Chemistry Chemical Physics* **2010,** *12* (20), 5375-5388.
75. Nachtigallova, D.; Barbatti, M.; Szymczak, J. J.; Hobza, P.; Lischka, H., The photodynamics of 2,4-diaminopyrimidine in comparison with 4-aminopyrimidine: The effect of amino-substitution. *Chemical Physics Letters* **2010,** *497* (1-3), 129-134.
76. Crespo-Hernandez, C. E.; Martinez-Fernandez, L.; Rauer, C.; Reichardt, C.; Mai, S.; Pollum, M.; Marquetand, P.; Gonzalez, L.; Corral, I., Electronic and structural elements that regulate the excited-state dynamics in purine nucleobase derivatives. *J Am Chem Soc* **2015,** *137* (13), 4368-81.
77. Martinez-Fernandez, L.; Arslancan, S.; Ivashchenko, D.; Crespo-Hernandez, C. E.; Corral, I., Tracking the origin of photostability in purine nucleobases: the photophysics of 2-oxopurine. *Phys Chem Chem Phys* **2019,** *21*, 13467-13473.
78. Lobsiger, S.; Sinha, R. K.; Trachsel, M.; Leutwyler, S., Low-lying excited states and nonradiative processes of the adenine analogues 7H-and 9H-2-aminopurine. *Journal of Chemical Physics* **2011,** *134* (11).

79. Cohen, B.; Hare, P. M.; Kohler, B., Ultrafast excited-state dynamics of adenine and monomethylated adenines in solution: Implications for the nonradiative decay mechanism. *Journal of the American Chemical Society* **2003,** *125* (44), 13594-13601.
80. Lobsiger, S.; Blaser, S.; Sinha, R. K.; Frey, H. M.; Leutwyler, S., Switching on the fluorescence of 2-aminopurine by site-selective microhydration. *Nat Chem* **2014,** *6* (11), 989-993.
81. Reichardt, C.; Wen, C. W.; Vogt, R. A.; Crespo-Hernandez, C. E., Role of intersystem crossing in the fluorescence quenching of 2-aminopurine 2 '-deoxyriboside in solution (vol 12, pg 1341, 2013). *Photoch Photobio Sci* **2013,** *12* (12), 2203-2203.
82. Caminati, W.; Maccaferri, G.; Favero, P. G.; Favero, L. B., Free Jet Absorption Millimeter Wave Spectrum of Purine. *Chemical Physics Letters* **1996,** *251*, 189-192.
83. Schneider, M.; Hain, T.; Fischer, I., Resonance-Enhanced Multiphoton Ionisation of Purine. *Chemphyschem* **2009,** *10* (4), 634-636.
84. Gonnella, N. C.; Roberts, J. D., Studies of the Tautomerism of Purine and the Protonation of Purine and Its 7-Methyl and 9-Methyl Derivatives by N-15 Nuclear Magnetic-Resonance Spectroscopy. *Journal of the American Chemical Society* **1982,** *104* (11), 3162-3164.
85. Majoube, M.; Millie, P.; Chinsky, L.; Turpin, P. Y.; Vergoten, G., Resonance Raman-Spectra for Purine. *Journal of Molecular Structure* **1995,** *355* (2), 147-158.
86. Borin, A. C.; Serrano-Andres, L.; Fulscher, M. P.; Roos, B. O., A theoretical study of the electronic spectra of N-9 and N-7 purine tautomers. *Journal of Physical Chemistry A* **1999,** *103* (12), 1838-1845.
87. Quinones, E.; Arce, R., Photochemistry and Photophysics of Purine Free Base and 6-Methylpurine. *Journal of the American Chemical Society* **1989,** *111* (21), 8218-8223.
88. Barbatti, M.; Lischka, H., Why water makes 2-aminopurine fluorescent? *Physical Chemistry Chemical Physics* **2015,** *17* (23), 15452-15459.
89. Seefeld, K. A.; Plützer, C.; Löwenich, D.; Häber, T.; Linder, R.; Kleinermanns, K.; Tatchen, J.; Marian, C. M., Tautomers and electronic states of jet-cooled 2-aminopurine investigated by double resonance spectroscopy and theory. *Physical Chemistry Chemical Physics* **2005,** *7* (16), 3021-3026.
90. Blaser, S.; Frey, H. M.; Heid, C. G.; Leutwyler, S., Gas-phase lifetimes of nucleobase analogues by picosecond pumpionization and streak techniques. *Chimia* **2014,** *68* (4), 260-3.
91. Sinha, R. K.; Lobsiger, S.; Trachsel, M.; Leutwyler, S., Vibronic Spectra of Jet-Cooled 2-Aminopurine center dot H2O Clusters Studied by UV Resonant Two-Photon Ionization Spectroscopy and Quantum Chemical Calculations. *Journal of Physical Chemistry A* **2011,** *115* (23), 6208-6217.
92. Perun, S.; Sobolewski, A. L.; Domcke, W., Ab initio studies of the photophysics of 2-aminopurine. *Mol Phys* **2006,** *104* (5-7), 1113-1121.
93. Smolarek, S.; Rijs, A. M.; Buma, W. J.; Drabbels, M., Absorption spectroscopy of adenine, 9-methyladenine, and 2-aminopurine in helium nanodroplets. *Physical Chemistry Chemical Physics* **2010,** *12* (48), 15600-15606.
94. Serrano-Andres, L.; Merchan, M.; Borin, A. C., Adenine and 2-aminopurine: Paradigms of modern theoretical photochemistry. *Proceedings of the National Academy of Sciences of the United States of America* **2006,** *103* (23), 8691-8696.
95. Rachofsky, E. L.; Ross, J. B. A.; Krauss, M.; Osman, R., CASSCF investigation of electronic excited states of 2-aminopurine. *Journal of Physical Chemistry A* **2001,** *105* (1), 190-197.
96. Santhosh, C.; Mishra, P. C., Electronic spectra of 2-aminopurine and 2,6 diaminopurine: phototautomerism and fluorescence reabsorption. *Spectrochimica Acta A* **1991,** *47*, 1685-1693.

97. Holmen, A.; Norden, B.; Albinsson, B., Electronic transition moments of 2-Aminopurine. *J.Am.Chem.Soc.* **1997,** *119*, 3114.
98. Neely, R. K.; Magennis, S. W.; Dryden, D. T. F.; Jones, A. C., Evidence of tautomerism in 2-aminopurine from fluorescence lifetime measurements. *Journal of Physical Chemistry B* **2004,** *108* (45), 17606-17610.
99. Kang, H.; Chang, J.; Lee, S. H.; Ahn, T. K.; Kim, N. J.; Kim, S. K., Excited-state lifetime of adenine near the first electronic band origin. *Journal of Chemical Physics* **2010,** *133* (15).
100. Kang, H.; Lee, K. T.; Jung, B.; Ko, Y. J.; Kim, S. K., Intrinsic lifetimes of the excited state of DNA and RNA bases. *Journal of the American Chemical Society* **2002,** *124* (44), 12958-12959.
101. Kang, H.; Jung, B.; Kim, S. K., Mechanism for ultrafast internal conversion of adenine. *Journal of Chemical Physics* **2003,** *118* (15), 6717-6719.
102. Luhrs, D. C.; Viallon, J.; Fischer, I., Excited state spectroscopy and dynamics of isolated adenine and 9-methyladenine. *Physical Chemistry Chemical Physics* **2001,** *3* (10), 1827-1831.
103. Plützer, C.; Nir, E.; de Vries, M. S.; Kleinermanns, K., IR-UV double-resonance spectroscopy of the nucleobase adenine. *Physical Chemistry Chemical Physics* **2001,** *3* (24), 5466-5469.
104. Plützer, C.; Kleinermanns, K., Tautomers and electronic states of jet-cooled adenine investigated by double resonance spectroscopy. *Physical Chemistry Chemical Physics* **2002,** *4* (20), 4877-4882.
105. Buchner, F.; Ritze, H. H.; Lahl, J.; Lubcke, A., Time-resolved photoelectron spectroscopy of adenine and adenosine in aqueous solution. *Physical Chemistry Chemical Physics* **2013,** *15* (27), 11402-11408.
106. Pancur, T.; Schwalb, N. K.; Renth, F.; Temps, F., Femtosecond fluorescence up-conversion spectroscopy of adenine and adenosine: experimental evidence for the pi sigma* state? *Chemical Physics* **2005,** *313* (1-3), 199-212.
107. Gustavsson, T.; Sharonov, A.; Onidas, D.; Markovitsi, D., Adenine, deoxyadenosine and deoxyadenosine 5 '-monophosphate studied by femtosecond fluorescence upconversion spectroscopy. *Chemical Physics Letters* **2002,** *356* (1-2), 49-54.
108. Smith, V. R.; Samoylova, E.; Ritze, H. H.; Radloff, W.; Schultz, T., Excimer states in microhydrated adenine clusters. *Physical Chemistry Chemical Physics* **2010,** *12* (33), 9632-9636.
109. Kwok, W. M.; Ma, C. S.; Phillips, D. L., Femtosecond time- and wavelength-resolved fluorescence and absorption spectroscopic study of the excited states of adenosine and an adenine oligomer. *Journal of the American Chemical Society* **2006,** *128* (36), 11894-11905.
110. Gengeliczki, Z.; Callahan, M. P.; Svadlenak, N.; Pongor, C. I.; Sztaray, B.; Meerts, L.; Nachtigallova, D.; Hobza, P.; Barbatti, M.; Lischka, H.; de Vries, M. S., Effect of substituents on the excited-state dynamics of the modified DNA bases 2,4-diaminopyrimidine and 2,6-diaminopurine. *Phys Chem Chem Phys* **2010,** *12* (20), 5375-88.
111. Mason, S. F., Purine Studies. Part II. The Ultra-violet Absorption Spectra of Some Mono- and Poly-substituted Purines. *Journal of the Chemical Society* **1954**, 2071-2081.
112. Rottger, K.; Siewertsen, R.; Temps, F., Ultrafast electronic deactivation dynamics of the rare natural nucleobase hypoxanthine. *Chemical Physics Letters* **2012,** *536*, 140-146.
113. Lin, J.; Yu, C.; Peng, S.; Akiyama, I.; Li, K.; Lee, L. K.; Lebreton, P. R., Ultraviolet Photoelectron Studies of the Ground-State Electronic-Structure and Gas-Phase Tautomerism of Hypoxanthine and Guanine. *Journal of Physical Chemistry* **1980,** *84* (9), 1006-1012.

114. Villabona-Monsalve, J. P.; Noria, R.; Matsika, S.; Peon, J., On the Accessibility to Conical Intersections in Purines: Hypoxanthine and its Singly Protonated and Deprotonated Forms. *Journal of the American Chemical Society* **2012,** *134* (18), 7820-7829.
115. Chen, J. Q.; Kohler, B., Ultrafast nonradiative decay by hypoxanthine and several methylxanthines in aqueous and acetonitrile solution. *Physical Chemistry Chemical Physics* **2012,** *14* (30), 10677-10682.
116. Guo, X. G.; Lan, Z. G.; Cao, Z. X., Ab initio insight into ultrafast nonadiabatic decay of hypoxanthine: keto-N7H and keto-N9H tautomers. *Physical Chemistry Chemical Physics* **2013,** *15* (26), 10777-10782.
117. Guo, X. G.; Zhao, Y.; Cao, Z. X., A QM/MM MD insight into photodynamics of hypoxanthine: distinct nonadiabatic decay behaviors between keto-N7H and keto-N9H tautomers in aqueous solution. *Physical Chemistry Chemical Physics* **2014,** *16* (29), 15381-15388.
118. Guo, X. G.; Yuan, H. J.; An, B. B.; Zhu, Q. L.; Zhang, J. L., Ultrafast excited-state deactivation of 9-methylhypoxanthine in aqueous solution: A QM/MM MD study. *Journal of Chemical Physics* **2016,** *144* (15).
119. Guo, X.; Yuan, H.; An, B.; Zhu, Q.; Zhang, J., Ultrafast excited-state deactivation of 9-methylhypoxanthine in aqueous solution: A QM/MM MD study. *J Chem Phys* **2016,** *144* (15), 154306.
120. Yamazaki, S.; Sobolewski, A. L.; Domcke, W., Photophysics of xanthine: computational study of the radiationless decay mechanisms. *Physical Chemistry Chemical Physics* **2009,** *11* (43), 10165-10174.
121. Changenet-Barret, P.; Kovacs, L.; Markovitsi, D.; Gustavsson, T., Xanthines Studied via Femtosecond Fluorescence Spectroscopy. *Molecules* **2016,** *21* (12).
122. Wachtershauser, G., An all-purine precursor of nucleic acids. *Proc Natl Acad Sci U S A* **1988,** *85* (4), 1134-5.
123. Rachofsky, E. L.; Ross, J. B. A.; Krauss, M.; Osman, R., CASSCF Investigation of Electronic Excited States of 2-Aminopurine. *The Journal of Physical Chemistry A* **2001,** *105* (1), 190-197.
124. Lobsiger, S.; Blaser, S.; Sinha, R. K.; Frey, H. M.; Leutwyler, S., Switching on the fluorescence of 2-aminopurine by site-selective microhydration. *Nat Chem* **2014,** *6* (11), 989-93.
125. Smolarek, S.; Rijs, A. M.; Buma, W. J.; Drabbels, M., Absorption spectroscopy of adenine, 9-methyladenine, and 2-aminopurine in helium nanodroplets. *Phys Chem Chem Phys* **2010,** *12* (48), 15600-6.
126. Yamazaki, S.; Sobolewski, A. L.; Domcke, W., Photophysics of xanthine: computational study of the radiationless decay mechanisms. *Phys Chem Chem Phys* **2009,** *11* (43), 10165-74.
127. Callahan, M. P.; Crews, B.; Abo-Riziq, A.; Grace, L.; de Vries, M. S.; Gengeliczki, Z.; Holmes, T. M.; Hill, G. A., IR-UV double resonance spectroscopy of xanthine. *Phys Chem Chem Phys* **2007,** *9* (32), 4587-91.
128. Ligare, M.; Siouri, F.; Bludsky, O.; Nachtigallova, D.; de Vries, M. S., Characterizing the dark state in thymine and uracil by double resonant spectroscopy and quantum computation. *Phys Chem Chem Phys* **2015,** *17* (37), 24336-41.
129. Brady, B. B.; Peteanu, L. A.; Levy, D. H., The electronic spectra of the pyrimidine bases uracil and thymine in a supersonic molecular beam. *Chemical Physics Letters* **1988,** *147* (6), 538-543.
130. Rottger, K.; Stellmacher, R.; Stuhldreier, M. C.; Temps, F., Ultrafast Electronic Deactivation Dynamics of Xanthosine Monophosphate. *Molecules* **2017,** *22* (1).

131. Rich, A., In *Horizons in Biochemistry*, Kasha, M.; Pullman, B., Eds. Academic Press: New York, 1962; pp 103-126.
132. Blas, J. R.; Luque, F. J.; Orozco, M., Unique tautomeric properties of isoguanine. *Journal of the American Chemical Society* **2004,** *126* (1), 154-164.
133. Robinson, H.; Gao, Y. G.; Bauer, C.; Roberts, C.; Switzer, C.; Wang, A. H. J., 2 '-deoxyisoguanosine adopts more than one tautomer to form base pairs with thymidine observed by high-resolution crystal structure analysis. *Biochemistry-Us* **1998,** *37* (31), 10897-10905.
134. Eschenmoser, A., Hexose Nucleic-Acids. *Pure Appl Chem* **1993,** *65* (6), 1179-1188.
135. Sugiyama, H.; Ikeda, S.; Saito, I., Remarkably stable parallel-stranded oligonucleotides containing 5-methylisocytosine and isoguanine. *Journal of the American Chemical Society* **1996,** *118* (41), 9994-9995.
136. Roberts, C.; Chaput, J. C.; Switzer, C., Beyond guanine quartets: cation-induced formation of homogenous and chimeric DNA tetraplexes incorporating iso-guanine and guanine. *Chem Biol* **1997,** *4* (12), 899-908.
137. Seela, F.; Wei, C. F.; Kazimierczuk, Z., Substituent Reactivity and Tautomerism of Isoguanosine and Related Nucleosides. *Helv Chim Acta* **1995,** *78* (7), 1843-1854.
138. Sepiol, J.; Kazimierczuk, Z.; Shugar, D., Tautomerism of Iso-Guanosine and Solvent-Induced Keto-Enol Equilibrium. *Z Naturforsch C* **1976,** *31* (7-8), 361-370.
139. Nir, E.; Imhof, P.; Kleinermanns, K.; de Vries, M. S., REMPI spectroscopy of laser desorbed guanosines. *Journal of the American Chemical Society* **2000,** *122* (33), 8091-8092.
140. Piuzzi, F.; Mons, M.; Dimicoli, I.; Tardivel, B.; Zhao, Q., Ultraviolet spectroscopy and tautomerism of the DNA base guanine and its hydrate formed in a supersonic jet. *Chemical Physics* **2001,** *270* (1), 205-14.
141. Chin, W.; Mons, M.; Dimicoli, I.; Piuzzi, F.; Tardivel, B.; Elhanine, M., Tautomer contribution's to the near UV spectrum of guanine: towards a refined picture for the spectroscopy of purine molecules. *Eur Phys J D* **2002,** *20* (3), 347-355.
142. Mons, M.; Piuzzi, F.; Dimicoli, I.; Gorb, L.; Leszczynski, J., Near-UV resonant two-photon ionization spectroscopy of gas phase guanine: Evidence for the observation of three rare tautomers. *Journal of Physical Chemistry A* **2006,** *110* (38), 10921-10924.
143. Seefeld, K.; Brause, R.; Häber, T.; Kleinermanns, K., Imino tautomers of gas-phase guanine from mid-infrared laser spectroscopy. *Journal of Physical Chemistry A* **2007,** *111* (28), 6217-6221.
144. Marian, C. M., The guanine tautomer puzzle: Quantum chemical investigation of ground and excited states. *Journal of Physical Chemistry A* **2007,** *111* (8), 1545-1553.
145. Choi, M. Y.; Miller, R. E., Four tautomers of isolated guanine from infrared laser spectroscopy in helium nanodroplets. *Journal of the American Chemical Society* **2006,** *128* (22), 7320-7328.
146. Alonso, J. L.; Pena, I.; Lopez, J. C.; Vaquero, V., Rotational Spectral Signatures of Four Tautomers of Guanine. *Angew Chem Int Edit* **2009,** *48* (33), 6141-6143.
147. Canuel, C.; Mons, M.; Piuzzi, F.; Tardivel, B.; Dimicoli, I.; Elhanine, M., Excited states dynamics of DNA and RNA bases: Characterization of a stepwise deactivation pathway in the gas phase. *Journal of Chemical Physics* **2005,** *122* (7), 074316-7.
148. Yamazaki, S.; Domcke, W.; Sobolewski, A. L., Nonradiative Decay Mechanisms of the Biologically Relevant Tautomer of Guanine. *Journal of Physical Chemistry A* **2008,** *112* (47), 11965-11968.

149. Barbatti, M.; Szymczak, J. J.; Aquino, A. J. A.; Nachtigallova, D.; Lischka, H., The decay mechanism of photoexcited guanine − A nonadiabatic dynamics study. *Journal of Chemical Physics* **2011,** *134*, 014304.
150. Chen, H.; Li, S. H., Ab initio study on deactivation pathways of excited 9H-guanine. *Journal of Chemical Physics* **2006,** *124* (15).
151. Heggen, B.; Lan, Z. G.; Thiel, W., Nonadiabatic decay dynamics of 9H-guanine in aqueous solution. *Physical Chemistry Chemical Physics* **2012,** *14* (22), 8137-8146.
152. Miles, H. T.; Frazier, J.; Howard, F. B., Tautomerism and Protonation of Guanosine. *Science* **1963,** *142* (359), 1458-&.
153. Onidas, D.; Markovitsi, D.; Marguet, S.; Sharonov, A.; Gustavsson, T., Fluorescence properties of DNA nucleosides and nucleotides: A refined steady-state and femtosecond investigation. *Journal of Physical Chemistry B* **2002,** *106* (43), 11367-11374.
154. Miannay, F. A.; Gustavsson, T.; Banyasz, A.; Markovitsi, D., Excited-State Dynamics of dGMP Measured by Steady-State and Femtosecond Fluorescence Spectroscopy. *Journal of Physical Chemistry A* **2010,** *114* (9), 3256-3263.
155. Karunakaran, V.; Kleinermanns, K.; Improta, R.; Kovalenko, S. A., Photoinduced Dynamics of Guanosine Monophosphate in Water from Broad-Band Transient Absorption Spectroscopy and Quantum-Chemical Calculations. *Journal of the American Chemical Society* **2009,** *131* (16), 5839-5850.
156. Peon, J.; Zewail, A. H., DNA/RNA nucleotides and nucleosides: direct measurement of excited-state lifetimes by femtosecond fluorescence up-conversion. *Chemical Physics Letters* **2001,** *348* (3-4), 255-262.
157. Pecourt, J. M. L.; Peon, J.; Kohler, B., Ultrafast internal conversion of electronically excited RNA and DNA nucleosides in water. *Journal of the American Chemical Society* **2000,** *122* (38), 9348-9349.
158. Pecourt, J. M. L.; Peon, J.; Kohler, B., DNA excited-state dynamics: Ultrafast internal conversion and vibrational cooling in a series of nucleosides. *Journal of the American Chemical Society* **2001,** *123* (42), 10370-10378.
159. Perun, S.; Sobolewski, A. L.; Domcke, W., Ab initio studies on the radiationless decay mechanisms of the lowest excited singlet states of 9H-adenine. *Journal of the American Chemical Society* **2005,** *127* (17), 6257-6265.
160. Picconi, D.; Ferrer, F. J. A.; Improta, R.; Lami, A.; Santoro, F., Quantum-classical effective-modes dynamics of the pi pi* -> n pi* decay in 9H-adenine. A quadratic vibronic coupling model. *Faraday Discuss* **2013,** *163*, 223-242.
161. Broo, A., A theoretical investigation of the physical reason for the very different luminescence properties of the two isomers Adenine and 2-Aminopurine. *J.Phys. Chem.* **1998,** *A 102*, 526-531.
162. Plasser, F.; Crespo-Otero, R.; Pederzoli, M.; Pittner, J.; Lischka, H.; Barbatti, M., Surface Hopping Dynamics with Correlated Single-Reference Methods: 9H-Adenine as a Case Study. *J Chem Theory Comput* **2014,** *10* (4), 1395-1405.
163. Chen, J. Q.; Zhang, Y. Y.; Kohler, B., Excited States in DNA Strands Investigated by Ultrafast Laser Spectroscopy. *Top Curr Chem* **2015,** *356*, 39-87.

IV THE SECOND WINDOW OF HISTORY: ORGANIC RESIDUE ANALYSIS OF CACAO IN MAYA POTTERY

The previous chapter showed in great detail how a photochemical technique can be applied to the question of life on an early earth. To answer this, detail was given on two projects in preparation for publication as well as a highlight review of a subject of interesting alternative and canonical nucleobases. Our technique of LD-JC-REMPI-MS, as the next chapter will show, can be applied also as an analytical technique. The molecular targets for the analysis in this chapter are xanthine derivatives, relying on the spectroscopy for xanthines developed in the previous chapter. Due to its low limit-of-detection (LOD) and great specificity in isolating a single analyte from a complex sample, it excels as an analytical technique. The degree of shot-to-shot variations though is the one significant drawback in this application, making absolute concentration difficult to determine. The ability as an analytical technique makes it a perfect choice to partner with fields such as archeology to help answer interdisciplinary questions of interest.

IV.1 SPECTROSCOPY AS A TOOL FOR ARCHAEOLOGISTS

By definition, "archeology is the study of past cultures through the material remains people left behind[164]." Physical artifacts are the evidence that archaeologists use to construct cultural narratives. Information such as the location of settlements and distribution of objects within settlements can reveal much cultural information. Vessel and tool use was often inferred through interpretation of images and through modern day ethnographic

descriptions. Analysis of artifacts makes it possible to empirically determine data about a tool to help understand its construction and use[165]. Archeologists can collaborate with analytical chemists for the study of artifacts to extract extra information such as what residues might remain from the vessels contents, or identify paint or the soil mixture found in a pottery piece (also called a sherd)[164].

Initially in the chemical study of artifacts, inorganic markers were the most important because they were easier to identify then organic material. Organic compounds are crucial to identify many materials as it can be a marker for resin[166, 167], fat[168-170], oil[171, 172], wax[173, 174], beeswax[174-176], and even food[177]. The study of organic material in archeological artifacts is termed organic residue analysis (ORA). One of the earliest studies of ORA, was done on bog butters[178]. Organic residues can appear as physical deposit of material crusted on the interior or exterior surface of the vessel but most commonly found as absorbed residues preserved inside the vessel walls. Once a residue sample is collected, archaeological biomarkers are used to discern the chemical makeup of the residue. “Biomarkers (biological markers) are indicator compounds that can be used as tracers for geological and environmental processes”[164]. Biomarkers includes a wide range of organic compounds-proteins, lipids, amino acids, nucleic acids, carbohydrates[179]. The requirements for a biomarker is that it survives burial, is unique to a particular substance, and is detectable by an analytical technique[180].

Initially ORA was done by using spectroscopic methods like IR, Raman, and NMR to identify functional groups. While useful this still leaves much uncertainty in the identification of the compounds present in the residue. Utilizing techniques like GC/MS and different forms of LC/MS allowed for separation of complex sample to identify the individual components.

As discussed previously, our technique LD-JC-REMPI-MS can also be applied to the study of complex mixtures. Previously, we have analyzed complex mixtures of PAH's as soot residue on archaeological fragments. As well as, studied carbonaceous dust in meteorites to determine the alternative canonical nucleobases present[65]. Additionally, this technique has been applied to ORA directly through the identification of wine in Nubian pottery[5] and cacao in Maya pottery[181]. The following section details an intense study of the LD-JC-REMPI-MS Fintechnique applied to identify cacao in Maya pottery with the intention of describing access and distribution. This study was done in collaboration with Dr. Anabel Ford who designed the archaeological question and contextualized the result, showing the data provided invaluable insights as to the role of cacao ceremonially with the Maya and assumptions on the distribution of cacao. Additionally, all pieces in the study were acquired and selected by Dr. Ford, Director of the MesoAmerican Research Center, who has conducted excavations at the Classic Maya center, El Pilar, in Belize and Guatemala. In this dissertation I will focus on my chemical contributions to the project.

IV. 2 CACAO- THE BEVERAGE OF THE GODS

Cacao is a decadent drink made from the pods of *Theobroma cacao*[182]. These pods are dried roasted, and ground then mixed with hot water, sometimes frothed and often have many spices added to them for additional flavor[182, 183]. This beverage is a key participant in ceremonies associated with marriage and death. This key ceremonial role is evident through the extravagant vessels that archeologists have found cacao present in[182-184]. This association with the religious elite and intricate vessels of great worth cause cacao to be associated with the elite population. Archeologists and anthropologists have yet to really question this assumption of cacao as a drink available only to the socially elite. If cacao is so important ceremonially and is also grown by lower social classes, it is believable the access to cacao would be more widely distributed than previously assumed. The majority of past studies have focused solely on vessels forms that would have been associated with an elite population[182, 183, 185-189]. In contrast, our study focuses mostly on sherds that would be associated with farmers or craftsman and not with an elite population. All sherds were provided by our collaborator Anabel Ford and are from the site El Pilar. The study includes 54 samples, 13 of these are from our original study while the other 41 are a new addition.

IV. 3 METHODOLOGY BACKGROUND

Cacao is made from the seeds of the plant *Theobroma cacao* which has three main varieties- Criollo, Forastero, and Trinitario[190, 191]. These varieties contain many different compounds with the class of methylxanthines indicative of cacao as they are present in high concentration and mostly unique to cacao. Methylxanthines is a class of molecules with oxo- and methyl-

groups substituted onto a purine base structure. Part of this class of methylxanthines includes caffeine, theobromine, and theophylline. Theobromine since it is found in the highest concentration of the methylxanthines in cacao was chosen as the biomarker.

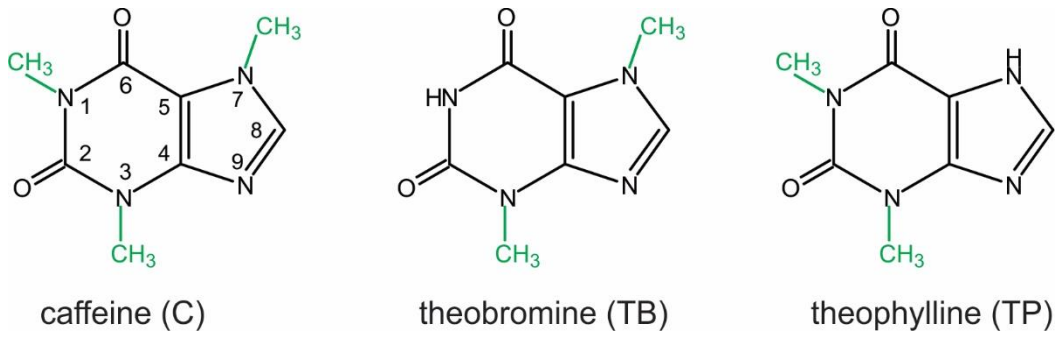

Figure 18- molecular structure of the three methylxanthines- caffeine, theobromine, and theophylline

The search for cacao began in 1989 with a paper published by Hurst that used theobromine alone as the biomarker for cacao in a decorative bowl from Rio Azul[188]. This paper was part of the larger biomarker revolution which sought to identify single compounds unique to a particular substance that would survive the burial process and still be detectable in an archeological sherd. Theobromine was this biomarker as it meets the two conditions of surviving burial and of being unique to cacao[179].

As the search for cacao moved to North America, theobromine alone was no longer suitable to indicate cacao in organic residues. In North America, black drink was brewed from two species of holly plant (*Ilex vomitoria and Ilex cassine*). Like cacao, black drink contains two of the three methylxanthines- caffeine and theobromine. One of the species of holly plant, *Ilex vomitoria* has a ratio of 5 to 1 caffeine to theobromine. I. cassine has a ratio of 2 to 1 caffeine

to theobromine. Similarly, Criollo, the variety of cacao most likely grown by the Maya, has a ratio of 1 to 2-3 caffeine to theobromine[182, 183, 190, 192].

While theobromine and caffeine are both limited as unique biomarkers for cacao, theophylline is found to be the best choice of the three as the biomarker for cacao. Caffeine, theobromine, and theophylline can be found in 100 species of plants. While these methylxanthines are extremely common in plants, only a few plants have a high concentration. Additionally, theophylline is usually found in much smaller concentrations than theobromine or caffeine[193-195]. Theophylline can be found in 7 plants: *Camellia sinensis, Coffea arabica, Ilex paraguariensis, Paullinia cupana, Theobroma bicolor, Theobroma angustifolium,* and *Theobroma cacao.*

The Asian plant, *Camellia sinensis*, with 2-4 ppm of theophylline in its leaf, is native to China and Japan, but present today in Hawaii, South Carolina, and Brazil[196]. *Coffea arabica*, native to the area of Ethiopia, is widespread now, known from most equatorial latitudes. *C. arabica* has minimal amounts of theophylline, 5 ppm in the seed and in the endosperm from immature fruits but not in mature fruits[197]. The South American *Ilex paraguariensis*, used as the herb mate from Argentina and Paraguay, has 500 ppm of theophylline in the leaf[198, 199]. There is also *Paullinia cupana* found in the Amazon Basin with 2500 ppm theophylline in the seeds[200]. As for genus Theobroma, it is known from the neotropical lowlands of Amazon and Mesoamerica. According to our database search there are three species of the genus Theobroma that have theophylline. *T. bicolor* (seed 200 ppm, fruit 500 ppm, testa 200 ppm,

petiola 53-273 ppm) and *T. angustifolium* (seed 90 ppm, fruit 0 ppm, testa 110 ppm, petiola 50 ppm) have less theophylline than *T. cacao* (seed 4739 ppm, fruit 0 ppm, testa 130-257 ppm, petiola 58-188 ppm). Our database search has made it clear that T. cacao is unique in its region for TP. This gives us confidence that any TP detected in our samples will be from cacao as no other natural sources make sense. Additional to the literature sources, Dr. Duke's Phytochemical and Ethnobotanical Databases (HTTPS://PHYTOCHEM.NAL.USDA.GOV) was used to determine the 7 plants with significant amounts of theophylline and the US Department of Agriculture GRIN-Global database to determine the regional location of each of these plants (HTTPS://NPGSWEB.ARS-GRIN.GOV/GRINGLOBAL).

IV.4 DESIGNING THE STUDY TECHNIQUES

Analyzing the pottery involved five steps: sample preparation, extraction, sample-graphite combination, analytical method. The methods that were used in this study were based on the techniques used previously with attention given to improving the method as well.

IV.4.a SAMPLE PREPARATION

In past papers, many different sample preparation techniques have been debated and used widely by archaeologists in studies identifying cacao residues. The most common sample preparation techniques are the burr method[184, 187, 201], the burr and grind method [202-206], and the waterwash method[207-209]. The burr method uses sandpaper or some other

scraping tool to remove the exterior surface of the interior of a vessel. The burr-and-grind method uses a Dremel bit to remove all the exterior surfaces from a small portion of the vessel. This portion is then chipped off and ground up. The water wash method is the only nondestrucitve method. In this method cold water is run down the interior surface of the vessel and collected.

While the waterwash method is the least destructive it is also the method that leads to very little extraction of the biomarkers for the pottery which is one of the reasons that make it undesirable for use. The other two methods which produce a powdered pottery sample can be extracted much more efficiently.

The burr and grind method has been found to introduce the least contamination into the sample which is crucial due to the ubiquitousness in modern culture of caffeine and, to some extent, theobromine. Washburn in their highly respected 2014 study raised the issue of dust contamination as creating false positives for cacao in the archeological record. When comparing positive identification of caffeine to dust contamination only 24 out of 61 samples were still valid[208]. In King's study, contaminant led him to suspend any conclusions from his samples[201]. Crown's most recent study from 2018 concludes that this can be prevented by using the more damaging burr and grind method over the burr method or the waterwash method which would include surface contamination in the analysis[202]. For these reasons, this study chose to use the burr-and-grind method for the sample preparation.

IV.4.b EXTRACTION

Extraction of the biomarkers from the pottery sample is the second step in the method. Method development was done as part of this study to see the effects of extraction on the ratio of caffeine to theobromine. Since multiple previous studies had used the ratio of theobromine and caffeine to distinguish between black drink and cacao, this study wanted to see if the extraction method was unequally extracting the two biomarkers creating a misrepresentation of the source of the biomarkers.

The extraction method is where the ratios of caffeine and theobromine are most likely to be distorted. Washburn in 2011 analyzed their results and found that overall caffeine was found in twice the concentration of theobromine which directly contradicts the 1:10 ratio in cacao. They spiked a Hopi vessel with a 12:1 theobromine to caffeine solution and performed their standard water wash extraction method. Their analysis confirmed that caffeine was preferentially extracted over theobromine which led them to the conclusion that theobromine complexes better with the inner matrix of the clay. In 2013, Washburn did another study to analyze the disproportionate extraction of the methylxanthines. They spiked modern Pueblo vessels with different ratios of theobromine and caffeine, took water washes of the spiked vessels and then analyzed the resulting samples. In some samples, caffeine was preferentially recovered and in others the amount recovered was identical. They say that an initial sample ratio of 6:1 theobromine to caffeine could result in the seen values, but this ratio doesn't match any variety of cacao.

The most common method is to take 500mg of ground pottery sample collected either through the burr or burr-and-grind method add 3mL of water heat at 80 C˚ for 30 min. This extraction process is done three times for each sample, all extractions are combined, and concentrated to 1mL before analysis. Crown and Hurst in 2018 compared this method to the water wash method. They soaked shards of an unslipped earthenware vessel and soaked them in a cup of coffee for 24hrs. They then analyzed the shards through the water wash method and through their standard burr and grind method and extraction. They found that the burr and grind method and subsequent extraction method extracts four times more than the water wash method[202]. No study has checked if theobromine and caffeine are preferentially or equally extracted by this method.

To study the efficiency of the extraction method, an unglazed, unslipped low fired bisque clay pot in the pinch pot style was furnished from a local pottery studio. Then this pot was soaked in an equimolar solution of theobromine, theophylline, and caffeine and heated for 48 hrs and then allowed to just sit covered for 48 hrs. The pot was then dried upside down, and smashed into pieces. The pieces of pottery were prepared for extraction by the burr and grind method. All pottery examined in the samples was ground together to ensure homogeneity among the various samples. Then 300 mg of pottery was extracted by 3 mL of either water or ethanol for 30 min at either 80 C˚ for water or 70 C˚ for ethanol. The liquid from the first extraction was pipetted into a separate vial and the clay had 3 mL of solvent re-

added and heated for another 30 min at the same temperature. Afterwards, the mixture was filtered and combined with the first extraction. Each condition was analyzed in triplicate.

All samples were analyzed utilizing UPLC-MS. A calibration curve was run twice as well as each sample was run twice with blanks between each sample. Analysis was done under the same conditions as Washburn 2011[209]. Figure 19 shows that the extraction with water extracts more theobromine than caffeine or theophylline. In comparison, if ethanol is used instead of water then the amount of each methylxanthine extracted is fairly equal with only 9% variance in the concentration of the three biomarkers. In order to more accurately see the ratio of caffeine to theobromine, ethanol was chosen as the extraction liquid.

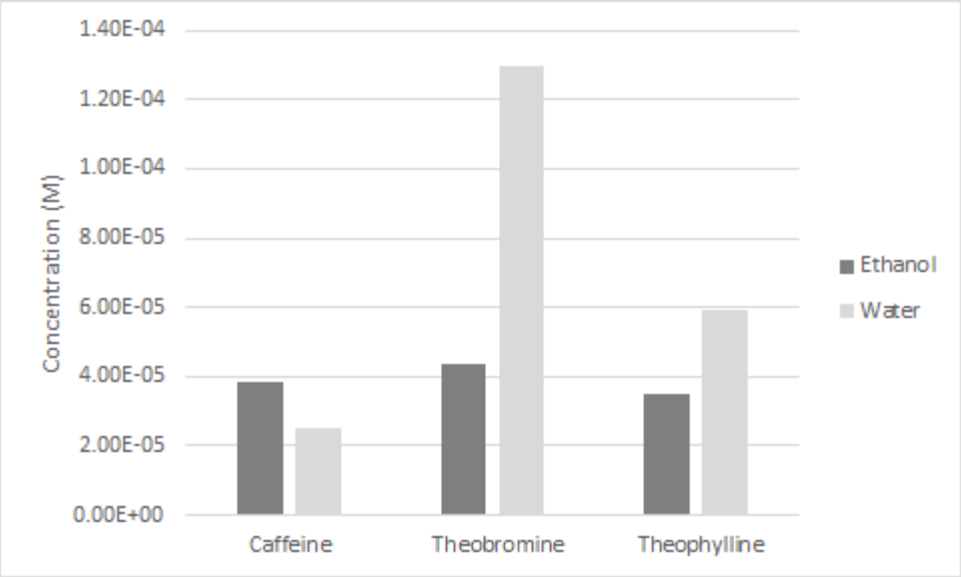

Figure 19- Results of the model extraction showing that when water is used as the extraction medium theobromine is preferentially extracted. In contrast, ethanol extracts the three methylxanthines equally with only a 9% difference in concentration.

IV.4.c SAMPLE-GRAPHITE COMBINATION

To allow for analysis of a liquid sample a new method had to be developed. Our technique of LD-JC-REMPI-MS, usually mixes a pure solid sample with graphite powder abrading a graphite bar and rubbing the graphite powder sample mixture on top. A new method had be developed that allowed for the combination of liquid sample and solid graphite in a manner where each sample could be isolated without drastically increasing the number of graphite bars to analyze. A small amount of graphite powder was weighed out and then an aliquot of the liquid extraction was added. This mixture was heated gently until the sample was totally dry. If the graphite powder was added directly to the bar this would result in 120 bars needing to be analyzed. If a method could be developed that placed all three replicates of one sample on the same bar then the analysis time could be drastically reduced.

A test was done with standards of theobromine, theophylline and caffeine mixed with graphite. Instead adding this directly to a graphite bar strips of double sided tape and carbon double sided tape were laid down with the sample powder adhered on top. The addition of the tape did not prevent signal and would allow for three samples to all be on the same bar. Since the double sided carbon tape provided the best signal over the normal double sided tape, it was used for all future studies.

IV.4.d DESIGN OF THE ANALYTICAL TECHNIQUE

LD-JC-REMPI-MS was used in this study due to the combination of wavelength and mass distinction as well as high sensitivity. The wavelength and mass selectivity allows for isomers

like theobromine and theophylline to be distinguishable. Techniques must also be incredibly sensitive to allow for usage in the detection of archeological materials. As this technique is usually used for photochemical rather than analytical studies some changes had to be made.

Our research group had previously published a study looking for cacao in Maya pottery. In developing an analytical method for this study initially, duplication of the past results was tried. In the previous study gold bars or gold bars with stainless steel pegs were used for the desorption step. This requires that the desorption wavelength be changed from 1064 nm to 266 nm or 532 nm. Under these conditions though with graphite powder and solid standards added to the top of the bars very little signal was gotten. Unable to make this easily work, our method would rely on a graphite substrate and 1064 nm desorption laser. The idea of graphite pegs on a metal bar was considered but the small surface area of the pegs allows for very few measurements of the sample. With a larger area with sample applied it is possible to take many measurements of the sample. Double sided tape was applied to a graphite bar with graphite standard mixture applied to the tape. This application of sample produced a lot of signal and would allow for multiple samples to occupy the same graphite bar.

For the first step, concentration standards were developed and analyzed by our technique. The wavelength was varied to determine where the transitions are for each of the three molecules of interest. The highest absorption peak was chosen for each of the three as the main resonant wavelength. The resonant wavelength is the wavelength that the laser would

be at when collecting the signal measurements. For theophylline this is 280.65 nm, theobromine 281.6 nm and caffeine 281.65 nm.

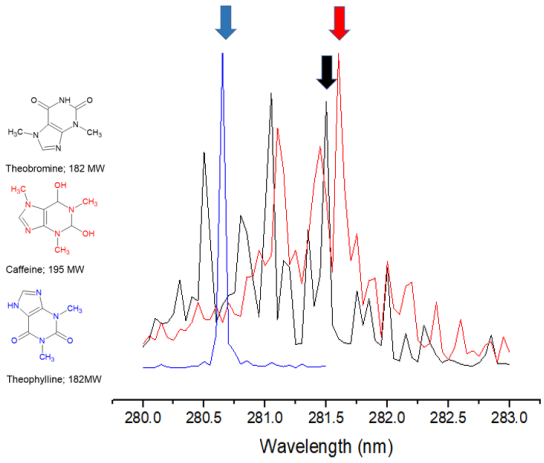

Figure 20- R2PI spectra of theobromine, caffeine, and theophylline with arrows showing peak used for analytical measurements.

Concentration standards were made of standard solutions of theophylline, theobromine, and caffeine in equal amounts. These standards were then run multiple times on multiple days to ensure that they always produced the same signal. There were extreme variations in the signal of these standards due to issues with the way that labview collected the data from the oscilloscope and due to the shot-to-shot variations due to differences in laser intensity between different shots. The reproducibility of the signal was the most significant barrier to using LD-JC-REMPI-MS as an analytical technique. There were multiple steps to reducing signal variations in the technique- 1) ensuring that the same number of volts on the oscilloscope always produced the same signal readout in labview 2) designing a scan that

allowed for the collection of multiple iterations of signal 3) reducing and quantifying the shot-to-shot and scan-to-scan variations.

In solving the first issue, a scan was developed such that the final signal measurement was the average of 12 shots of signal subtracted from the average of 3 shots of background. In this case, background refers to the oscilloscope reading when the desorption laser is not firing. This method of subtracting the background from the signal allowed the oscilloscope to be set to any voltage offset without affecting the final signal measurement. The design of this scan also allowed for 12 measurements of signal to be taken and averaged for a final value.

Even with these steps the variability in the signal is still high due to shot to shot variations in the laser intensity. Analysis was done of 30 scans on a bar of theophylline to quantify the shot to shot variation. Over these 30 scans it was found that there was a 27 % variance in the signal with this being the relative standard deviation between the 30 scans. Within each scan the relative standard deviation between the 12 shots of signal is 39 % when averaged over the 30 scans. Thus, the variation between scans is less than the variation between shots.

Reproducibility of the technique while a crucial problem to minimize and quantify, the sensitivity of the technique was also essential to the success of the study. Archeological fragments exposed to cacao would have very small amounts of theophylline requiring extremely high sensitivity in the chosen analytical technique. Our previous study had shown that the LOD was on the order of 10's of pg but with a drastic change in method the LOD needed to be re-established. Five standards were made of caffeine, theobromine, and

theophylline in 2900, 1950, 780, 78, and 39 pg. The LOD will be different for each of the three compounds as each biomarker has different ionization efficiencies. Theophylline is detected the best, 4.4 times better than theobromine, with caffeine 2.7 times better. The LOD is lowest with theophylline at 52 pg with caffeine 85 pg and theobromine 228 pg. A signal of 1.5 is used for the calculation of LOD as that is 3 times the standard deviation in the background.

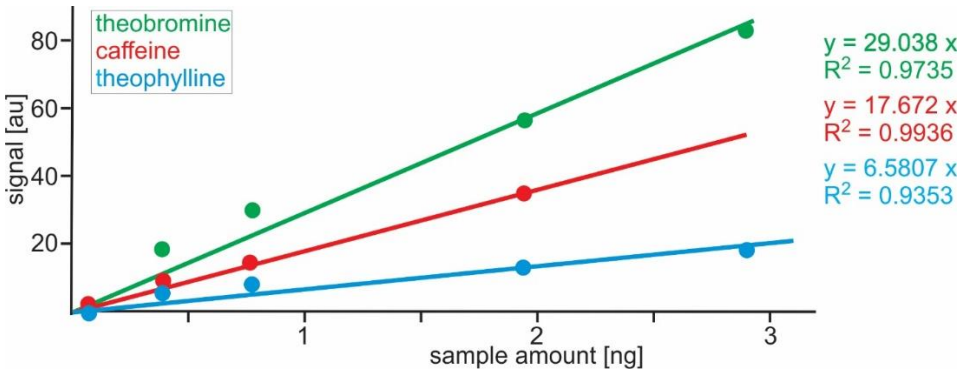

Figure 21- Concentration curve for theobromine, caffeine, and theophylline used to calculate LOD.

IV. 5 ANALYTICAL RESULTS AND DISCUSSION

In our previous study, a set of 13 vessels were analyzed from the El Pilar area and compared those with 7 vessels from SE US[181]. Twelve of the thirteen Maya samples can be attributed to cacao due to the presence of TP (Table 1). The vessels from the Maya area represent Maya centers, large residential units, as well as a small residential unit in the river valley that was recorded as a zone of cacao production at the time of the conquest.

Table 1: *Analysis of Maya Samples from previous study*[181]

Catalog #	Site	Form	Theobromine	Caffeine	Theophylline
578	281-34	Vase base	Positive	Positive	Positive
16463G	272-145	Vase base	Positive	Positive	Positive
2009	278-46	Vase base	Positive	Positive	Positive
4209	Yaxox	Vase base	Positive	Positive	Positive
16535Z	272-145	Vase base	Positive	Positive	Positive
16359AB	272-145	Vase base	Positive	Positive	Positive
13394AO	281-21	Vase base	Positive	Positive	Positive
14321V	278-26	Vase base	Positive	Positive	Positive
14328K	278-26	Vase base	Positive	Positive	Positive
143325U	278-26	Vase base	Positive	Positive	Positive
14320M	278-26	Vase base	Negative	Negative	Negative
14319O	278-26	Vase base	Positive	Positive	Positive
14342V	278-26	Vase base	Positive	Positive	Positive

The current work expands the sample set of Maya vessels to incorporate wider domestic settings as well as examples of more vessel forms in order to address this question of elite access to cacao. The samples represent ceramic vessels as ancient Maya belongings from civic and domestic contexts, including large to small residential units in the El Pilar area. Our results demonstrate that the mild stimulant, cacao, appears to have been widely distributed among elite and non-elite populations.

Table 2: *Analytical Results of Archaeological Samples in this Study from the El Pilar Area. Shading indicates that the signal is higher than the cut off value of 1.5.*

#	Catalog #	Site	Form	TB	C	TP	TP/C rat
1	10157	MC214A	Bowl rim	0.38	2.78	1.16	-
2	1313	278-077	Plate rim	0.7	3.72	0.99	-
3	1016A	Bacab Na	Plate rim	0.52	1.28	1.85	0.84
4	1307	278-077	Plate rim	0.3	5.8	2.04	0.2
5	2005	El Pilar	Plate base	0.3	3.48	0.96	-
6	14387A	278-066	Vase base	0.2	0.15	0.79	-
7	14387AS	278-066	Vase base	0.52	2.06	2.78	0.79
8	14387AS	278-066	Vase base	0.355	2.47	1.72	0.41

9	14387AQ	278-066	Vase base	0.99	10.60	1.4	-
10	16484 HM	272-182	Vase base	0.17	0.18	0.15	-
11	15496AH	272-182	Vase base	0.905	3.48	3.13	0.52
12	16499 AI	272-182	Vase base	0.32	0.88	2.67	-
13	16484HI	272-182	Vase base	0.77	1.11	3.41	-
14	16484HE	272-182	Vase base	0.79	0.36	2.28	-
15	16527CJ	272-182	Vase base	1.09	0.83	3.79	-
16	16445H	272-182	Vase base	0.52	2.24	2.05	0.53
17	16484HW	272-182	Vase base	0.815	1.24	1.71	-
18	165310O	272-136	Vase base	0.24	0.47	6.95	-
19	16589A	272-136	Vase base	0.32	0.89	1.48	-
20	13133A	281-21	Vase base	0.01	0	1.12	-
21	13171H	281-21	Vase base	0.42	0	0.98	-
22	13171E	281-21	Vase base	0.43	0.27	0.65	-
23	13184Q	281-21	Vase base	0.28	0.19	0.62	-

24	16425N	272-145	Vase base	0.37	0	1.03	-
25	165890A	272-145	Vase base	0.59	4.23	0.87	-
26	16378H	272-145	Vase base	0.42	2.69	1.19	-
27	16535AA	272-145	Vase base	0.64	1.71	3.32	1.13
28	16578H	272-145	Vase base	1.15	1.9	1.1	-
29	16425N	272-145	Vase base	0.58	2.69	1.3	-
30	14230AL	272-220	Vase base	0.56	0.47	1.75	-
31	14230ALL	272-220	Vase base	0.28	1.64	7.58	2.69
32	16170FE	272-145	Bowl rim	0.215	3.77	1.11	-
33	3656	272-145	Vase tripod	1.24	3.77	1.71	0.26
34	16170FT	272-145	Bowl rim	0.69	2	1.57	0.46
35	16170 FF	272-145	Bowl rim	0.5	2.62	1.225	-
36	4798A	El Pilar	Jar rim	1.37	5.79	3.65	0.37
37	16359A	272-145	Jar rim	0.16	13.36	0.85	-
38	16427A	272-145	Jar rim	0.38	10.29	0.7	-

39	4684	El Pilar	Jar rim	0.42	11.91	0.52	-
40	4675	El Pilar	Jar rim	0.69	7.56	0.07	-
41	4751	El Pilar	Jar rim	0.98	10.3	0.62	-

As shown above 41 samples were measured for theobromine, caffeine and theophylline. None of the 41 samples had a significant amount of theobromine, meaning that it never exceeded the 228 pg LOD. Caffeine was found in a significant amount in 25 samples with 18 for theophylline. Eleven samples were positive for both caffeine and theophylline. Using the condition that detection of theophylline is the best indication of cacao presence, 18 of our 41 samples would be positive for cacao.

For the 11 samples positive for caffeine and theophylline, their ratio can be calculated and compared to those previously reported. Our results show a theophylline to caffeine ratio ranging from 0.2 to 2.69 while other studies showed a ratio of 6.12, 7.31, 7.34, and 26.9[201, 205, 208]. Additionally, none of these ratios correspond to the ratio found in raw Criollo cacao. Somewhere between the raw plant to analysis from an archaeological sample, the ratio is changed dramatically, reducing the reliability of this variable.

IV.6 BIBLIOGRAPHY

5. Callahan, M. P.; Gengeliczki, Z.; de Vries, M. S., Resonant Two-Photon Ionization Mass Spectrometry of Jet-Cooled Phenolic Acids and Polyphenols. *Analytical Chemistry* **2008,** *80*, 2199-2203.

65. Callahan, M. P.; Smith, K. E.; Cleaves, H. J.; Ruzicka, J.; Stern, J. C.; Glavin, D. P.; House, C. H.; Dworkin, J. P., Carbonaceous meteorites contain a wide range of extraterrestrial nucleobases.

Proceedings of the National Academy of Sciences of the United States of America **2011,** *108* (34), 13995-13998.
164. Organic Residue Analysis and Archaeology: Guidance for Good Practice. England, H., Ed. 2017.
165. Loughmiller-Cardinal, J., Distinuishing the uses, functions, and purposes of classic maya "chocolate" containers: not all cups are for drinking. *Ancient Mesoamerica* **2019,** *30*, 13-30.
166. Stern, B.; Heron, C.; Corr, L.; Serpico, M.; Bourriau, J., Compositional Variations in Aged and Heated Pistacia Resin Found in late Bronze Age Canaanite Amphorae and Bowls from Amarna, Egypt. *Archaeometry* **2003,** *45* (3), 457-469.
167. Lambert, J. B.; Frye, J. S.; Poinar, G. O. J., Amber from the Dominican Republic: analysis by nuclear magnetic resonance spectrsocopy. *Archaeometry* **1985,** *27*, 43-51.
168. Dudd, S. N.; Evershed, R. P., Direct demonstration of milk as an element of archaeological economies. *Science* **1998,** *282*, 1478-1481.
169. Mottram, H. R.; Dudd, S. N.; Lawrence, G. J.; W., S. A.; Evershed, R. P., New chromatographic, mass spectrometric and stable isotope approaches to the classification of degraded animal faats preserved in archaeological pottery. *Journal of Chromatography A* **1999,** *833*, 209-221.
170. Copley, M. S.; Berstan, R.; Dudd, S. N.; Docherty, G.; Mukherjee, A. J.; Straker, V.; Payne, S., Direct chemical evidence for widespread dairying in prehistoric Britain. *PNAS* **2003,** *100*, 1524-1529.
171. Condamin, J.; Formenti, F.; Metais, M. O.; Michel, M.; Blond, P., The application of gas chromatography to the tracing of oil in ancient amphorae. *Archaeometry* **1976,** *18*, 195-201.
172. Kimpe, K.; Jacobs, P. A.; Waelkens, M., Analysis of oil used in late Roman oil lamps with different mass spectrometric techniques revealed the presence fo predominantly olive oil together with traces of animal fat. *Journal of Chromatography A* **2002,** *937*, 87-95.
173. Evershed, R. P.; Heron, C.; Goad, L. J., Epicuticular wax components preserved in potsherds as archaeological indicators of leafy vegetables in ancient diets. *Antiquity* **1991,** *65*, 540-544.
174. Charters, S.; Evershed, R. P.; Blinkhorn, P. W.; Denham, V., Evidence for the mixing of fat and wax in archaeological ceramics. *Archaeometry* **1995,** *37*, 13-128.
175. Heron, C.; Nemcek, N.; Bonfield, K. M.; Dixon, D.; Ottaway, B. S., The chemistry of Neolithic beeswax. *Naturwissenschaften* **1994,** *81*, 266-269.
176. Evans, K.; Heron, C., Glue, disinfectant and chewing gum: natural products chemistry in archaeology. *Chemistry and Industry* **1993,** *12*, 446-449.
177. Barnard, H.; Ambrose, S. H.; Beehr, D. E.; Forster, M. D.; Lanehart, R. E.; Malainey, M. E.; Parr, R. E.; Rider, M.; Solazzo, C.; Yohe, R. M., Mixed results of seven methods for organic residue analysis applied to one vessel with the residue of a known foodstuff. *Journal of Archaeological Science* **2007,** *34* (1), 28-37.
178. Thornton, M. D.; Morgan, E. D.; Celoria, F., The composition of bog butter. *Science and Archaeology* **1970,** *2/3*, 20-25.
179. Evershed, R. P., Organic Residue Analysis in Archaeology: The Archaeological Biomarker Revolution. *Archaeometry* **2008,** *50* (6), 895-924.
180. McGovern, P. E.; Hall, G. R., Charting a Future Course for Organic Residue Analysis in Archaeology. *Journal of Archaeological Method and Theory* **2015,** *23*, 592-622.

181. Owens, S. C.; Berenbeim, J. A.; Ligare, M. R.; Gulian, L. E.; Siouri, F. M.; Boldissar, S.; Tyson-Smith, S.; Wilson, G.; Ford, A.; Vries, M. S. d., Direct Analysis of Xanthine Stimulants in Archaeological Vessels by Laser Desorption Resonance Enhanced Multiphoton Ionization. **2017**.
182. McNeil, C. L., The Biology, Antiquity, and Modern Uses of the Chocolate Tree (Theobroma cacao L.). In *Chocolate in Mesoamerica: A Cultural History of Cacao*, McNeil, C., Ed. Florida Scholarship Florida, 2009.
183. Henderson, J. S.; Joyce, R. A., Brewing Distinction: The Development of Cacao Beverages in Formative Mesoamerica. In *Chocolate in Mesoamerica: A Cultural History of Cacao*, McNeil, C., Ed. Florida Scholarship Online: Florida, 2009.
184. Powis, T. G.; Valdez, F.; Hester, T. R.; Hurst, W. J.; Tarka, S. M., Spouted Vessels and Cacao Use among the Preclassic Maya. *Latin American Antiquity* **2002,** *13* (1), 85-106.
185. Loughmiller-Cardinal, J., Distinguishing the Uses, Functions, and Purposes of Classic Maya 'Chocolate' Containers: Not All Cups Are for Drinking. *Ancient Mesoamerica* **2018,** *30* (1), 1–18.
186. Reents-Budet, D., The social context of Kakaw drinking among the ancient Maya. In *Chocolate in Mesoamerica : a cultural history of cacao*, McNeil, C. L., Ed. University Press of Florida: Gainesville, 2006; pp 220-223.
187. Powis, T. G.; Hurst, W. J.; Rodriquez, M. d. C.; C., P. O.; Blake, M.; Cheetham, D.; Coe, M. D.; Hodgson, J. G., The Origins of Cacao Use in Mesoamerica. *Mexicon* **2008,** *30* (2), 35-38.
188. Hurst, W. J.; Martin, R. A. J.; Tarka, S. M. J.; Hall, G. D., Authentication of cacao in maya vessels using high-performance liquid chromatograpic techniques. *Journal of Chromatography A* **1989,** *466*, 279-289.
189. Ardren, T., *Her cup for sweet cacao : food in ancient Maya society*. University of Texas Press: Austin, 2021.
190. Pelaez, P. P.; Bardon, I.; Camasca, P., Methylxanthine and catechin content of frech and fermented cacoa beans, dried cocoa benas, and cocoa liquor. . *Scientia Agropecuaria* **2016,** *7*.
191. Ogata, N.; Gomez-pompa, A.; Taube, K. A., The domestication and distributio of theobroma L. in the Neotropics. In *Chocolate in Mesoamerica: A Cultural History of Cacao*, McNeil, C., Ed. Florida Scholarship Online: Florida, 2009.
192. Gasco, J., Soconusco Cacao Farmers Past and Present. In *Chocolate in Mesoamerica: A Cultural History of Cacao*, McNeil, C., Ed. Florida Scholarship Online: Florida, 2009.
193. Ashihara, H.; Crozier, A., Biosynthesis and Metabolism of Caffeine and Related Purine Alkaloids in Plants. *Advances in Botanical Research* **1999,** *30*, 117-205.
194. Ashihara, H.; Suzuki, T., Distribution and Biosynthesis of Caffeine in Plants. *Frontiers in Bioscience* **2004,** *9*, 1864-1876.
195. Ashihara, H.; Kato, M.; Crozier, A., Distribution, Biosynthesis and Catabolism of Methylxanthines in Plants | SpringerLink. In *Methylxanthines*, Fredholm, B. B., Ed. SpringerLink: 2021; Vol. 200, pp 11-31.
196. Jalal, M. A. F.; Collin, H. A., Estimation of Caffeine, Theophylline and Theobromine in Plant Material. *New Phytology* **1975,** *76*, 277-281.
197. Mazzafera, P.; Crozier, A.; Magalhaes, A. C., Caffeine Metabolism in *Coffea Arabica* and Other Species of Coffee. *Phytochemistry* **1991,** *30* (12), 3913-3916.
198. Cardozo, E. L. J.; Ferrarese-Filho, O.; Filho, L. C.; Ferrarese, M. d. L. L.; Donaduzzi, C. M.; Sturion, J. A., Methylxanthines and phenolic compounds in mate (*Ilex paraguariensis* St. Hil.) progenies grown in Brazil. *Journal of Food Composition and Analysis* **2007,** *20* (7), 553-558.

199. Clifford, M. N.; Ramirez-Martinez, J. R., Chlorogenic acids and purine alkaloids contents of Maté (Ilex paraguariensis) leaf and beverage. *Food Chemistry* **1990,** *35* (1), 13-21.
200. Meurer-Grimes, B.; Berkov, A.; Beck, H., Theobromine, theophylline, and caffeine in 42 samples and products of Guaraná (Paullinia cupana , Sapindaceae). *Economic Botany* **2021,** *52* (3), 293-301.
201. King, A.; Powis, T. G.; Cheong, K. F.; Gaikwad, N. W., Cautionary tales on the identification of caffeinated beverages in North America. *Journal of Archaeological Science* **2017,** *85*, 30-40.
202. Crown, P. L.; Ward, T. J.; Hurst, w. J.; Bravenec, A. D.; Ali, S. U.; Klugh, J.; Sturm, J.; Williams, K., Caffeine Connections and Conundrums: Issues in Methylxanthine Recovery from Archaeological Ceramics. *Papers of the Archaeological Society of New Mexico* **2018,** *44*, 95-106.
203. Crown, P. L.; Hurst, J., Evidence of cacao use in the Prehispanic American Southwest. *PNAS* **2009,** *106* (7), 2110-2113.
204. Crown, P. L.; Emerson, T. E.; Gu, J.; Hurst, W. J.; Pauketat, T. R.; Ward, T., Ritual Black Drink consumption at Cahokia. *PNAS* **2012,** *109* (35), 13944-13949.
205. Crown, P. L.; Gu, J.; Hurst, J.; Ward, T. J.; Bravenec, A. D.; Ali, S.; Kebert, L.; Berch, M.; Redman, E.; Lyons, P. D.; Merewether, J.; Phillips, D. A.; Reed, L. S.; Woodson, K., Ritual Drinks in the pre-Hispanic US Southwest and Mexican Northwest. *PNAS* **2015,** *112* (37), 11436-11442.
206. Reber, E. A.; Kerr, M. T., The persistence of caffeine in experimentally produced black drink residues. *Journal of Archaeological Science* **2012,** *39* (7), 2312-2319.
207. Washburn, D. K.; Washburn, W. N.; Shipkova, P. A., Cacao consumption during the 8th century at Alkali Ridge, southeastern Utah. *Journal of Archaeological Science* **2013,** *40* (4), 2007-2013.
208. Washburn, D. K.; Washburn, W. N.; Shipkova, P. A.; Pelleymounter, M. A., Chemical analysis of cacao residues in archaeological ceramics from North America: consideration of contamination, sample size and systematic controls. *Journal of Archaeological Science* **2014,** *50*, 191-207.
209. Washburn, D. K.; Washburn, W. N.; Shipkova, P. A., The prehistoric drug trade: widespread consumption of cacao in Ancestral Pueblo and Hohokam communities in the American Southwest. *Journal of Archaeological Science* **2011,** *38* (7), 1634-1640

V THE THIRD WINDOW OF HISTORY: SPECTROSCOPY TO UNDERSTAND THE PHOTOCHEMICAL AND MEDICINAL PROPERTIES OF HISTORICAL PIGMENTS

There is no need to explain the importance and role of artistic works of historic and cultural significance. Conservationists have shown that time fades pigments, darkens varnishes, creates tears, causes warping, and generally totally changes the appearance of a work of art. The effective conservation and preservation of works of art to prevent time from taking its toll requires an indepth knowledge of the composition of the work of art to undo and mitigate damages. Art works are complex in composition a mix of inorganic pigments and organic pigments, glues, waxes, oils, and varnishes. Each component has to be separately identified to allow for appropriate treatment. Scientific research into the materials of paintings can greatly aid conservationists and preservationists. Scientist can offer up additional information such as sketches below paint and identification of pigments. Additionally, science can help us to understand why some pigments are affected more drastically by time while others are not.

A great example of this differentiation is exemplified by the anthraquinones and the differences in behavior of alizarin and purpurin. Our lab in a study published by Berenbeim et al. studied the spectroscopy of several anthraquinone dyes[210]. Anthraquinone dyes are of interest because they are traditional organic red pigments found from natural sources like madder, and cochineal. Within this large class of dyes several of the pigments are well known by conservationist to fade drastically over time. Two of the pigments alizarin and

purpurin were commonly used in paintings and are still used as food dyes, though one was found to fade while the other was lightfast. Purpurin fades over time while alizarin maintains its color. This is due to their differences in excited state lifetime and the fact that alizarin dissipates excess energy on a fast timescale.

The anthraquinones are not the only class of organic pigments that were used frequently in antiquity. Another common dye of interest to this dissertation is indigo an organic blue pigment used widely throughout the ancient world. Indigo is not only interesting in regards to its wide use in paintings, mosaics and other historical works of art but also scientifically as a model compound to better understand hydrogen and proton transfer dynamics. One reason that indigo was used so widely as a pigment is its lack of fading due to a fast excited state lifetime. This fast excited state lifetime has been studied previously by our group by Haggmark et al[211]. Preliminary work has been done to deuterate indigo to better understand the mechanism of hydrogen and proton transfer. This preliminary work will be presented in the following chapter.

The other pigment of interest in this dissertation is actually not used as a pigment but instead has been shown to have key medicinal properties- curcumin. Curcumin is the compound that gives turmeric its bright orange-yellow color as well as results in the medicinal properties of turmeric. Understanding the photochemistry of curcumin leads to a better understanding of its possible medicinal properties. As its photochemistry is likely

dominated by fast proton/hydrogen transfer, studying its photochemistry also helps the broader scientific understanding of this mechanism.

V.1 CHARACTERIZING THE PHOTOCHEMISTRY OF DEUTERATED INDIGO

Indigo is famous as a dye for multiple reason. It is the only historically used organic blue dye[212]. It is the only dye to successfully make the large scale transition from a natural dye to a synthetic dye. Indigo is found naturally in the leaves of *Isatis Indigofera* and *Isatis tinctoria* as well as from the mollusc *Murex trunculus*[213]. Indigo was used historically primarily as a vat dye in which the reduced form is soluble and can then act as a dye. Leuco-indigo is the colorless reduced form that is soluble in water. Back in the Greek and Roman periods indigo was used as a pigment instead of a dye as was traditional. In Egypt, many burial cloths were dyed with indigo[213]. Many of these artifacts still retain their color when dyed or painted with indigo. In 1883, Adolf von Baeyer determined the chemical structure of indigo and began the synthesis of indigo. By 1900, the production of synthetic indigo is now in full swing by Badische Anilin und Soda-Fabrik (BASF).

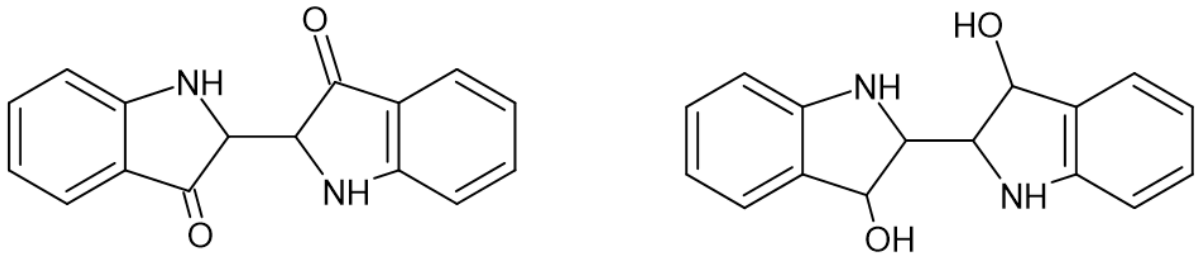

Figure 22- Molecular structure of indigo (left) and leuco- indigo (right)

Indigo's photostability comes from a fast excited state decay due to excited-state intramolecular proton transfer (ESIPT). The dynamics of indigo have been studied in the past in the gas phase, solution and theoretically. Overall the dynamics can be boiled down to indigo absorbing into a ππ* state[214]. In the S_1 (ππ*) state, the lowest energy form is the diketo form. From there most studies agree that the major deactivation mechanism is ESPT[214-219]. From the S_1 (ππ*) state, the quantum yield for fluorescence and intersystem crossing are extremely low and highly unlikely to be major mechanisms. The nature of ESPT in indigo is highly argued about. There is disagreement on whether it is a single or double PT, if ESPT involves photoisomerization, and if it is intra- or inter- molecular ESPT.

The work of multiple in depth studies agrees that the ESPT happens by the keto state undergoing rapid single proton transfer that relies on tunneling as the energy barrier for ESPT is roughly 10 kcal/mol rather than photoisomerization. ESPT converts the diketo form into the enol form which then decays in 20-130 ps.

In 2018, a thorough study on indigo and its dynamics was published by Haggmark[211]. Because past studies had established the presence of a barrier for ESPT to happen, it was this study's attempt to characterize the barrier height. Our technique allows for lifetimes to be ascribed to individual vibronic transitions as well as using various ionization wavelengths to try to map the barrier height. The results and calculations show that the barrier to achieve PT in the S_1 state is only 0.11 eV high. Interestingly, the dynamics of indigo involve not only the di-keto form but the PES also leads to two wells each corresponding to one of two different forms of the keto-enol tautomer. One of these forms has a smaller S_1/S_0 gap leading to fast radiationless decay pathways. In detail, in the ground state calculations there are two stable forms the diketo and the keto-enol due to HT. In the excited state, the keto enol has PT character instead. Past studies have not revealed any of these mechanisms of indigo, prompting our desire to study it in the deuterated form to better support and elucidate our proposed dynamics.

Indigo was deuterated by the following procedure by Joseph R. A. Kincaid in order to allow for comparison of the photodynamics of deuterated and undeuterated indigo.

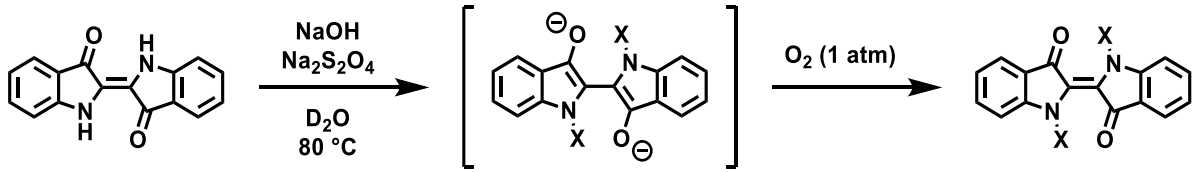

Scheme 1- deuteration procedure for indigo

To a flame-dried 2 dram vial was added a PTFE-coated magnetic stir bar, indigo (0.1 mmol, 26.2 mg), NaOH (100 mg), and sodium dithionite (100 mg). The vial was fitted with a rubber septum and the headspace purged with argon with the use of a vent needle. To the vial was added 3 mL of degassed D_2O and the mixture was heated to 80 °C with stirring until a transparent yellow solution was obtained. The reaction was allowed to cool to room temperature and O_2 was bubbled through the solution with an O_2-filled balloon and vent needle, and the product precipitated as a dark-blue solid. Product was recovered via centrifugation, the supernatant was discarded, and the product was washed several times with D_2O by resuspending and centrifuging. Product was then dried on vacuum overnight.

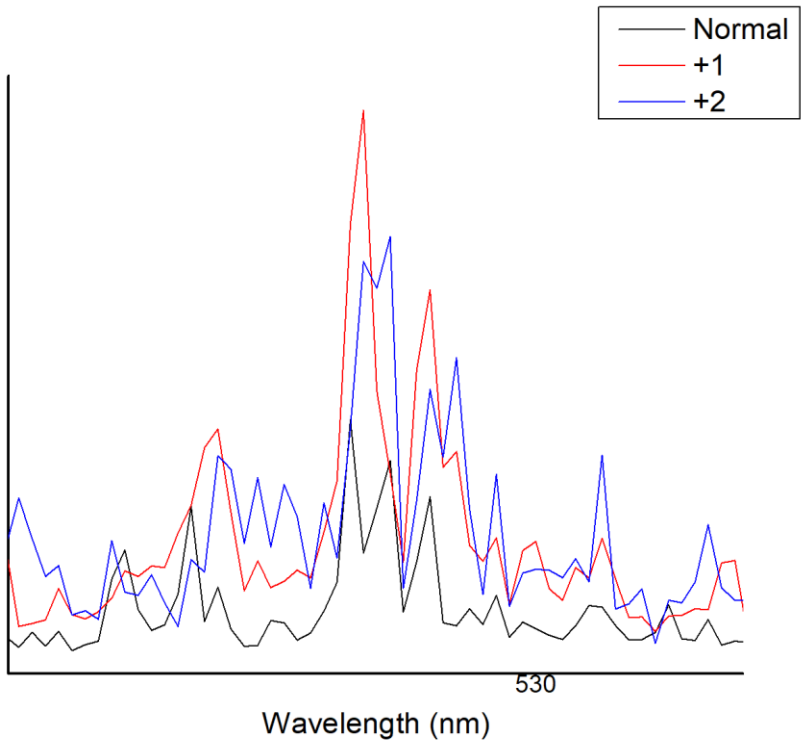

Figure 22- Unnormalized signal measurements of all isotopemers of indigo to show relative mass intensity.

Effectiveness of indigo deuteration was established through the mass spectrometry portion of our technique. With the wavelength resonant for the origin transition, the relative mass intensity of the three forms was established. The mass intensity showed that very little of the un-deuterated indigo was present while the +1 and +2 deuterated forms were roughly equal in population. It is important to note that some portion of the mass spectrum will be the result of the C_{13} portion of the lower mass peak overlapping with the peak of interest.

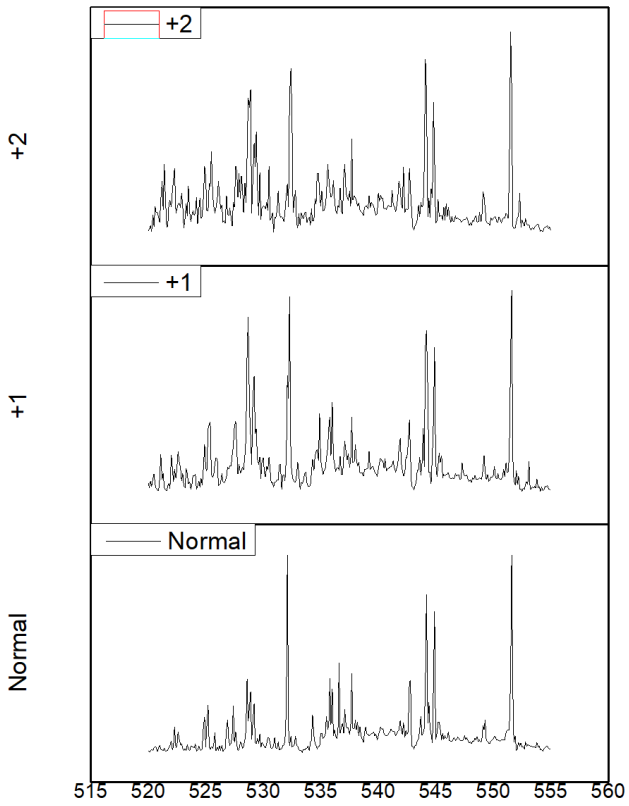

Figure 23- R2PI spectra of indigo taken with ps 213 nm as ionization laser.

Figure 23 depicts the R2PI spectra of undeuterated indigo, singly deuterated indigo (+1) and doubly deuterated indigo (+2). The initial origin transitions look remarkably the same in

width and intensity among the isotopomers. As excess energy is added though, the peaks change in intensity and even broaden in the +1 and +2 form. This could be indicative of a change in dynamics.

Previously, it was shown that for the origin to +700 cm-1 excess energy there were two lifetime decays. Past 700 cm-1 excess energy, there was only a single decay that changed as more excess energy was added. As the dynamics of indigo are determined by the height of the barrier for both ESPT and the barrier between the two keto-enol forms, the addition of deuteration is expected to increase the barrier for both, drastically changing the excited state dynamics. To better understand the effect of deuteration on dynamics, pump probe measurements will need to be done.

V.2 THE MEDICINAL PROPERTIES OF CURCUMIN STUDIED PHOTOCHEMICALLY

Extensive research has been conducted exploring the medicinal applications of curcumin; ranging from antioxidant properties to Alzheimer's treatment[220]. Historically, curcumin has been widely used in Chinese and Indian traditional medicine.[220] This created an interest in curcumin and analogous structures of curcumin for their possible use in drug exploration[221-223]. A thorough review by Nelson et al. disagrees with curcumin's functionality in most of these applications, but does agree with the labeling of curcumin as a PAIN (pan-assay interference compound) and IMP (invalid metabolic panaceas).[220]

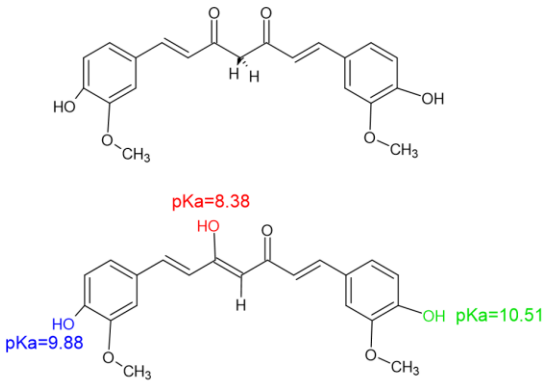

Figure 24- The structures of top: the di-keto tautomer and bottom: the mono-enol tautomer of curcumin. The mono-enol tautomer also has the pKa values of the three acidic protons recorded.

Curcumin is a bright yellow di-phenolic compound that is responsible for the bright hue and medicinal properties of turmeric[224]. It contains a beta diketone group in between two phenolic moieties. As shown by a thorough study by Balasubramanian, the charge separation in curcumin due to the polar enolic and phenolic groups placement between a hydrophobic bridge is important to its medicinal abilities. This charge separation is what allows curcumin to pass through the blood-brain barrier [224]. Because of this importance, many studies have calculated the electronic charge distribution of the highest occupied molecular orbital (HOMO) and lowest unoccupied molecular orbital (LUMO) electronic states. All calculations agree that the HOMO and LUMO have highly delocalized charge with the HOMO of π character and the LUMO of π* character [222, 223, 225-228]. The electronic structure of curcumin is also important because it determines if and how a ligand will interact in a binding site. The Kumaradhas group has reported multiple studies using molecular docking analysis to

understand the binding of curcumin with acetylcholinesterase for the prevention of Alzheimer's disease and has described in detail the two main mechanisms by which this happens [229-231].

Curcumin's excited state dynamics are dominated by deactivation of the S_1 state. Absorption and emission spectra have been characterized in a variety of solvents. A number of transient absorption and fluorescence upconversion studies have determined lifetimes for the major decay pathways of the S_1 state [232-236]. Laser flash photolysis has been done to characterize the triplet state[237]. H atom abstraction is also important to the medicinal abilities of curcumin because that provides its antioxidant abilities[238]. The excited state dynamics favor either intermolecular and intramolecular proton or hydrogen atom transfer, depending on how the solvent affects the hydrogen bonding environment around the enolic groups [232, 235]. Nonpolar, aprotic solvents do not affect the intramolecular hydrogen bond, allowing for excited state intramolecular proton transfer (ESIPT)[236]. More protic solvents interfere with the hydrogen bonding, favoring intermolecular excited state proton transfer (ESPT). Polar solvents further perturb the intramolecular hydrogen bonding, increasing the fluorescence rate, lifetime, and Stokes shift[239]. So far, no isotope effect has been observed to definitively identify ESIPT as a major decay pathway. Santin et al. found theoretically that MeOH lowers the barrier to proton tunneling, increasing the likelihood of proton transfer[225]. This conclusion agrees well with experimental work that has used deuteration to observe the intermolecular proton transfer[240]. Barik et al. found that the fluorescence quantum yield decreases with

increasing solvent polarity and deuteration has little effect which suggests that intermolecular hydrogen transfer is only partially responsible for the non-radiative decay process.[241]

The results shown below are from a publication in preparation which characterizes the lifetime and decay mechanisms of curcumin in the gas phase. These results are the first to unambiguously assign the gas phase tautomer of curcumin, and measure the lifetime of gas phase decay pathways. Surprisingly, deuteration only slightly perturbed the curcumin's absorption properties, and did not affect the excited state dynamics at all, contributing to the past discussions of ESIPT.

Curcumin was deuterated by dissolving it in deuterated methanol (CD_3OD) for 24 hours. This process was repeated three times to increase deuteration. The central enolic hydrogen should be the first site of deuteration as it is the most acidic, followed by the two phenolic enol moieties[242].

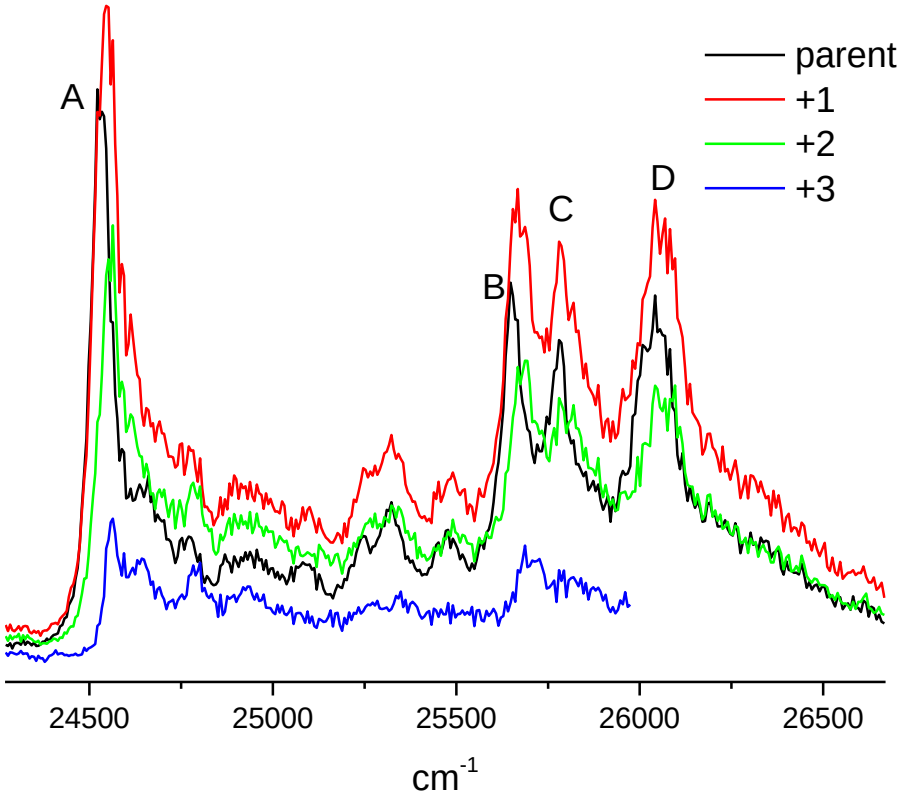

Figure 23- REMPI spectra of curcumin showing two key absorption sections corresponding to different excited states.

The R2PI spectrum of the parent mass provided signal in two spectral regions, around 24600 cm^{-1} and 25700 cm^{-1} (Fig. 25). Origin transitions, labeled as A and B, were then followed by broad, featureless regions of lower signal. The first spectral region only had a single sharp peak A (24515 cm^{-1}) which matches well with the $S_0 \rightarrow S_1$ origin transition found in other experimental studies as well as the origin calculated by theory. Benassi et al. calculated the absorption maximum of the enol tautomer in vacuum to be 419 nm (23866 cm^{-1}) [226]. This is

on par with experimental and calculated absorption maxima in most solutions [223, 224, 232-236, 240, 243, 244].

The second region had three peaks- B (25657 cm^{-1}), C (25780 cm^{-1}) and D (26041 cm^{-1}). Peak B matches well with calculations for the $S_0 \rightarrow S_2$ origin transition. No solution phase study reported seeing the absorption band for the S_2 state, as it is likely hid with in the extremely broad peak for the S_1 state. Both states are $\pi\pi^*$ making them highly allowed and likely to have a measurable absorption. The large energy separation between the two origin transitions also matches well with two different electronic states rather than higher level vibrational bands within the same electronic state. Normally, our technique distinguishes narrow individual vibronic transitions. Here, higher-energy vibronic transitions after the origin transition appear as broad regions of signal. It is likely that hidden within these broad bands are multiple narrow vibronic transitions. The broadening is due to the large size of curcumin as well as the density of lower energy modes. Other papers believed that the broadness in solution was due to different isomers but our results showed that this is not the case in the gas phase.

The mono-, di- and tri- deuterated forms have very similar two color-REMPI spectra with only a slight blue-shift as the mass is increased (Fig. 3). This slight blue shift upon increased deuteration is in line with solution phase studies[233, 245]. It is likely caused by a lowering of the zero point energy upon deuteration[246]. The slight blue shift is probably due to a shift in the zero point energy due to the deuteration. The data were collected simultaneously and were

not normalized. Therefore the intensities observed were the actual intensities relative to each other. The position of the deuterium can be estimated by the pKA values of the three hydrogens of curcumin. Since the enolic proton is the most acidic it is likely to be the first deuteration spot. The second and third deuteration must occur on the two phenolic protons[247]. The weak intensity of the trideuterated form was due to a much smaller ratio of the trideuterated species in the sample as revealed by the mass spectrum of the compound. Not all signal at the higher masses can be contributed to that mass since there is also a contribution from ^{13}C isotopes. Consequently, 83% of +1 is from that form, 72% for +2 and 52% for +3.

Curcumin can be found as syn-diketo, anti-diketo, or enol tautomers that readily undergo keto-enol tautomerization. The two diketo forms are energetically degenerate and almost all theoretical calculations agree that the mono-enol form is energetically favored both in vacuo and most solvents[221, 223-225, 228, 248, 249]. [244].

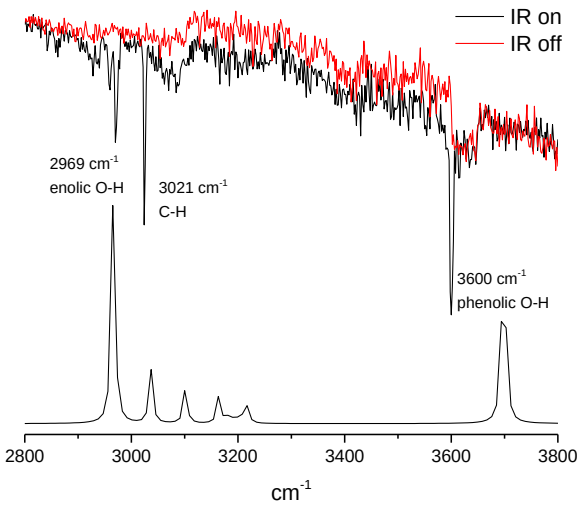

Figure 26- Mode 1 IR-UV double resonance. Red is background while back is burn spectrum. Bottom trace is the theoretical IR spectrum at the b3lyp/6-31+g(d) level.

We assign the single observed tautomer with IR-UV double resonant spectroscopy Mode 1. The IR spectrum shows three peaks – 2969 cm^{-1}, 3021 cm^{-1} and 3600 cm^{-1}. Previously theory calculation can be used to assign stretches to our spectra [226, 228, 248]. The stretch at 2969 cm^{-1} has been attributed by theory to the enolic O-H stretch. While the stretch at 3021 cm^{-1} is most likely due to several overlapping C-H bonds. Finally the 3600 cm^{-1} stretch has been attributed to the phenolic O-H stretch[248].

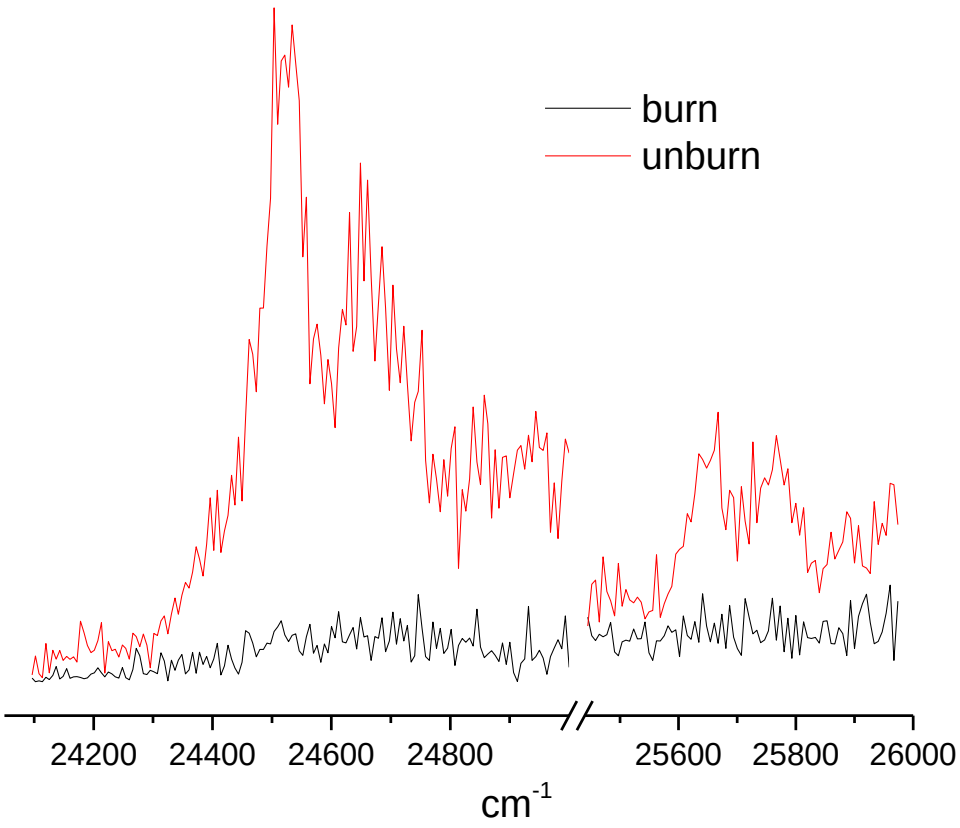

Figure 27- Mode 2 IR-UV Double Resonance Mode 2 spectrum proving that only one tautomer is present.

IR-UV Double Resonance Mode 2 was used to discern how many tautomers were present in the spectrum (Fig. 27). For this, the IR laser was parked on the 3600 cm^{-1} transition. This is the transition for the phenolic stretches not the enolic stretch. The phenolic stretch does slightly shift depending on tautomer. As the width of our pulse is extremely narrow it is

possible to only excite the phenolic stretch of the mono-enol form. It is clear from the IR-UV spectrum that all peaks shown in the REMPI spectrum are from the same tautomer evidenced by the loss in signal at all visible energies scanned.

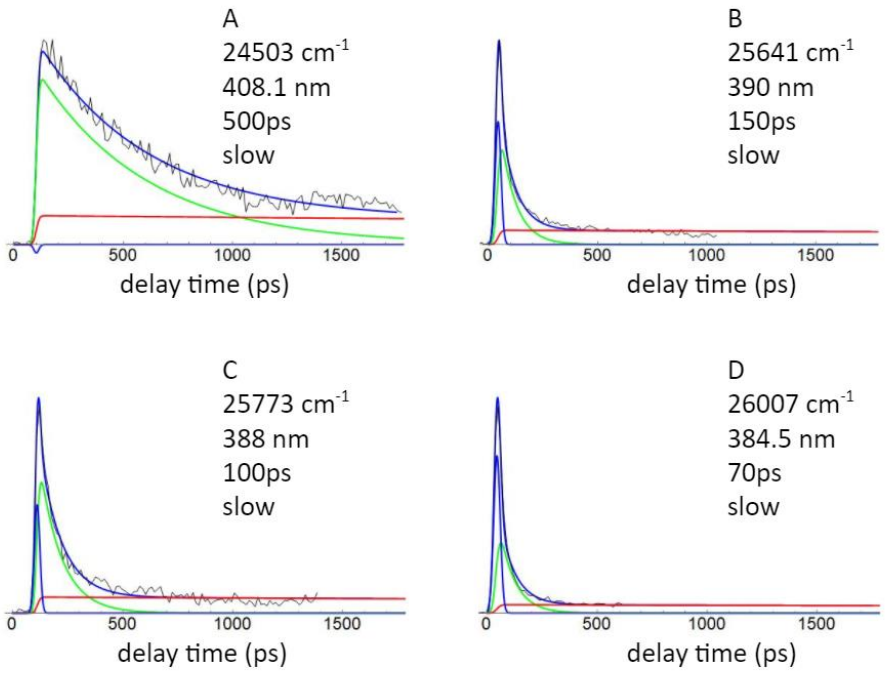

Figure 28- Pump probe spectra of the four vibrational bands. In each spectrum, black is experimental data, blue total fit, green IRF, and red decay function.

Pump probe measurments were recorded for all four peaks, designated A-D, with the undeuterated and mono- bi- and tri- deuterated forms to characterize the lifetimes of the transitions. All pump probes traces were fit with a monoexponential decay as well as a bi-exponential decay (Figure 28). According to the monoexponential decay fitting, the S_1 state (Fig. 28a) had the longest lifetime at 632 ps with the S_2 origin (Fig. 28b) being slightly shorter

at 442 ps with the lifetime decreasing as excess energy was added. All higher energy transitions in the S_2 state also saw a decrease in lifetime. The bi-exponential fit shows that all transitions have a long lifetime component . The lifetime of the other transitions matches fairly well the lifetimes found in the monoexponential fitting of the decay. The bi-expontial fit does calculate shorter lifetimes for the S_2 state decay with the origin having a lifetime of 150 ps and all higher energy transitions shorter at 70 ps.

Our results have yielded three interesting conclusions. (1) The tautomer of curcumin in the gas phase has been verified experimentally to be the mono-enol tautomer. Our Mode 1 IR-UV, proved that there was only one tautomer present in our system and the mode 2, found the IR stretches of that tautomer. When matched to theory it is clear that the tautomer observed is in fact the mono-enol and not the diketone as predictied in previous studies.

(2) None of the decay pathways detected in our system can be attributed to any sort of hydrogen transfer. Curcumin was triply deuterated and the R2PI spectra and pump-probe spectra were taken for all isotopomers. There was no difference in the decay lifetimes upon deuteration of all acidic hydrogens. If one of the observed relaxation pathways involved proton transfer of any sort then it is expected that deuteration would cause the lifetime to increase by a factor of 1.5 to 2. Since no change in lifetime is observed upon deuteration then it is safe to assume that none of our decays can be attributed to proton transfer. This is not to say that ESIPT cannot still be an important decay pathway of curcumin. This only means that if it occurs that it happens on a faster timescale than that measurable of our instrument.

(3) Finally the last conclusion is that in the gas phase two decay pathways have been observed. The pump probe shows a decay that varies in time from 630 ps to 150 ps and a longer decay greater than 5 ns. Possible decay pathways will be discussed later.

Below it will be discussed how these conclusions as well as our data fit into the variety of solvation studies done on curcumin.

Our study is the first gas phase study and thus the first to see individual vibronic transitions rather than the broad bands found in solution. Our R2PI spectra observed transitions to both the S1 and S2 state. Solution phase studies have found that the absorption band of curcumin is highly dependent on the solvent due to the hydrogen bonding nature and polarity of the system[236, 239]. One thorough study by Nardo measures the absorption and relaxation processes in a variety of solvents[239]. In most solvents, the absorption spectrum is a broad structureless band with a maximum around 430 nm. Polarity and hydrogen-bonding ability of the solvent can greatly affect the absorption band. In protic solvents, this broad band has a weak shoulder which resolves into two separate bands in cyclohexane. These two peaks redshift from 408 nm and 429 nm in cyclohexane (aprotic nonpolar) to 433 nm in ethylene glycol (polar protic). Usually data collected in cyclohexane will match the closest to gas phase data. The origin transition for $S_0 \rightarrow S_1$ at 24515 cm^{-1} (A) matches well to 408 nm peak in cyclohexane. Another lower energy 429 nm peak is observed in cyclohexane. Multiple authors attribute the 429 nm peak to the presence of the diketo tautomer[237, 239]. Since our

technique only includes the cis enol tautomer, we do not expect to observe this second transition.

The broad absorption band seen in the more polar solution phase studies contains multiple electronic transitions. In the gas phase we can resolve a second electronic transition ($S_0 \rightarrow S_2$ at 389.76 nm; 25656 cm^{-1}). It is unusual, though not unheard of, to observe more than one bright electronic state in the gas phase. Typically only the lowest energy bright state is observed, because electronic states are separated by a significant amount of energy and higher energy states are more difficult to observe due to their more extreme dynamics. This does not appear to be the case for curcumin. This is due to the relative proximity in energy between S_1 and S_2 and their high absorption cross sections. It is further enhanced by their relatively long lived excited states.

As also described above, our IR data reveals that in the gas phase there is indeed only one tautomer present and we assign this tautomer as the mono-enol form. This fits with theory which stated that the mono-enol is expected in gas phase because it is the lowest in energy. In addition the fact that the triply deuterated form of curcumin is observed further shows that it is unlikely the di-keto form is observed. Again, we expect the central enolic hydrogen to be deuterated first as it is the most acidic, followed by the two phenolic enol groups[242].

The decay pathways observed in our instrument can offer interesting insight to the current solution phase theories of curcumins dynamics. Unlike our two lifetimes at 400-100 ps and 1500 ps. Solution phasestudies observe roughly three decays. These decay processes typically

occur on the 20 ps, 200 ps, and the 1000 – 2000 ps timescales. All investigators agree that the shortest pathway is due to solvation, a process we will not observe in the gas phase. The latter two decays are more controversial, with a couple of different explanations proposed. A measurable ISC yield with a lifetime on the order of microseconds has also been observed.

The first proposed decay pathway attributes the short lifetime from solvation decay and the intermediate is from ESIHT[232-234]. Petrich et al. uses deuteration of curcumin and femtosecond fluorescence upconversion spectroscopy to support this pathway. They found a 12 ps and 70 ps component in MeOH and an 12 ps and 120 ps in MeOH-d_4. Additionally they measured lifetimes of 20 ps and 105 ps in ethylene glycol and 20 ps and 200 ps in ethylene glycol-d_2. Deuteration extends the time of the longer relaxation process in both solvents. The shorter lifetime was attributed to solvation, while the longer lifetime was attributed to ESIHT, assigned from the observed isotope effect. Because of the significant change in dipole moment upon excitation solvation is expected to influence the excited state dynamics, supported by the sensitivity of the Stokes shift. Solvation does still play a role in the relaxation of the excited state but it happens extremely quickly [232-234]. A study by Erez et al which used fluorescence up conversion in EtOH and 1-proponal to look at the decay at different temperatures and excitation wavelengths also agree that the major non-radiative process is solvent-controlled proton transfer.

The second proposed decay pathway attributes the short lifetime to solvation decay as well but assigns the intermediate decay to interaction with the solvent and fluorescence. Ghosh

et al. did a thorough study using transient absorption and fluorescence upconversion in 15 different solvents looking into this mechanism [236]. Unlike past studies they found that these lifetimes are highly wavelength dependent. The lifetimes measured at 520 nm are not applicable because the multiple decays are actually just due to a large number of differently solvated species. Only when measured at the red edge of the spectra 640-660 nm can the fully solvated S1 state be monitored. This wavelength dependence shows the faster process is due to interaction with the solvent. Solvation involves the formation of intermolecular hydrogen or deuterium bonds between the solute and the solvent. Stretching vibrations in hydrogen/deuterium induce nonradiative deactivation of the excited state, hence the longer lifetimes in deuterated solvents. This yields a lifetime of 130 ps in MeOH or 220 ps in MeOH-d_4. They argue this isotope effect is due to solvation and not the originally proposed ESIHT. ESIHT (and its corresponding isotope effect) cannot be observed with these spectroscopic techniques in curcumin due to the molecule's symmetry. Further, ESIHT should be on the hundreds of femtoseconds timescale. They agree with past studies that the lifetimes of the 57 ps and 256 ps are from the cis-enol and trans-diketo conformers respectively[235, 239].

Our study observes a decay pathway with a lifetime of 632 ps at the origin of the lowest energy singlet excited state, with decreasing lifetime with excess energy. Additionally, a much longer lifetime is observed at all energies as well. Solution phase studies saw three lifetimes 20 ps, 120 ps and 1500 ps. According to solution phase studies, the only possible decay pathways of curcumin are ESIHT, solvation, ISC or fluorescence. Comparison of the dynamics

between environments is not straightforward. The polarity of the solvent not only affects the electronic structure of curcumin, but also the hydrogen-bonding environment, which potentially has a significant role in the dynamics. Further, because solvation is a major decay process, the viscosity of the solvent is also relevant. Viscosity of solvents change, irrespective of polarity. Therefore, relaxation trends going from more polar solvents to less polar solvents to gas phase are not evident.

Due to the gas phase, both solvation and ESIPT can be ruled out as relaxation mechanisms in our system. With the lack of any isotope effect, both described pathways for solvated curcumin can also be safely rejected as well, including ESIHT. For the faster decay process we measured, that only realistically leaves fluorescence and a separate nonradiative decay pathway as possibilities. The fluorescence yield and lifetime both decrease as the solvent polarity decreases, to $\Phi_{fl} = 0.006$ and $\tau = 57$ ps in cyclohexane[239, 250]. Extrapolating to the gas phase, fluorescence is highly unlikely to be the major relaxation pathway for curcumin. Further, Kasha's rule discourages fluorescence from S_2, meaning the yield of the faster process would drop off precipitously at the higher energies probed, if fluorescence was the dominant mechanism. Therefore, this relaxation must be from another nonradiative decay mechanism.

Unfortunately, the literature discusses very little on other nonradiative relaxation processes. Without concerted theoretical calculations, the nature of this process is difficult to discern. It can safely be assumed that the relaxation does not involve any sort of geometrical distortion

with a significant contribution from H/D, as an isotope effect would likely be observed. Upon excitation, the process must overcome some potential energy barrier as it relaxes back to the ground state, as the process speeds up with increased energy.

With regards to the 15000 ps decay component also observed, this is likely from ISC. This process has been observed for curcumin in solution as well, with increasing ISC yield as solvent polarity decreased [250, 251]. Quantum yields from ISC exceeded 0.1 in both benzene and cyclohexane making it a strong candidate for this much longer process in the gas phase.

Overall, the excited state dynamics proposed here for curcumin in the gas phase are significantly different than the models developed for curcumin in solution. While the dynamics of solvated curcumin are dominated by solvation and proton/hydrogen transfer, *in vacuo* it appears to be mainly from a yet undescribed nonradiative pathway. Whatever this process is, triply deuterating curcumin did not change the dynamics at all.

The longest decay is the decay seen from the triplet state or from the much lower population diketo tautomer. The origin has a small ISC rate to the triplet state so it is not surprising that this decay is not observed. In different solvents the triplet state has a quantum yield of 0.03 to 0.12 and a lifetime ranging from 1 to 10 μs[235 251]. The lifetime is highly dependent on concentration due to self quenching [251]. This ISC pathway in solution is also supported by curcumin's ability to generate single oxygen. Further, we only observe the mono-enol tautomer, thus no contribution from the diketo tautomer.

Our data elucidates the deactivation mechanisms of two electronic states. Curcumin was triply deuterated but none of the isotopomers showed any differences in their vibrational spectra or in the excited state dynamics. A lack of observed change in dynamics with deuteration means that if ESIPT is a major relaxation pathway it is likely too fast for us to observe. We expect the vibronic spectra between separate isotopomers to be more different if ESIHT was the dominant process due to the deuterium present. The deuterium would shift the frequency of individual vibronic bands, due to the change in mass. Further, the lifetime of any vibronic band that decays via ESIHT would be affected by the deuterium, causing the relative broadness of that band to be modulated. Thus, the single decays of hundreds of picoseconds that we experimentally observe cannot be due to ESIPT, nor solvation. Our data supports that of Ghosh and others who state that the intermediate lifetime decay is not ESIPT and expects that the ESIPT are instead much faster likely on a fs lifetime.

ISC is possible but it is unlikely as the lifetime is usually on the order of microseconds, which we do not observe. Fluorescence of the mono-enolic form in solution usually ranges from 50-350 ps which is of the same order that we observe at all transition energies. Flourescence has also been observed in many solution phase studies and the lifetime matches that observed in solution (Nardo 2008) This lifetime could also be from internal conversion (IC) rather than fluorescence since the flourescent quantum yield is low in solution, IC is a major decay pathway in solution[235].

The emission of curcumin is found to be highly Stokes shifted based on the polarity and hydrogen bond forming nature of the solvent [232, 235-237, 241, 252, 253]. The argument that Stokes shifting is due to solvent polarity is strengthened by a study of fluorescence in deuterated solvents [241]. The QY for fluorescence ranges from 0.006 to 0.174 depending on the solvent as well as changing whether it is a mono-, di- or tri-exponential decay. Nardo attributes these three processes to fluorescence of either cis- enol form as the shortest lifetime, cis-trans isomerization as the intermediate, or anti diketo as the longest lifetime component [239]. Mukerjee also agrees that the different emissions are likely from different tautomers or intramolecular conformational changes[254].

We do not exclude the possibility that the main relaxation process observed in gas phase is a different nonradiative pathway. This means that this yet unknown nonradiative pathway is not disturbed by any of the three sites of deuteration. If this is the case, more theoretical calculations would be needed to explain this.

Curcumin has been studied spectroscopically in the gas phase using REMPI. This technique allowed for a more direct comparison to theoretical calculations and observation of the excited state dynamics near the threshold excitation. Up to three deuteriums were added to curcumin to understand if and how deuteration affected the structure and dynamics. Only the mono-enol tautomer was observed in the gas phase, in agreement with theoretical calculations. Deuteration did not appear to have a significant effect on curcumin's absorption properties, nor any effect on its excited state dynamics, at least near threshold excitation.

Moreover, two distinct excited electronic states were observed, uncommon in the gas phase. These states are also well-described by theory. Two decay pathway were observed, on the order of hundreds of picoseconds and nanoseconds. The shorter decay is assigned to a nonradiative pathway that has not yet been thoroughly studied. The longer decay is likely from ISC. The popular ESIPT pathway is not observed, as there is no isotope effect and the ubiquitous solvation mechanism does not apply here.

The dynamics of curcumin have a long ways to go before they are understood. ESIPT still has not been convincingly resolved in solution. Admittedly, that may be difficult with most spectroscopic techniques due to symmetry. The longer, several hundred picosecond decay process needs to be more thoroughly studied theoretically to explain what is occurring. Finally, it needs to be identified if these processes are the same for the gas phase and solution phase.

BIBLIOGRAPHY

210. Berenbeim, J. A.; Boldissar, S.; Owens, S. C.; Haggmark, M. R.; Gate, G.; Siouri, F. M.; Cohen, T.; Rode, M. F.; Patterson, C. S.; de Vries, M. S., Excited state intramolecular proton transfer in hydroxyanthraquinones: toward predicting fading of organic red colorants in art. *Science Advances* **2019,** *5* (9).

211. Haggmark, M. R.; Gate, G.; Boldissar, S.; Berenbeim, J. A.; Sobolewski, A. L.; de Vries, M. S., Evidence for competing proton-transfer and hydrogen transfer reactions in the S1 state of indigo. *Chemical Physics* **2018,** *515*, 535-542.

212. Christie, R. M., Why is Indigo Blue? *Biotechnic & Histochemistry* **2007,** *82* (2), 51-56.

213. Clark, R. J. H.; Cooksey, C. J.; Daniels, M. A. M.; Withnall, R., Indigo, woad, and Tyrian Purpule: important vat dyes from antiquity to the present. *Endeavour* **1993,** *17* (4), 191-199.

214. Bernardino, N. D.; Brown-Xu, S.; Gustafson, T. L.; de Faria, D. L. A., Time-Resolved Spectroscopy of Indigo and of a Maya Blue Stimulant. *The Journal of Physical Chemistry C* **2016,** *120*, 21905-21914.

215. Iwakura, I.; Yabushita, A.; Kobayashi, T., Kinetic isotope effect on the proton-transfer in indigo carmine. *Chemical Physics Letters* **2010,** *484*, 354-357.

216. Izumi, I.; Atushi, Y.; Takayoski, K., Why is Indigo Photostable over Extremely Long Periods? *Chemistry Letters* **2009,** *38* (11), 1020-1021.
217. Chatterley, A. S.; Horke, D. A.; Verlet, J. R. R., On the intinsic photophysics of indigo: a time-resolved photoelectron spectroscopy study of the indigo carmine dianion. *Phys Chem Chem Phys* **2012,** *14*, 16155-16161.
218. Moreno, M.; Ortiz-Sanchez, J. M.; Gelabert, R.; Lluch, J. M., A theoretical study of the photochemistry of indigo in its neutral and dianionic (leucoindigo) forms. *Phys Chem Chem Phys* **2013,** *15*, 20236-20246.
219. Pina, J.; Sarmento, D.; Accoto, M.; Gentili, P. L.; Vaccaro, L.; Galvao, A.; Seizas de Melo, J. S., Excited-State Proton Transfer in Indigo. *The Journal of Physical Chemistry B* **2017,** *121*, 2308-2318.
220. Nelson, K. M.; Dahlin, J. L.; Bisson, J.; Graham, J.; Pauli, G. F.; Walters, M. A., The Essential Medicinal Chemistry of Curcumin. **2017**.
221. Sun, Y.-M.; Zhang, H.-Y.; Chen, D.-Z.; Liu, C.-B., Theoretical Elucidation on the Antioxidant Mechanism of Curcumin: A DFT Study. *Org. Lett* **2002,** *4* (17).
222. Naama, J. H.; Alwan, G. H.; Obayes, H. R.; Al-Amiery, A. A.; Al-Temimi, A. A.; Kadhum, A. A. H.; Mohamad, A. B., Curcuminoids as antioxidants and theoretical study of stability of curcumin isomers in gaseous state. *Research on Chemical Intermediates* **2012,** *34*, 4047-4059.
223. Galasso*, V.; Kovač, B.; Modelli, A.; Ottaviani, M. F.; Pichierri, F., Spectroscopic and Theoretical Study of the Electronic Structure of Curcumin and Related Fragment Molecules. *Journal of Physical Chemistry A* **2008,** *112* (11), 2331-2338.
224. Balsubramanian, K., Molecular Orbital Basis for Yellow Curry Spice Curcumin's Prevention of Alzheimer's Disease. *Journal of Agricultural and Food Chemistry* **2006,** *54* (10), 3512-3520.
225. Santin, L. G.; Toledo, E. M.; Carvalho-Silva, V. H.; Camargo, A. J.; Gargano, R.; Oliveira, S. S., Methanol Solvation Effect on the Proton Rearrangement of Curcumin's Enol Forms: An Ab Initio Molecular Dynamics and Electronic Structure Viewpoint. *Journal of Physical Chemistry C* **2016,** *120* (36), 19923-19931.
226. Benassi, E.; Spagnolo, F., A Combined Theoretical and Experimental Approach to the study of the structural and Electronic Properties of Curcumin as a Function of the Solvent. *Journal of Solution Chemistry* **2009,** *39* (1), 11-29.
227. Benassi, E.; Spagnolo, F., A theoretical study about the structural, electronic and spectroscopic properties of the ground and singlet excited states of curcuminoidic core. *Theoretical Chemistry Accounts* **2009,** *124*, 235-250.
228. Benassi, R.; Ferrari, E.; Lazzari, S.; Spagnolo, F.; Saladini, M., Theoretical study on Curcumin: A comparison of calculated spectroscopic properties with NMR, Uv-vis and IR experimental data. *Journal of Molecular Structure* **2008,** *892* (1-3), 168-176.
229. Parameswari, A. R.; Rajalakshmi, G.; Kumaradhas, P., A combined molecular docking and charge density analysis is a new approach for medicinal research to understand drug-receptor interaction: Curcumin-AChE model. *Chemico-Biological Interactions* **2015,** *225*, 21-31.
230. Devipriya, B.; Kumaradhas, P., Molecular flexibility and the electrostatic moments of curcumin and its derivatives in the active site of p300: A theoretical charge density study. *Chemico-Biological Interactions* **2013,** *204* (3), 153-165.
231. Saravanan, K.; Kalaiarasi, C.; Kumaradhas, P., Understanding the conformational flexibility and electrostatic properties of curcumin in the active site of rhAChE via molecular docking,

molecular dynamics, and charge density analysis. *Journal of Biomolecular Structure and Dynamics* **2017,** *35* (16), 3627-3647.
232. Adhikary, R.; Mukherjee, P.; Kee, T. W.; Petrich, J. W., Excited-State Intramolecular Hydrogen Atom Transfer and Solvation Dynamics of the Medicinal Pigment Curcumin. *Journal of Physical Chemistry B* **2009,** *113* (15), 5255-5261.
233. Adhikary, R.; Carlson, P. J.; Kee, T. W.; Petrich, J. W., Excited-State Intramolecular Hydrogen Atom Transfer of Curcumin in Surfactant Micelles. *Journal of Physical Chemistry B* **2010,** *114* (8), 2997-3004.
234. Kee, T. W.; Adhikary, R.; Carlson, P. J.; Mukherjee, P.; Petrich, J. W., Femtosecond Fluorescence Upconversion Investigations on the Excited State Photophysics of Curcumin. *Australian Journal of Chemistry* **2011,** *64* (1), 23-30.
235. Khopde, S. M.; Priyadarsini, K. I.; Palit, D. K.; Mukherjee, T., Effect of Solvent on the Excited-state Photophysical Properties of Curcumin. *Photochemistry and photobiology* **2007,** *72* (5), 625-631.
236. Ghosh, R.; Mondal, J. A.; Palit, D. K., Ultrafast Dynamics of the Excited States of Curcumin in Solution. *Journal of Physical Chemistry B* **2010,** *114* (37), 12129-12143.
237. Chignell, C. F.; Bilskj, P.; Reszka, K. J.; Motten, A. G.; Sik, R. H.; Dahl, T. A., Spectral and Photochemical Properties of Curcumin. *Photochemistry and photobiology* **1994,** *59* (3), 295-302.
238. Slobodan V. Jovanovic, †; Steen Steenken; Charles W. Boone, a.; Simic‖, M. G., H-Atom Transfer Is A Preferred Antioxidant Mechanism of Curcumin. *Journal of the American Chemical Society* **1999,** *121* (41), 9677-9681.
239. Nardo, L.; Paderno, R.; Andreoni, A.; Masson, M.; Haukvik, T.; Tonnesen, H. H., Role of H-bond Formation in the Photoreactivity of Curcumin. *Spectroscopy* **2008,** *22*, 187-198.
240. Erez, Y.; Presiado, I.; Gepshtein, R.; Huppert, D., Temperature Dependence of the Fluorescence Properties of Curcumin. *Journal of Physical Chemistry A* **2011,** *115* (40), 10962-10971.
241. Barik, A.; Goel, N. K.; Priyadarsini, K. I.; Mohan, H., Effect of Deuterated Solvents on the Excited State Photophysical Properties of Curcumin. *Journal of Photoscience* **2004,** *11* (3), 95-99.
242. Anjomshoa, S.; Namazian, M.; Noorbala, M. R., The Effect of Solvent on Tautomerism, Acidity and Radical Stability of Curcumin and Its Derivatives Based on Thermodynamic Quantities. *Journal of Solution Chemistry* **2016,** *45* (7), 1021-1030.
243. Akulov, K.; Simkovitch, R.; Erez, Y.; Gepshtein, R.; Schwartz, T.; Huppert, D., Acid Effect on Photobase Properties of Curcumin. *Journal of Physical Chemistry A* **2014,** *118* (13), 2470-2479.
244. Manolova, Y.; Deneva, V.; Antonov, L.; Drakalska, E.; Momekova, D.; Lambov, N., The Effect of the water on the curcumin tautomerism: A quantitative approach. *Spectrochimica Acta Part A: Molecular and Biomolecular Spectroscopy* **2014,** *132*, 815-820.
245. Adhikary, R.; Mukherjee, P.; Kee, T. W.; Petrich, J. W., Excited-State Intramolecular Hydrogen Atom Transfer and Solvation Dynamics of the Medicinal Pigment Curcumin. *J phys Chem B* **2009,** *113*, 5255 - 5261.
246. Douhal, A. L., Francoise; Zewail, Ahmed H., Proton-transfer reaction dynamics. *Chemical Physics* **1996,** *207*, 477-498.
247. Zhao, Q.; Kong, D.-X.; Zhang, H.-Y., Excited-State pKa values of Curcumin. *Natural Product Communications* **2007,** *3* (2), 229-232.
248. Kolev, T. M.; Velcheva, E. A.; Stamboliyska, B. A.; Spiteller, M., DFT and experimental studies of the structure and vibrational spectra of curcumin. *Properties, Dynamics, and Electronic Structure of Atoms and Molecules* **2005,** *102* (6), 1069-1079.

249. Anjomshoa, S.; Namazian, M.; Noorbala, M. R., The Effect of Solvent on Tautomerism, Acidity and Radical Stability of Curcumin and Its Derivatives Based on Thermodynamic Quantities. *Journal of Solution Chemistry* **2016,** *45*, 1021-1030.
250. Khopde, S. M.; Priyadarsini, K. I.; Palit, D. K.; Mukherjee, T., Effect of Solvent on the Excited-state Photophysical Properties of Curcumin. *Photochem Photobio* **2000,** *72* (5), 625 - 631.
251. Gorman, A. A.; Hamblett, I.; Srinivasan, V. S.; Wood, P. D., Curcumin-derived transients: A Pulsed Laser and Pulse Radiolysis Study. *Photochemistry and photobiology* **1994,** *59* (4), 389-398.
252. Bong, P. H., Spectral and Photophysical Behaviors of Curcumin and Curcuminoids. *Bulletin of the Korean Chemical Society* **2000,** *21* (1), 81-86.
253. Barik, A.; Priyadarsini, K. I.; Mohan, H., Excited State Photophysical Properties of Curcumin and its Methoxy Derivative in Benzene. *Oriental Journal of Chemistry* **2002,** *18* (3).
254. Mukerjee, A.; Sorensen, T. J.; Ranjan, A. P.; Raut, S.; Gryczynski, I.; Vishwanatha, J. K.; Gryczynski, Z., Spectroscopic Properties of Curcumin: Orientation of Transition Moments. *The Journal of Physical Chemistry B* **2010,** *114* (39), 12679-12684.